NASA
Technical
Memorandum

NASA TM - 103544

APPLICATIONS OF LOW LIFT TO DRAG RATIO AEROBRAKES USING ANGLE OF ATTACK VARIATION FOR CONTROL

By J.A. Mulqueen

Preliminary Design Office
Program Development Directorate

June 1991

NASA
National Aeronautics and
Space Administration
George C. Marshall Space Flight Center

MSFC - Form 3190 (Rev. May 1983)

NASA
National Aeronautics and Space Administration

Report Documentation Page

1. Report No. NASA TM- 103544	2. Government Accession No.	3. Recipient's Catalog No.

4. Title and Subtitle Applications of Low Lift to Drag Ratio Aerobrakes Using Angle of Attack Variation for Control	5. Report Date June 1991
	6. Performing Organization Code
7. Author(s) J.A. Mulqueen	8. Performing Organization Report No.
	10. Work Unit No.
9. Performing Organization Name and Address George C. Marshall Space Flight Center Marshall Space Flight Center, Alabama 35812	11. Contract or Grant No.
	13. Type of Report and Period Covered Technical Memorandum
12. Sponsoring Agency Name and Address National Aeronautics and Space Administration Washington, DC 20546	14. Sponsoring Agency Code NASA

15. Supplementary Notes

Prepared by Preliminary Design Office, Program Development Directorate.

16. Abstract

This report investigates several applications of low lift to drag ratio aerobrakes which use angle-of-attack variation for control. These applications are: return from geosynchronous or lunar orbit to low Earth orbit and planetary aerocapture at Earth and Mars. A number of aerobrake design considerations are reviewed. It was found that the flow impingement behind the aerobrake and the aerodynamic heating loads are the primary factors that control the sizing of an aerobrake. The heating loads and other loads, such as maximum acceleration, are determined by the vehicle ballistic coefficient, the atmosphere entry conditions, and the trajectory design. Several formulations for defining an optimum trajectory are reviewed, and the various performance indices that can be used are evaluated. The "nearly grazing" optimal trajectory was found to provide the best compromise between the often conflicting goals of minimizing the vehicle propulsive requirements and minimizing vehicle loads. The relationship between vehicle and trajectory design is investigated further using the results of numerical simulations of trajectories for each aerobrake application. The data show the sensitivity of the trajectories to several vehicle parameters and atmospheric density variations. The results of the trajectory analysis show that low lift to drag ratio aerobrakes, which use angle-of-attack variation for control, can potentially be used for a wide range of aerobrake applications.

17. Key Words (Suggested by Author(s)) Aerobraking, Aerocapture, Lunar Missions, Mars Missions	18. Distribution Statement Unclassified – Unlimited

19. Security Classif. (of this report) Unclassified	20. Security Classif. (of this page) Unclassified	21. No. of pages 99	22. Price NTIS

NASA FORM 1626 OCT 86

For sale by the National Technical Information Service, Springfield, VA 22161-2171

TABLE OF CONTENTS

Page

LIST OF ILLUSTRATIONS

LIST OF ILLUSTRATIONS (Continued)

LIST OF ILLUSTRATIONS (Continued)

LIST OF TABLES

LIST OF SYMBOLS

A	aerobrake reference area, frontal area
$\mathbf{A}$	aerodynamic force vector
A/B	abbreviation for aerobrake
AFE	Aeroassist Flight Experiment
B	inverse scale height (depth of penetration into the atmosphere)
C	(1) characteristic velocity; (2) a constant
cg	center of mass (or center of gravity)
C_3	hyberbolic excess velocity squared ($\mathrm{km}^2/\mathrm{s}^2$)
C_A	axial aerodynamic force coefficient
C_D, CD	aerodynamic drag coefficient
C_{D_0}	drag coefficient at zero lift
C_D*	drag coefficient at maximum lift to drag ratio
C_L, CL	aerodynamic lift coefficient
C_L*	lift coefficient at maximum lift to drag ratio
C_m	aerodynamic pitching moment coefficient
$C_{m_{cg}}$	pitching moment coefficient at the center of mass (or center of gravity)
C_{m_α}	stability derivative, partial derivative of the pitching moment coefficient with respect to angle of attack
C_N	aerodynamic normal force coefficient
C_y	aerodynamic side force coefficient
d	aerobrake reference length, aerobrake diameter
D	aerodynamic drag force
E*	maximum lift to drag ratio
g	acceleration due to gravity

g_w	ratio of wall enthalpy to total enthalpy
$g_{\max}$	maximum acceleration load
GEO	geosynchronous Earth orbit
$h_{p_{\text{tol.}}}$	target vacuum periapsis altitude tolerance
H	Hamiltonian function
I_{sp}	specific impulse (seconds)
J	functional in optimization formulation
k	a constant used in dimensionless equations of motion ($k^2 = Br$)
k_i	boundary constraints for the functional J
K	degrees Kelvin
L	aerodynamic lift force
LaRC	Langley Research Center
LTV	lunar transfer vehicle
LEO	low Earth orbit
L/D	lift to drag ratio
m	(1) vehicle mass; (2) meters
$\dot{m}$	mass flow rate of vehicle engines
M	(1) payload ratio performance index; (2) free stream Mach number
M_{cg}	total moment about the center of mass (or center of gravity)
N	Newtons
p_i	adjoint functions in the Hamiltonian
q	dynamic pressure (N/m^2)
$q_{\max}$	maximum dynamic pressure
Q	integrated aerodynamic convective heating load
$\dot{Q}$	aerodynamic convective heating rate

r	radial distance from center of planet to vehicle
$\dot{r}$	rate of altitude change
r_n, R_N	aerobrake nose radius at stagnation point
R_E	Reynolds number
s	dimensionless arc length of trajectory
t	(1) time; (2) metric ton (1,000 kg)
$\mathbf{T}$	thrust force vector
TPS	thermal protection system
$T_{0_{\max}}$	maximum stagnation point temperature
$\mathbf{u}$	control function
v	dimensionless kinetic energy
V	velocity
$\dot{\mathbf{V}}$	time rate of change of velocity (acceleration)
W	watts
x	distance along the vehicle x axis
x_{cg}	x coordinate of the vehicle center of mass (or center of gravity)
$x_{cg_{np}}$	x coordinate of vehicle neutral point
x_R	x coordinate of the vehicle moment reference point
$\dot{x}_i$	an equation of motion
z	altitude drop, distance from the top of the atmosphere
z_{cg}	z coordinate of the vehicle center of mass (or center of gravity)
z_R	z coordinate of the vehicle moment reference point
α, ALPHA	angle of attack
β, m/C_DA	ballistic coefficient
γ	orbital flight path angle

Γ	thrust acceleration vector ($\Gamma = \mathbf{T}/m$)
δ	aerobrake rake-off angle
ΔV	delta velocity (change in velocity)
θ	(1) flow impingement angle, (2) longitude, (3) aerobrake cone angle
λ	normalized lift coefficient
μ	(1) gravitational constant; (2) a constant in the adjoint function
ρ	atmospheric density
σ	bank angle
σ_B	aerobrake mass density (mass/frontal area)
τ	normalized time of flight
φ	latitude
ψ	heading angle

TECHNICAL MEMORANDUM

APPLICATIONS OF LOW LIFT TO DRAG RATIO AEROBRAKES USING ANGLE OF ATTACK VARIATION FOR CONTROL

I. INTRODUCTION

As the utilization of outer space increases for a wide range of endeavors, from commercial ventures to human exploration of the solar system, the search for technologies and techniques which would maximize the benefits is increasing. One technological area that is receiving considerable attention is space transportation. If space transportation can be performed with maximum efficiency, the cost can be minimized. One of the primary objectives in studies of space transportation systems is to optimize vehicle performance so that payload mass or operational capabilities can be maximized.

Spacecraft aerobraking is one transportation technology that has great potential for increasing the performance capabilities of future space vehicles. Aerobraking is a technique in which a spacecraft passes through a region of a planet's atmosphere in order to alter its orbital trajectory. During the flight through the atmosphere, aerodynamic forces are used to change the spacecraft's velocity and direction of flight. The techniques and design issues associated with aerobraking and the potential applications of aerobraking have been investigated for many years. It is believed that aerobraking offers significant potential performance increases in applications related to orbital transfers and planetary orbital capture.

A. Applications of Aerobraking

During the early 1960's, the application of aerobraking to orbital transfers was first proposed. In 1962, H.S. London established that aerobraking could provide substantial performance advantages for orbital plane change maneuvers [1]. This application of aerobraking was called the synergetic plane change. This type of maneuver uses aerodynamic forces directed out of the orbital plane to turn the vehicle to a new direction. The synergetic plane change was studied extensively during the 1960's with peak activity around 1967. These studies focused on slender reentry vehicles with high lift to drag ratios (L/D) and metallic thermal protection systems (TPS) [2]. These concepts were the forerunners of the space shuttle and national aerospace plane.

The synergetic plane change maneuver is illustrated in figures 1-1 and 1-2 [3]. The synergetic plane change is accomplished with a combination of propulsive maneuvers plus the aerobraking maneuver [2]. The first maneuver is a propulsive deorbit to a shallow atmospheric entry. Some of the plane change could be performed during this maneuver if it would optimize the overall vehicle performance. Once in the atmosphere, the vehicle banks in order to rotate the lifting force out of the original orbit plane. This aerodynamic turn results in a rotation of the orbit plane [1]. This is illustrated in figure 1-2 [4]. In addition to a change in the orbit plane, the spacecraft's velocity is decreased during the aeropass. This results in a lowering of the orbit apoapsis.

In many applications of aerobraking it is necessary to perform a specified plane change and lower the orbit apoapsis to a specified altitude. The plane change that can be accomplished without causing the exit apoapsis to fall below the target altitude is often called the "free" plane change,

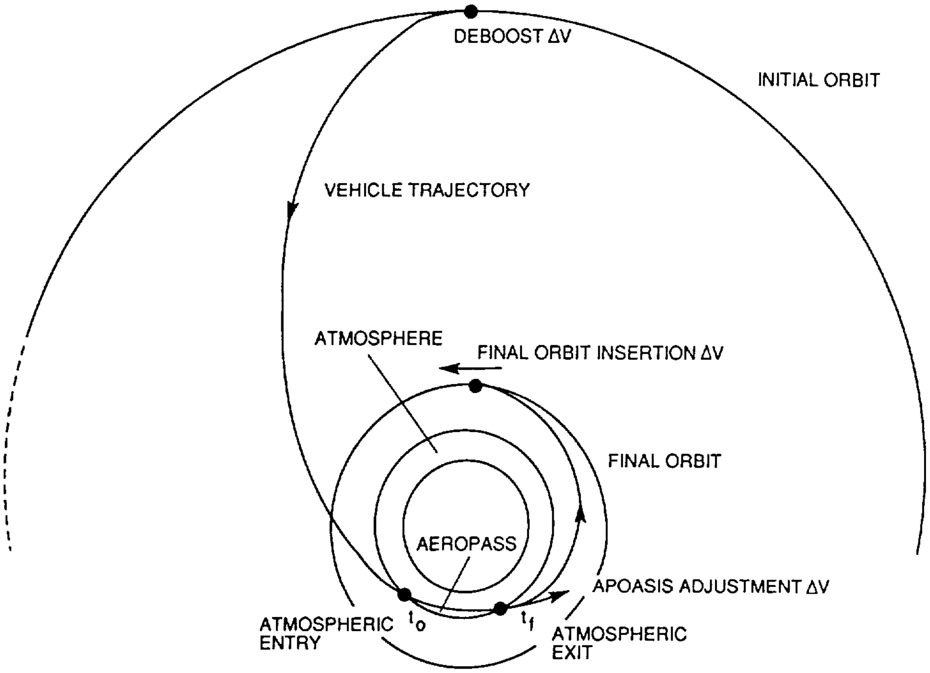

Figure 1-1. Aeroassisted orbital transfer.

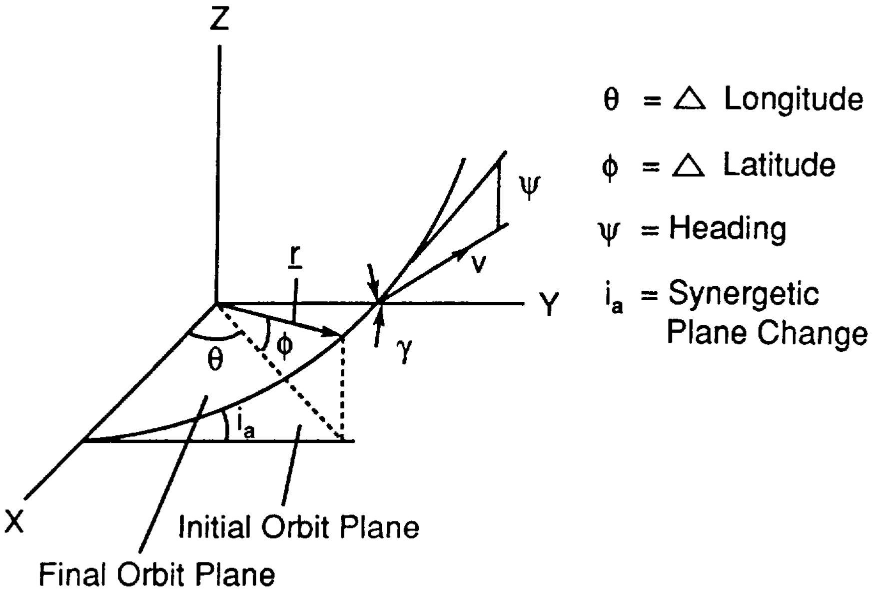

$$\cos i_a = \cos \phi_f \quad \cos \Psi_f$$

Figure 1-2. Atmospheric plane change.

since no propellant is needed [4]. If the desired plane change is greater than the achievable free plane change then a propulsive manuever could be used to perform part of the plane change or raise the orbit apoapsis back up to the target altitude. As shown in figure 1-1, this maneuver could take place either during the aeropass or immediately after atmospheric exit [1].

The final propulsive maneuver for the synergetic plane change occurs when the vehicle reaches the target apoapsis. This maneuver raises the orbit periapsis out of the atmosphere to the desired final periapsis altitude. In the synergetic plane change, propulsion is used primarily to lower and raise the orbit apsides, and aerodynamic force is used primarily to change the orbit plane [1].

Another application of aerobraking to orbital transfers makes use of aerodynamic forces for velocity changes only. In this application there is less need for lift since there is no atmospheric plane change. This type of aerobraking maneuver is called a coplanar aeroassisted orbital transfer. The purpose of the atmospheric pass is solely to dissipate energy in order to lower the apoapsis altitude [1]. This aerobrake application was studied in the 1960's and again in the early 1980's. These studies led to innovative approaches for carrying cargo to geosynchronous orbit or the Moon from a space station in low Earth orbit (LEO) using vehicle concepts with low L/D and low ballistic coefficients. They indicated that the application of aerobraking to orbital transfers could increase vehicle payload capabilities by as much as a factor of 2 over conventional all propulsive transfers [2]. The mission profile for a coplanar aeroassisted orbital transfer is similar to the synergetic plane change except there is no plane change in the atmosphere and there is no apoapse raising maneuver in the atmosphere or at atmospheric exit (fig. 1-1).

The significant potential for vehicle performance gains for aeroassisted orbital transfers in Earth orbital applications also exists for interplanetary missions. The application of aerobraking to planetary orbit capture maneuvers is an attractive option which was first studied from 1964 to 1968 and again beginning in 1979 [2].

Planetary aerocapture is illustrated in figure 1-3. A spacecraft arrives at a planet on a hyperbolic trajectory (relative to the planet) which penetrates the atmosphere. Once the vehicle enters the atmosphere, the aerodynamic drag slows the vehicle to a desired orbital velocity. Ideally, the velocity is reduced so as to achieve a target parking orbit apoapsis. When the vehicle reaches the apoapsis, a propulsive maneuver is used to raise periapsis out of the atmosphere to its final value. Just as in the coplanar aeroassisted orbital transfer, the purpose of the atmospheric pass is primarily to dissipate energy, however, there is no reason that a plane change could not also be performed. Aerocapture is essentially a transfer from a hyperbolic orbit to an elliptical orbit.

B. Topics of Discussion

There are numerous types of problems that must be addressed in the study of aerobrake applications. These problems include thermodynamics of hypersonic flight, TPS options, L/D selection and operational considerations such as control methods and guidance strategies. The solution of these problems is not always straight-forward and usually requires numerical methods. This reliance on numerical solutions which depend on many parameters makes it difficult to obtain truly general results for aerobraking analyses. The theory of optimal aeroassisted orbital transfer is considered to be in only the development stage. The goal of this development is to establish a sound basis for determining the best strategies for utilizing aerobraking and to describe the characteristics of the optimal strategies [1]. This report is an attempt to characterize the techniques and performance

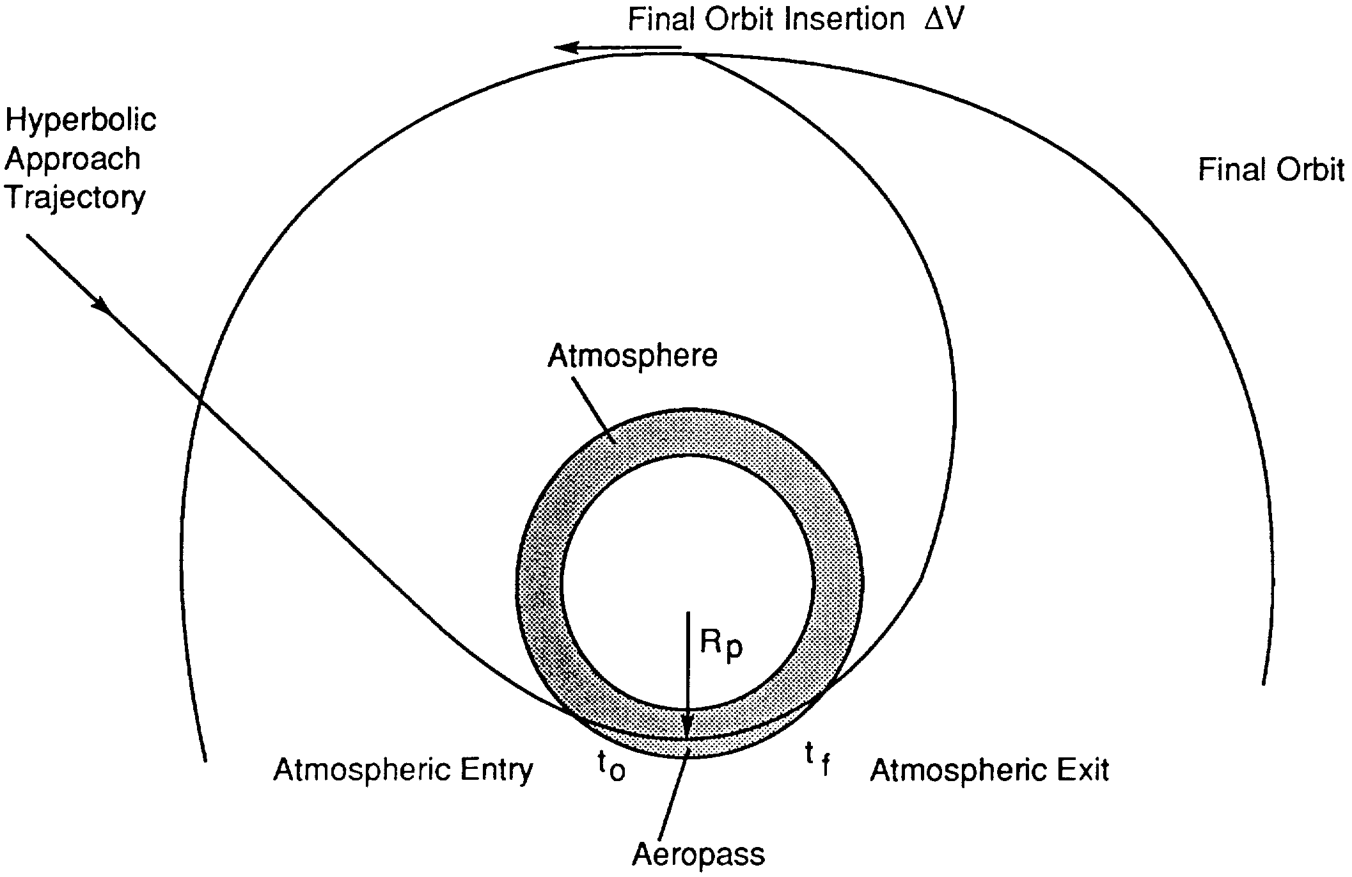

Figure 1-3. Planetary aerocapture.

of one aerobraking strategy as it could be applied to a number of applications. The strategy that will be studied will be the use of low L/D aerobrakes with angle of attack control. To better understand the reason for the selection of this strategy it is helpful to consider some of the topics which are being addressed in the current studies of aerobraking.

Two interrelated topics which are being addressed in aerobrake studies are aerobrake L/D requirements and aerobrake flight control strategies. Early studies of aerobraking focused on high L/D concepts while more recent studies have considered low L/D concepts. The high L/D aerobrakes have definite advantages in performing plane changes. However, since the lift force does not aid in slowing the vehicle down, there is no real need for high L/D for many orbital transfer applications. Low L/D aerobrakes may also offer more efficient payload packaging and better protection from the aerothermal environment than high L/D aerobrakes. If there is no atmospheric plane change, lift force is needed only for vehicle control. The amount of control required is dependent on the atmospheric conditions encountered, vehicle ballistic coefficient, and the control strategy that is employed. In this report the performance characteristics of low L/D aerobrakes for several mission applications will be determined, and some of the requirements for adequate vehicle control will be investigated.

The aerobrake control strategy is closely related to the L/D selection. Almost all aerobrake concepts that have been investigated have assumed "roll control" to guide the vehicle through the atmosphere. In this control strategy, ascent and descent in the atmosphere is controlled by rotating the lift vector about the velocity vector (bank angle). The bank angle is varied in order to change the vertical component of the lift vector and achieve a desired rate of ascent or descent. Any unwanted lateral component of lift is cancelled by alternating the bank angle from side to side. One reason that roll control has been assumed in many studies is because it was successfully used for reentry control for the Mercury, Gemini and Apollo spacecraft. It will also be used for the Aeroassisted Flight Experiment. An alternative control strategy is to vary the magnitude of the lift vector by rotating the vehicle about the pitch axis. This strategy varies lift by changing the vehicle angle of attack. It has not been studied as much as roll control but offers several potential advantages such as faster response times and elimination of lateral forces.

The second section of this report will address aerobrake design considerations. First, the aerodynamic characteristics of aerobrakes will be discussed. This discussion will begin with a description of the aerodynamic coefficients, followed by an explanation of the conditions required for static stability. The significance of L/D and ballistic coefficient will also be described. Another aspect of aerobrake design that will be discussed is aerodynamic heating. A discussion of aerobrake construction will address thermal protection system design and aerobrake mass estimation.

Section III will discuss the optimization of aerobrake trajectories. This will include two formulations that can be used, depending on the choice of a performance index. Several potential performance indices will be described and evaluated. The process used to determine a lift control function will be outlined. This control function will be used as a basis for the angle-of-attack variation for the aerobrake applications investigated in this report. To complete the discussion of the optimum control function, several vehicle control strategies which could be used will be described.

Section IV will contain the bulk of the data that was generated. This chapter will begin with a description of the computer program that was used to simulate the aerobrake trajectories and the techniques used to model the atmosphere. Data will include constant and variable angle-of-attack trajectories for several aerobrake applications. These applications include return from GEO, return from Lunar orbit, Earth aerocapture, and Mars aerocapture. The data will show the sensitivity of aerobrake trajectories and vehicle loads to angle of attack, ballistic coefficient, and atmospheric entry conditions. It will also be used to define target periapsis tolerances.

The final section of this report will summarize the characteristics of low L/D aerobrakes and the results of the trajectory and performance analyses. This section will include an overall assessment of the low L/D aerobraking strategy and summarize the conclusions that have been reached concerning aerobrake control requirements.

The study of aerobraking and its application to future space missions involves the analysis of a number of complex interrelated issues. As mentioned earlier, there is no definitive theory that can be applied to the analysis of aerobraking. Instead, current studies seek to identify the potential strategies for the application of aerobraking and the methodology to evaluate these strategies. The objective of this report is to study one possible control strategy for aerobraking and to evaluate the potential benefits for a number of applications. It is hoped that the results obtained and the analysis performed in this report will add to the overall body of knowledge from which a general theory of aerobraking optimization may be derived.

II. AEROBRAKE DESIGN CONSIDERATIONS

This section will describe some of the important design considerations that must be made in the design of aerobrakes. The most important design considerations for aerobrakes arise from their aerodynamic characteristics and the flight environments in which they operate. The unique configurations of aerobraked vehicles give them aerodynamic characteristics that are quite different from other atmospheric vehicles. These aerodynamic characteristics influence the sizing of the aerobrake and the stability of the vehicle during flight. The aerodynamic properties also determine the trajectory requirements for a particular orbital transfer and the dynamic and thermal loads experienced by the vehicle. These loads are also important factors which determine the mass of the aerobrake and the performance gain that is possible.

A. Aerodynamic Characteristics of Aerobrakes

1. Aerobrake Lift and Drag

There is a degree of uncertainty that exists in the analysis of the aerodynamic characteristics of aerobrakes since aerobraking is performed in the upper atmosphere. Figure 2-1 shows an approximate altitude profile of an aerobraking trajectory and the flow regimes that are experienced [5]. An aerobraked vehicle spends considerable time in the noncontinuum flow regimes [5]. Unfortunately, there has been little research in the aerodynamics of thermodynamics of noncontinuum flows [6]. Most of the aerodynamic data for aerobrakes has been developed using Newtonian aerodynamics for hypersonic conditions. Under these conditions, the dependence of the aerodynamic coefficients on Mach number and Reynolds number is disregarded [3], therefore, the aerodynamic coefficients depend only on angle of attack.

Many potential aerobrake shapes have been investigated. In this report, only low L/D aerobrakes will be described. Figure 2-2 shows three typical low L/D aerobrakes. The spherical aerobrake is based on the heat shield of the Apollo command module. The use of this shape allows the application of past research and flight data to aerobraking analyses. The sphere-cone configuration consists of a circular cone with a spherical section at the tip. The raked-off elliptical cone is defined as a cone with an elliptical cross section and a spherical tip which is "raked-off" at an oblique angle as shown in figure 2-3 [7]. This shape provides a higher L/D at low angles of attack. The configuration shown will be used for the planned aeroassist flight experiment (AFE).

Figure 2-4 shows the lift and drag coefficients for the three aerobrake shapes [8]. The aerodynamic coefficients for the spherical (Apollo), sphere-cone, and AFE configurations were calculated using the Mark IV Supersonic-Hypersonic Arbitrary Body Program [9]. This program uses the modified Newtonian pressure method to calculate pressure coefficients for each element of surface area on the aerobrake. The components of the pressure coefficients are then used to calculate the aerodynamic coefficients. The wind tunnel data shown in figure 2-4 was obtained using a 4-in diameter aerobrake model at a Mach number of 10.2 [10]. The AFE has been designed to fly at a specific angle of attack of 17° which puts the stagnation point at the center of the spherical tip. The aerodynamic data at other angles of attack are shown for illustrative purposes only.

The curves shown in figure 2-4 give an indication of the unique aerodynamic characteristics of aerobrakes. The drag decreases as the magnitude of the angle of attack increases. This is opposite of most aerodynamic vehicles. Another characteristic that is opposite of most aerodynamic vehicles is that aerobrakes experience positive lift (lift up) at negative angles of attack and negative lift (lift down) at positive angles of attack. This characteristic can be used to differentiate between aerobrakes and aerobodies (of lifting bodies). Vehicles having positive lift at positive angles of attack can be defined as aerobodies [11]. For this definition to hold true for nonsymmetrical aerobrakes such as the AFE, a further stipulation must be made that the bank angle is zero. If the AFE is flown

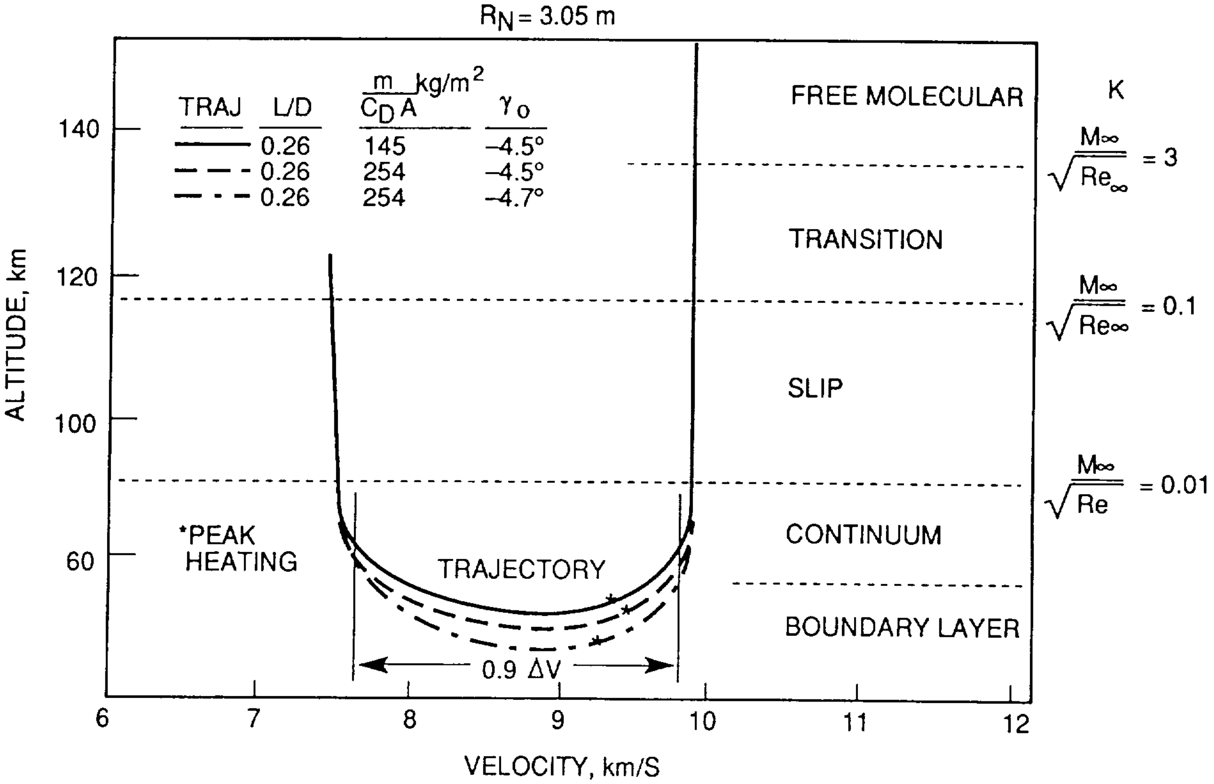

Figure 2-1. Aerobrake trajectories and flow regimes [5].

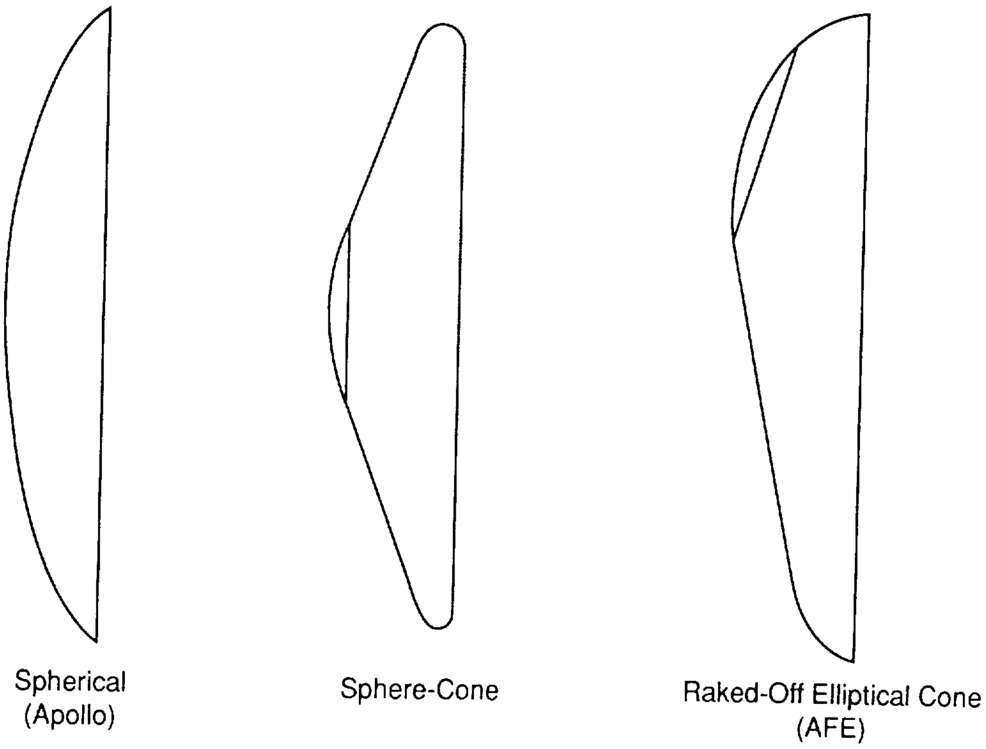

Figure 2-2. Low L/D aerobrake shapes.

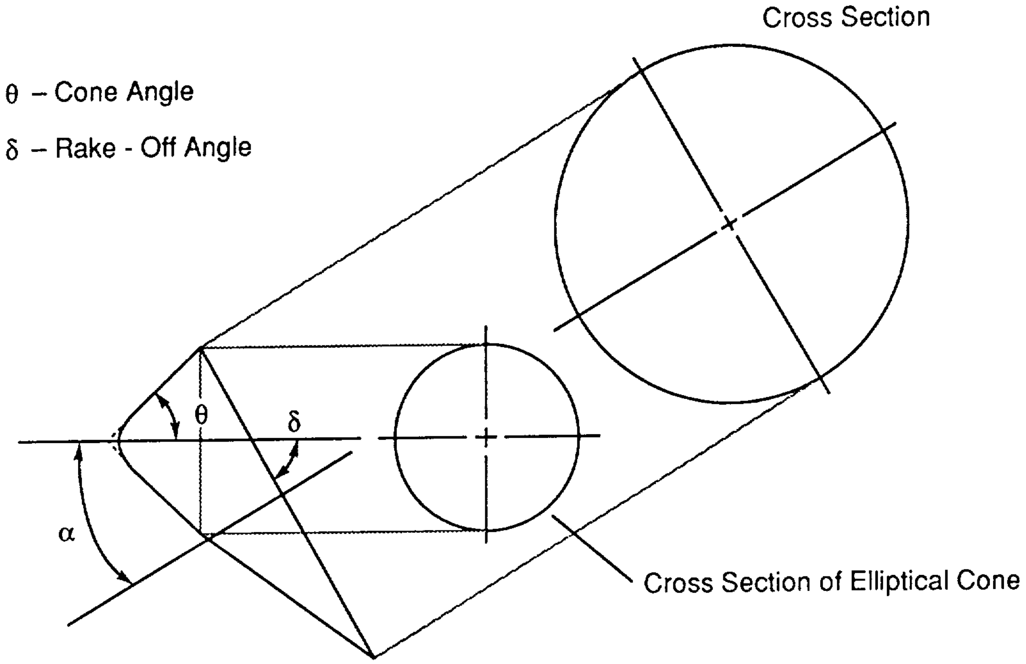

Figure 2-3. Raked-off elliptical cone configuration.

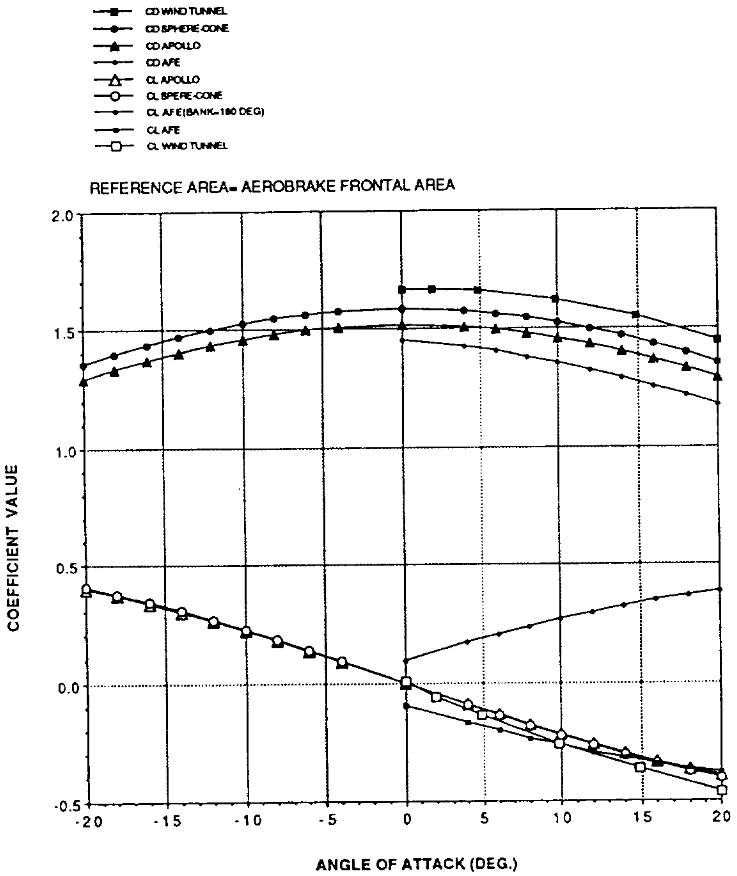

Figure 2-4. L/D coefficients for aerobrakes.

inverted (bank angle = 180°) then the lift is positive at positive angles of attack. The advantage of this will be explained later. It should be noted that there is no standard definition of aerobrake geometry or coordinate systems so care must be taken when referring to angles of attack and bank angles.

The direction of lift is an important factor in aerobraking because it influences the vertical movement of the vehicle in the atmosphere. Lift should work in harmony with drag in controlling the trajectory of the vehicle. If more drag is needed, the lift force should pull the vehicle down (deeper) in the atmosphere. If less drag is needed, the lift force should move the vehicle upward in the atmosphere [12]. Referring back to figure 2-4, it can be seen that this coordination of lift and drag exists at negative angles of attack for symmetrical aerobrakes (spherical, sphere-cone) and at a bank angle of 180° for the AFE (raked-off cone). Even though the most efficient coordination of lift and drag is achieved when lift is directed upward, it will be shown later that when a trajectory is optimized to minimize certain vehicle loads it is sometimes necessary to fly the aerobrake with lift directed downward.

2. Aerobrake Static Stability

One of the most important design considerations for aerobraked vehicles is the aerodynamic stability of the vehicle. The vehicle must be designed to maintain the proper flight attitudes in order to achieve the desired trajectory. It is beyond the scope of this report to investigate the dynamic stability of aerobraked vehicles, therefore, the discussion of aerodynamic stability will be limited to the necessary conditions for vehicle equilibrium (trim) and longitudinal static stability. These are preconditions for dynamic stability.

In the discussion of vehicle trim, it is necessary to define a vehicle coordinate system. This coordinate system is shown in figure 2-5. For the present discussion only, the spherical (Apollo) aerobrake shape will be considered. The x axis is defined by the central axis of the vehicle. The z axis is defined by the longitudinal plane of the vehicle. The origin is defined to be the center of the front of the aerobrake. In defining the aerodynamic forces and moments, the reference area (A) is the cross-sectional area of the aerobrake, the reference length (d) is the aerobrake diameter, and the moment reference point is the origin ($x = 0$, $z = 0$). It should be noted that the location of the moment reference point is arbitary, but it is tied to a particular set of aerodynamic coefficients. The aerodynamic coefficients for a spherical aerobrake are listed in table 2-1 [8].

When the vehicle attitude is maintained in a particular orientation, the aerodynamic forces and moments are in equilibrium, and the vehicle is in a "trimmed" configuration. The necessary condition for trim is that the sum of the moments about the vehicle center of gravity (cg) is zero. If the vehicle cg is located at the arbitary position shown in figure 2-5, the moments can be summed as follows:

$$M_{cg} = C_m\, q\, dA + C_N\, (X_{cg} - X_R) q^A - C_A (Z_{cg} - Z_R) q^A \ , \qquad (2\text{-}1)$$

the moment coefficient about the cg can be defined as:

$$C_{m_{cg}} = \frac{M_{cg}}{q\, d\, A} \ . \qquad (2\text{-}2)$$

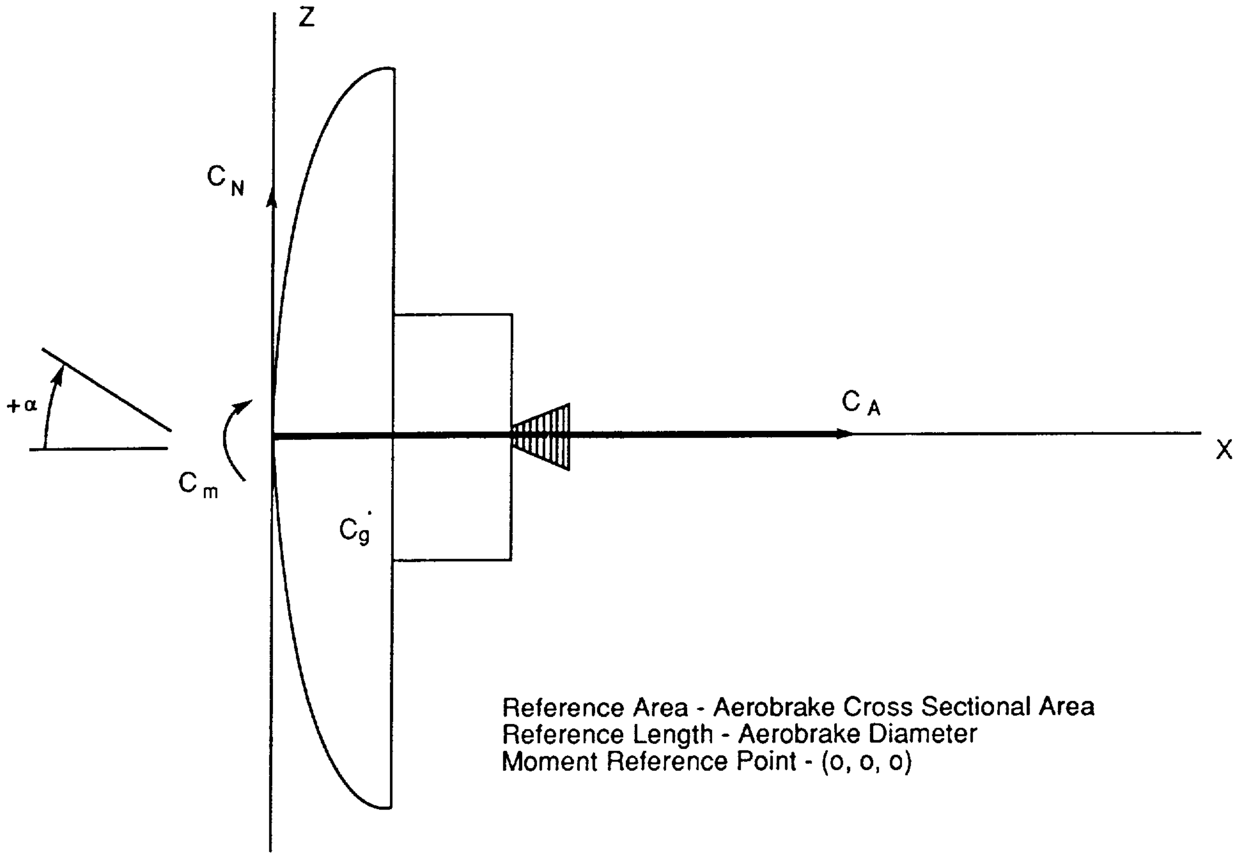

Reference Area - Aerobrake Cross Sectional Area
Reference Length - Aerobrake Diameter
Moment Reference Point - (o, o, o)

Figure 2-5. Aerobrake coordinate system.

Table 2-1. Aerodynamic coefficients for a spherical aerobrake.

REFERENCE AREA = AEROBRAKE FRONTAL AREA
REFERENCE LENGTH = AEROBRAKE DIAMETER
MOMENT REFERENCE POINT = FRONT CENTER OF AEROBRAKE (X=Y=Z=0.0)

ALPHA (DEG.)	L/D	CL	CD	CA	CN	CM
0	0.0	0.0	1.5167	1.5167	0.0	0.0
4	-0.0602	-0.0908	1.5072	1.5098	0.0146	-0.0135
6	-0.0905	-0.1353	1.4953	1.5013	0.0218	-0.0202
8	-0.1208	-0.1787	1.4789	1.4894	0.0289	-0.0268
10	-0.1514	-0.2207	1.4580	1.4741	0.0359	-0.0333
12	-0.1821	-0.2609	1.4328	1.4557	0.0427	-0.0396
14	-0.2131	-0.2990	1.4034	1.4340	0.0494	-0.0457
16	-0.2443	-0.3347	1.3702	1.4094	0.0559	-0.0516
18	-0.2759	-0.3678	1.3334	1.3818	0.0622	-0.0572
20	-0.3078	-0.3980	1.2933	1.3514	0.0683	-0.0626
22	-0.3400	-0.4251	1.2501	1.3183	0.0742	-0.0677
24	-0.3727	-0.4489	1.2043	1.2828	0.0798	-0.0724
26	-0.4058	-0.4693	1.1562	1.2449	0.0851	-0.0768
28	-0.4394	-0.4860	1.1062	1.2049	0.0902	-0.0809
30	-0.4733	-0.4992	1.0546	1.1629	0.0950	-0.0846

Using this definition, equation (2-1) can be rewritten in the following form:

$$C_{m_{cg}} = C_m + C_N\frac{(X_{cg}-X_R)}{d} - C_A\frac{(Z_{cg}-Z_R)}{d}\,. \tag{2-3}$$

The condition for trim is:

$$M_{cg} = C_{m_{cg}} = 0\,. \tag{2-4}$$

In deriving equation (2-3), an arbitrary cg location was used. The combinations of x_{cg} and z_{cg} that satisfy equation (2-3) define a line in the longitudinal plane called the trim line. This line can be defined by setting equation (2-3) equal to zero then solving for z_{cg} (normalized to z_{cg}/d)

$$\frac{Z_{cg}}{d} = \underbrace{\frac{C_m}{C_A}\frac{C_N}{C_A}\frac{X_R}{d} + \frac{Z_R}{d}}_{z\text{ intercept}} + \underbrace{\frac{C_N}{D_A}\frac{X_{cg}}{d}}_{\text{slope}}\,. \tag{2-5}$$

As long as the vehicle cg falls on the trim line, the vehicle will maintain a constant attitude. Since C_m, C_N, and C_A are functions of angle of attack, the trim line is also a function of angle of attack. Figure 2-6 shows the trim lines at various angles of attack for a spherical aerobrake [13].

Placing the cg on the desired trim line insures that the vehicle will be in equilibrium, but it does not guarantee that it will be in a stable equilibrium. Longitudinal static stability depends on the change in pitching moment when a disturbance causes a slight change in the angle of attack. The necessary condition for longitudinal static stability is defined as:

$$\frac{\partial C_{m_{cg}}}{\partial a} = C_{m_\alpha} < 0\,. \tag{2-6}$$

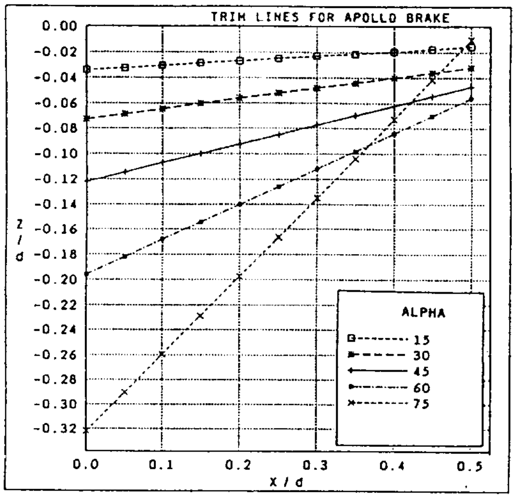

Figure 2-6. Trim lines for a spherical aerobrake.

Figure 2-7 shows an example of an aerobrake trimmed at an angle of attack of 15°. The plot of pitching moment coefficient versus angle of attack shows that C_{m_α} is negative and $C_{m_{cg}} = 0$ at $\alpha = 15°$. These conditions indicate that the vehicle possesses longitudinal static stability. For any disturbance causing an increase in angle of attack (clockwise rotation), the aerodynamic forces will cause an increase in $C_{m_{cg}}$ in the negative direction (counter-clockwise rotation). The opposite is true if a disturbance causes a decrease in angle of attack [12].

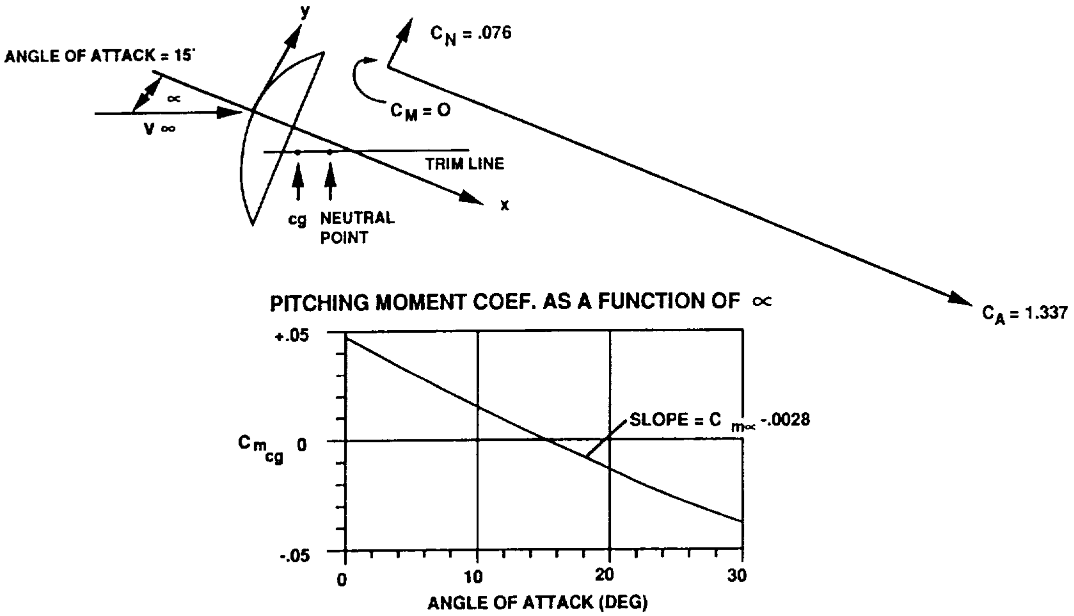

CONDITION FOR STATIC STABILITY: $C_{m_\alpha} < 0$

FOR ANY DISTURBANCE CAUSING AN INCREASE IN α (CLOCKWISE ROTATION) THE AERODYNAMIC FORCES WILL RESULT IN AN INCREASE IN C_m IN THE NEGATIVE DIRECTION (COUNTER-CLOCKWISE ROTATION)

Figure 2-7. Longitudinal static stability during aerobraking.

The value of C_{m_α} depends on the aerodynamic coefficients and the cg location. The relationship can be found by differentiating equation (2-3) with respect to angle of attack then using equation (2-5) to eliminate z_{cg} from the result.

$$C_{m_\alpha} = \frac{\partial C_m}{\partial \alpha} - \frac{\partial C_A}{\partial \alpha}\frac{C_m}{C_A} + \left(\frac{\partial C_N}{\partial \alpha} - \frac{\partial C_A}{\partial \alpha}\frac{C_N}{C_A}\right)\frac{(x_{cg} - x_R)}{d} \, . \qquad (2\text{-}7)$$

For a given trim condition (angle of attack), the aerodynamic coefficients are constant so the stability depends on the cg location. The cg location at which $C_{m_\alpha} = 0$ is called the neutral point. The x coordinate of this point can be found by setting equation (2-8) equal to zero and solving for x_{cg}:

$$X_{cg_{np}} = \frac{\left(\frac{C_m}{C_A} - \frac{\partial C_m}{\partial C_A}\right) d}{\left(\frac{\partial C_N}{\partial C_A} - \frac{C_N}{C_A}\right)} + X_R \, . \qquad (2\text{-}8)$$

For the example in figure 2-7, at a trim angle of attack of 15°, the neutral point is at $x = 0.7284d$. If the x_{cg} is greater than x_{np}, then C_{m_α} will be positive and the vehicle will be unstable. Obviously it is desirable to have the cg as far in front of the neutral point as possible. Equations (2-7) and (2-8) show that the stability is also a function of aerobrake diameter. As the diameter increases, C_{m_α} becomes negative, and the x_{np} increases so the vehicle becomes more stable. This indicates that stability considerations should be included in the process of sizing an aerobrake.

3. Flow Impingement Behind Aerobrakes

One of the more basic considerations in sizing an aerobrake is the flow condition behind the aerobrake. As the flow passes the edge of the aerobrake, it turns inward toward the center of the vehicle. The aerobrake must be sized such that this flow does not impinge on the payload behind the aerobrake. Figure 2-8 shows the impingement angle behind a spherical aerobrake as a function of angle of attack [14]. The data was extracted from reference 20. The most critical impingement occurs at the most forward edge of the aerobrake. The flow impingement angle is equal to the sum of the magnitude of the angle of attack and the flow turning angle.

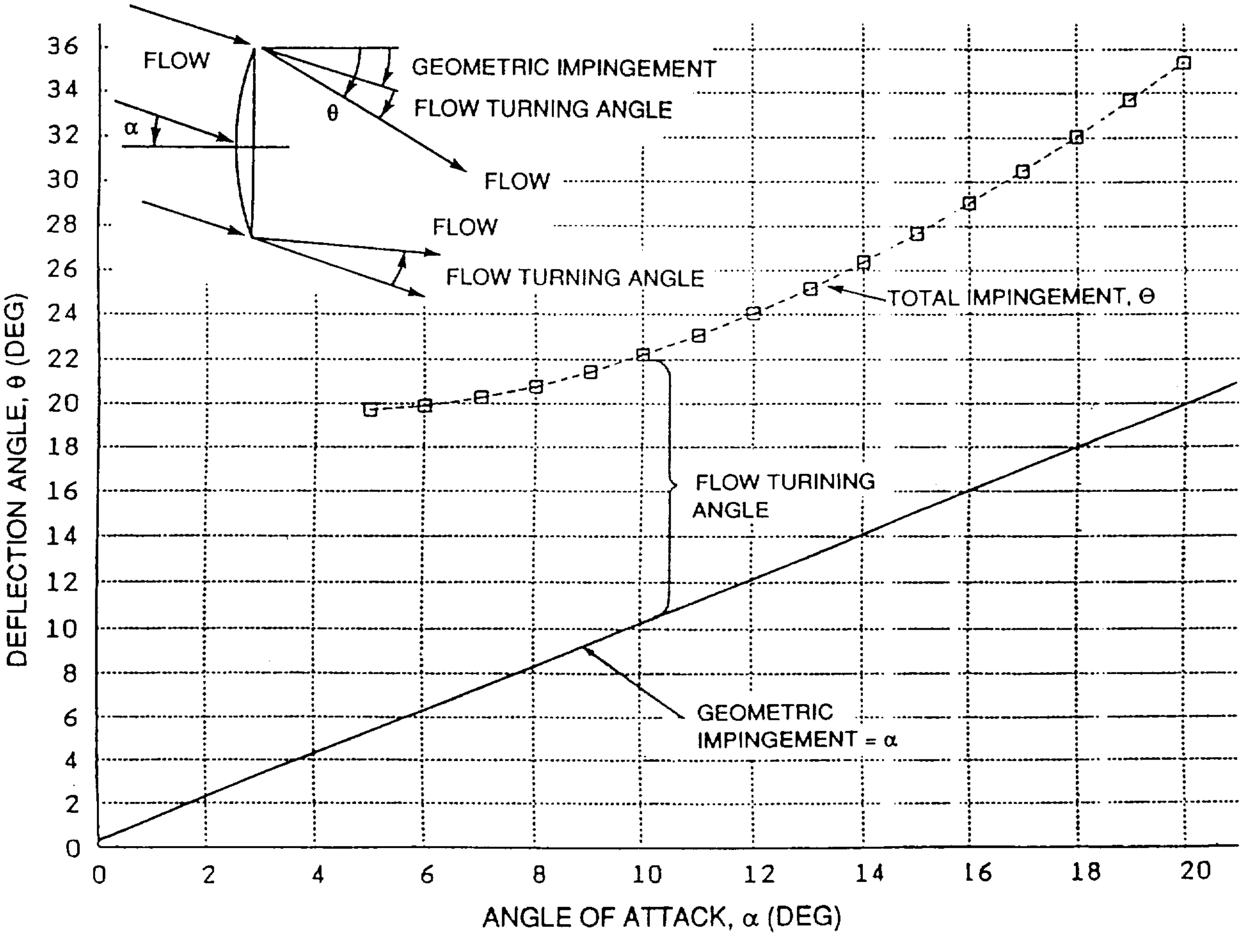

Figure 2-8. Flow impingement angle for an aerobrake.

4. Lift to Drag Ratio

It was indicated that the combined effects of lift and drag are important in controlling an aerobrake trajectory. This relationship has led to the use of the L/D as an important parameter in characterizing aerobrakes. The L/D, along with the ballistic coefficient, determines the aerodynamic control capability and influences the heating and acceleration loads on the vehicle [1]. Figure 2-9 shows the L/D and ballistic coefficients for typical aerospace vehicles [2]. L/D's greater than 1.5 require blended wing-body configurations. Most aerobrakes fall into the low- to mid-L/D range. The primary factor in choosing an L/D for an aerobrake is the type of mission to be flown. High-L/D aerobrakes ($L/D > 2.0$) have significantly greater plane change capability in the atmosphere than low L/D aerobrakes ($L/D < 0.8$). Unfortunately, the benefit of using a high L/D aerobrake to perform a synergetic plane change is counteracted by an increase in structural mass. In comparing high L/D aerobrakes to low L/D aerobrakes for missions returning from GEO, Talay et al. [2] found very little difference in payload capability, but the high L/D aerobrake had significantly higher aerodynamic heating and structural mass. These results were verified by Mease and Vinh [15]. Table 2-2 shows the relationship between L/D and several trajectory parameters for an aerobraked transfer from GEO to LEO. Based on these results, it appears that high L/D offers little or no advantage for this mission [2].

The previous conclusion could be interpreted from a different perspective as pointing out a disadvantage of the synergetic plane change rather than high L/D. The reason that the thermal and structural requirements are greater for the high L/D configuration is that the vehicle trajectory went deeper into the atmosphere to maximize the synergetic plane change. In aerobrake applications with no synergetic plane change, it has been found that increasing the L/D results in a decreased penetration into the atmosphere (if lift is downward) which decreases the vehicle loads [14]. Unfortunately in these cases, the mass penalty associated with the complex aerodynamic shapes can make high L/D configurations unattractive. It appears that high L/D aerobrakes do not provide any significant advantages for missions to high Earth orbit such as GEO or for missions that do not require synergetic plane changes such as return from lunar orbit or planetary orbital capture. This is one of the primary reasons for considering only low L/D aerobrakes in this report.

Figure 2-10 shows the L/D as a function of angle of attack for low L/D aerobrakes [8]. The symmetrical aerobrakes have very similar L/D characteristics while the raked-off cone (AFE) L/D is slightly higher in magnitude. Based on the analysis performed by Mayo, Lamb, and Romere [7], the L/D for low L/D aerobrakes at low angles of attack can be approximated by the following relationship:

$$\frac{L}{D} \approx \sin(\alpha) \; . \tag{2-9}$$

This formula is useful in making a first guess for the angle of attack required to achieve a desired L/D.

The choice of an L/D for an aerobrake application is complicated by the uncertainty in the aerodynamics of the vehicle in the upper atmosphere. G.D. Walberg has indicated that the L/D decreases at high altitudes due to viscous effects [2]. This phenomenon has been ignored in most aerobrake studies [1]. Maslin was the first to analyze aerobrake trajectories with this effect included. He developed an approximation for the L/D degradation at high altitudes [2]. Figure 2-11 shows the variation of maximum L/D with altitude for the space shuttle [2]. The solid curve represents wind tunnel and flight data, and the hatched band represents Maslan's approximation.

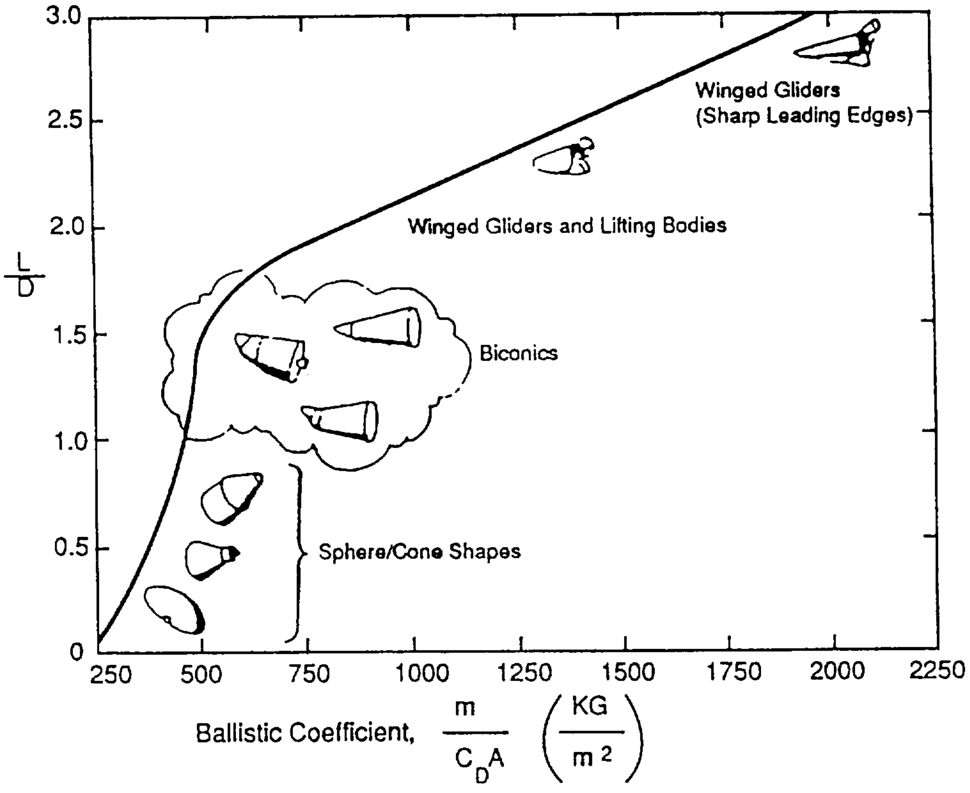

Figure 2-9. L/D's and ballistic coefficient values for typical lifting bodies [2].

Table 2-2. Aerobrake parameters for a GEO to LEO transfer.

	LIFT TO DRAG RATIO		
	LOW	MODERATE	HIGH
MAXIMUM L/D	0.845	1.5	2.9
MINIMUM ALTITUDE (KM)	58.8	58.2	51.5
MAX. DYNAMIC PRESSURE (N/M**2) X 0.001	15.9	18.6	44.2
MAX. CONVECTIVE HEATING RATE (W/CM**2)	193.1	222.8	361.4
MAX. ACCELERATION (EARTH g'S)	3.6	2.7	1.8

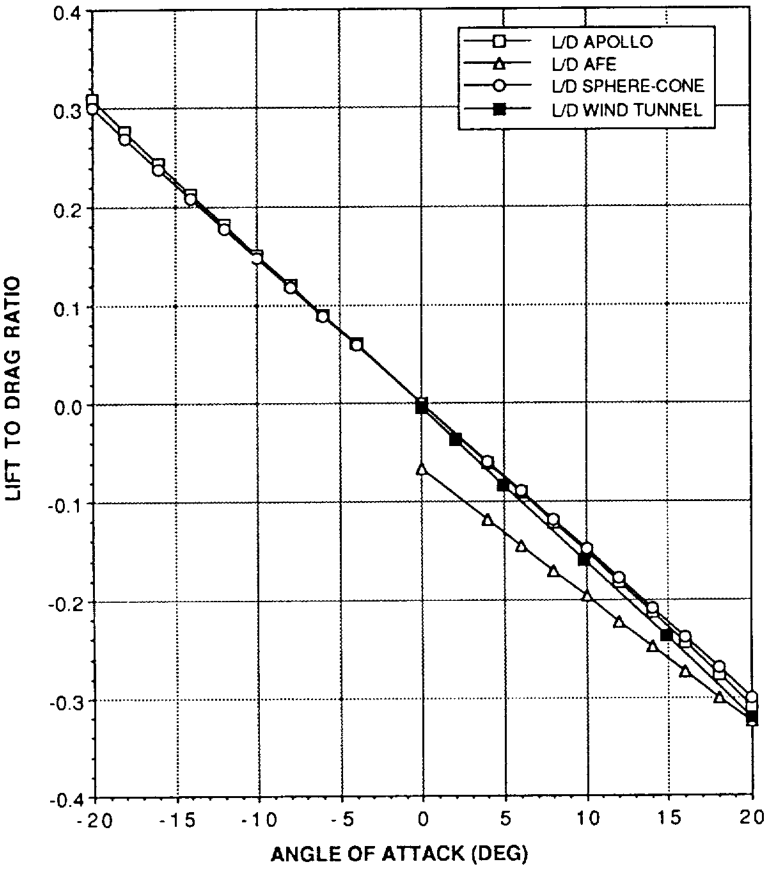

Figure 2-10. L/D's for aerobrakes.

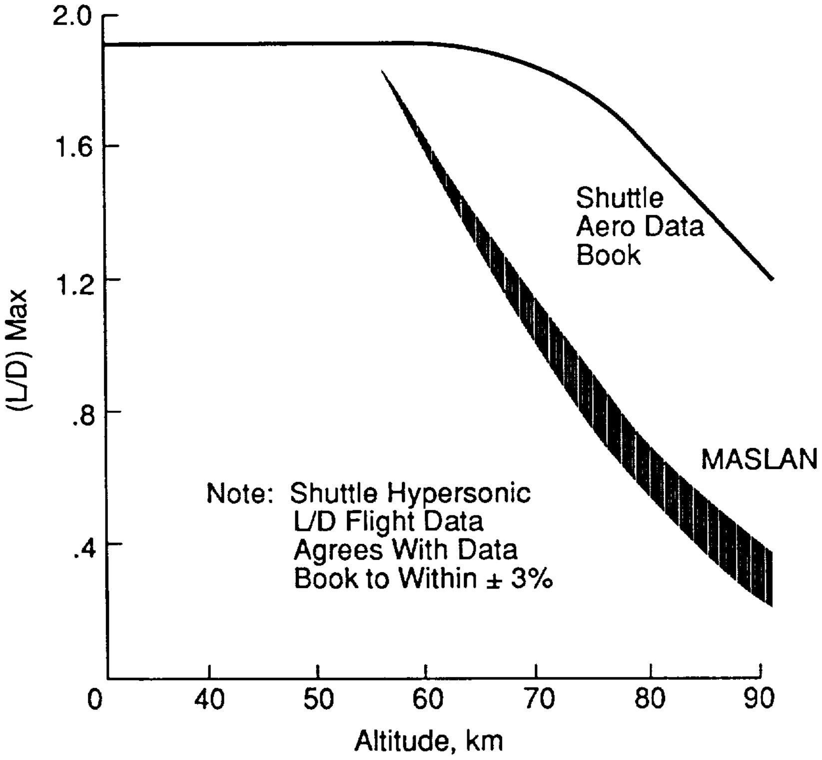

Figure 2-11. Degradation of maxim L/D at high altitude [2].

While it appears that Maslin's approximations underpredict the L/D at high altitudes, the shuttle data shows that there is still significant degradation of the L/D above 70-km altitude.

5. Ballistic Coefficient

The ballistic coefficient is a very important design parameter for aerobrakes. As mentioned earlier, it is closely related to the L/D in its influence on the vehicle and trajectory. The ballistic coefficient determines the structural and heating loads that are experienced during the aeropass as well as several other trajectory parameters. One of the objectives of this report is to investigate the relationship between the ballistic coefficient and the aerobrake control requirements. This relationship will be described in subsequent sections.

The ballistic coefficient is defined by the following equation:

$$\beta = \frac{m}{C_D A}. \tag{2-10}$$

It provides a measure of the capability of an aerodynamic drag force to change the kinetic energy (velocity) of the vehicle. The mass is an indicator of the vehicle's inertia, and the product of the drag coefficient and aerobrake cross-sectional area is an indicator of the drag force that can be generated. A high ballistic coefficient indicates that a larger drag force is required to achieve a given velocity change. For a given aerobrake ballistic coefficient, an increase in drag is achieved by flying the vehicle deeper in the atmosphere to achieve a greater dynamic pressure. This increases the vehicle structural and thermal loads [14].

Figure 2-9 shows that for most aerobraked vehicles the ballistic coefficients will not exceed 500 kg/m^2. Figure 2-12 shows the sensitivity of the ballistic coefficient to vehicle mass and aerobrake diameter. It shows that there are extremes to be avoided. There is a point at which increasing the diameter of the aerobrake has little benefit in lowering the ballistic coefficient due to the increase in aerobrake mass. There is also a point at which decreasing the diameter of the aerobrake (to reduce the mass) will result in a greatly increased ballistic coefficient which could result in an increase in structural and thermal loads..

6. Aerodynamic Heating

Aerodynamic heating is probably the most critical design factor that must be considered in aerobrake design. The thermal loads that are anticipated in most aerobrake applications require insulation materials which are at the limit of current technology. The heating loads influence the aerobrake material selection and sizing (diameter) and also constrain the atmospheric trajectories that can be flown. Unfortunately, the understanding of the thermal environments that will be encountered by aerobraked vehicles is not complete. There is evidence that chemical and thermodynamic nonequilibrium caused by the dissociation and recombination of air molecules will significantly influence the convective and radiative aerodynamic heating [2]. One of the primary objectives of the planned AFE is to determine the extent of nonequilibrium effects. There are two principle phenomena that may be present. They each have a different effect on the heating conditions.

Chemical nonequilibrium is the result of the catalysis of the aerobrake surface. The high temperatures near the aerobrake cause the air molecules to dissociate. A certain fraction of the atoms that strike the aerobrake surface would recombine due to catalysis effects. When they recombine, the energy of dissociation is left on the wall of the aerobrake and contributes to the heat flux [5]. There is evidence that finite wall catalysis could reduce the convective heating rate by up to one half of their equilibrium values [2]. Figure 2-13 [5] shows the effect of wall catalysis on the peak temperature for an aerobraked return from GEO.

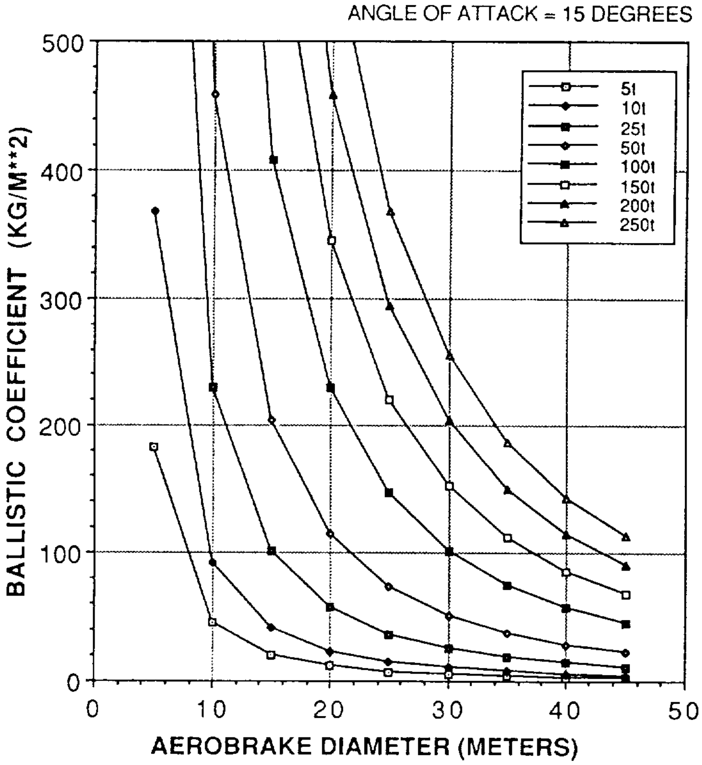

Figure 2-12. Sensitivity of ballistic coefficient to vehicle mass and aerobrake diameter.

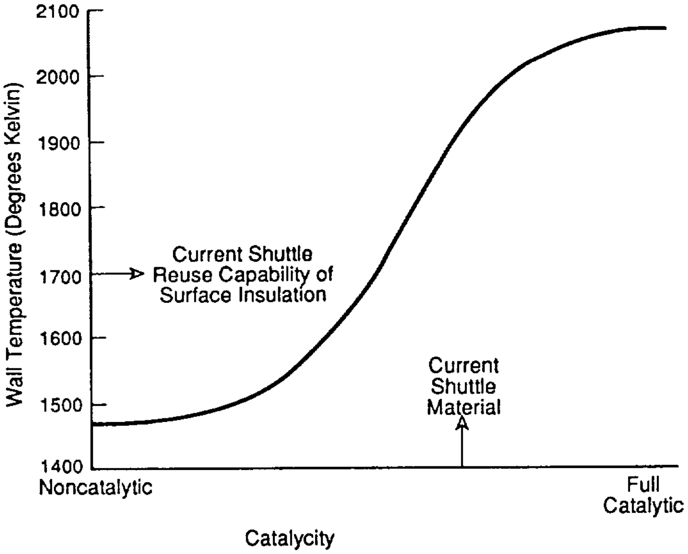

Figure 2-13. Representative peak temperature dependence on catalysis for GEO to LEO aerobraked transfers [5].

Another phenomenon that may exist in the aerothermal environment of an aerobrake is nonequilibrium shock layer radiation [2]. There is considerable disagreement on the extent of radiative heating and its effect. If nonequilibrium radiation occurs, it could increase the peak heating rate by 10 percent [5] to 100 percent [2]. The existence of nonequilibrium radiative heating may be the single most important question that exists concerning aeroassisted orbital transfers [2]. This question can only be answered through an actual flight test [2].

The potential effects of nonequilibrium conditions on the aerodynamic heating are important considerations in aerobrake design. Since aerobrakes will have velocities that are greater than reentry vehicles, catalysis effects will be even more evident. In the Earth's atmosphere there will be substantial nitrogen dissociation, so it would be beneficial to choose insulation materials with low nitrogen recombination rates [16]. Mars aerobrakes may require different materials to minimize the recombination of Mars atmospheric constituents (mostly carbon dioxide). The effects of catalysis and convective heating are reduced at higher altitudes due to the decrease in density. This indicates that it is desirable to use high-drag aerobrake configurations at very high altitudes [16].

In performing aerobrake trajectory analysis, it is impossible to accurately predict the aerodynamic heating environment without the use of Navier-Stokes solutions, viscous shock-layer solutions, and experimental verification [5]. To avoid these complications, the aerodynamic heating is characterized by an indicator that is much easier to calculate. The most common heating indicator is the stagnation point convective heating rate, defined by the following equation [1]:

$$\dot{Q} = c\,\rho^{0.5}\,V^{3.08}\ \mathrm{W/cm^2}, \tag{2-11}$$

where

$c = 1.83 \times 10^{-8}\, r_n^{-0.5}\,(1 - g_w)$

r_n = nose radius (m)

g_w = wall enthalpy/total enthalpy

ρ = density (kg/m^3)

V = velocity (m/s).

The value of the stagnation point heating rate is often used to determine the type and thickness of thermal insulation material for an aerobrake, even though wind tunnel tests have shown that the maximum heating actually can occur at the edge of the aerobrake [17].

For a given aeroassisted orbital transfer, the depth of penetration into the atmosphere depends on the L/D and the ballistic coefficient. Since the depth of penetration also influences the heating rate, there is a relationship between L/D, ballistic coefficient, and heating rate. This relationship for a GEO to LEO transfer is illustrated in figure 2-14 [5]. Note that in this graph the heating indicator is the product of the stagnation point heating rate and the nose radius. These data indicate that the heating rate is more sensitive to the ballistic coefficient than the L/D [5].

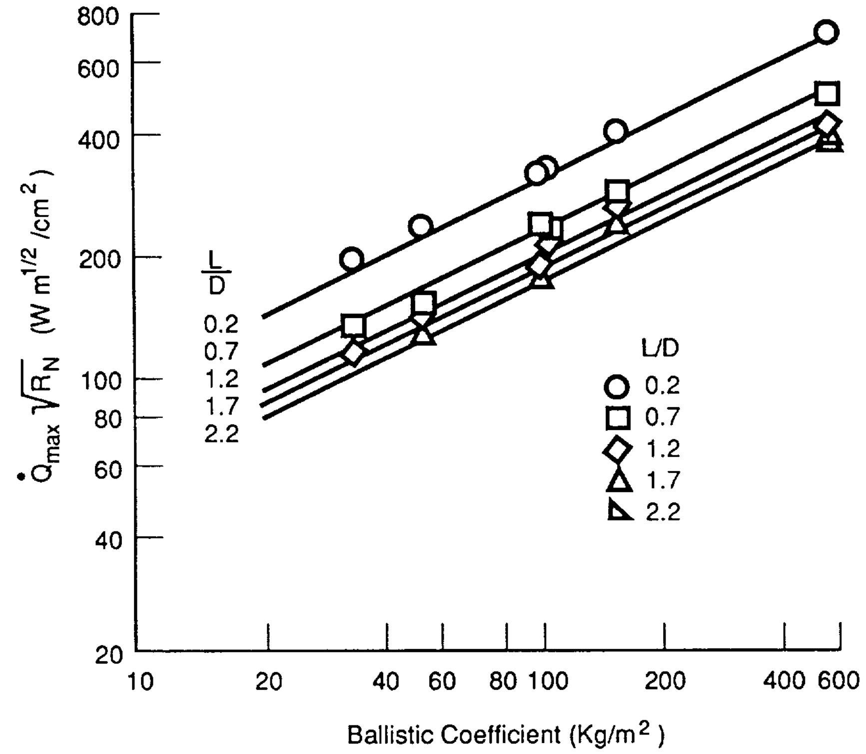

Figure 2-14. Correlation of peak reference heat flux with ballistic coefficient and L/D for GEO to LEO trajectories [5].

B. Aerobrake Construction

1. Aerobrake Thermal Protection

The aerodynamic heating environments that are anticipated for most aerobraking applications will require unique insulation materials to protect the structure of the aerobrake and the payload. Currently, there are two general types of thermal protection system materials that may be applicable for aerobrakes.

One type of TPS is the metallic standoff system. This system is composed of a metallic outer surface and a layer of insulation between the outer surface and the aerobrake structure. The metallic surface radiates some heat away, the rest of the heat is absorbed by the layer of insulation [1]. The type of metal used for the outer surface depends on the peak temperature that is experienced during the aeropass [18]. Figure 2-15 [18] shows the temperature ranges and weight per unit area for several metals. The thickness of the insulation layer depends on the accumulated (or integrated) heat load, Q [18], defined by the following equation [1]:

$$Q = \int_{t_0}^{t_f} \dot{Q}\, dt. \tag{2-12}$$

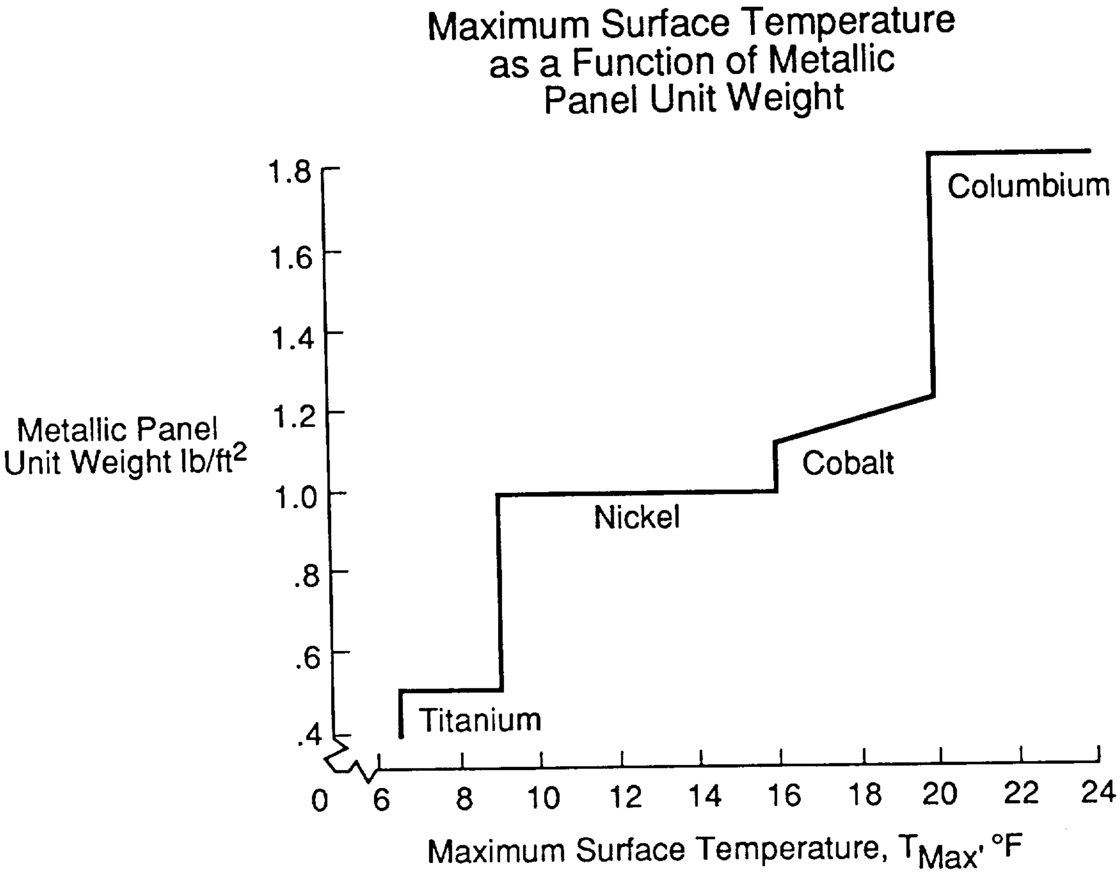

Figure 2-15. Metallic TPS weight per square foot versus maximum surface temperature [18].

To minimize the mass of the metallic standoff thermal protection system, it is desirable to have both a low $\dot{Q}_{max}$ and a low Q. Since these quantities have different sensitivities to the trajectory, a tradeoff between $\dot{Q}_{max}$ and Q is necessary. Garcia and Fowler found that the total TPS mass is reduced by minimizing $\dot{Q}_{max}$. The savings gained by reducing the mass of the metallic outer surface more than compensates for the increased insulation mass required due to the increased Q [18]. The sensitivity of $\dot{Q}_{max}$ and Q to the trajectory, specifically the depth of penetration into the atmosphere, will be discussed further in subsequent sections.

A second type of TPS is called reusable surface insulation (RSI). This type of TPS usually consists of ceramic tiles which are coated with a reaction cured glass. The tiles are attached to the vehicle structure with a felt strain isolation pad to allow deformation of the skin without damage to the tile [14]. This is the type of TPS used on most of the space shuttle. The thickness of RSI for an aerobrake depends on the integrated heat load [18] and the temperature limitations of the material [14]. Current RSI materials can withstand a maximum temperature of 1,645 K (2,500 °F) [18]. Future materials may have a limit as high as 2,500 K (4,100 °F) [6], which could significantly reduce the thermal protection system mass.

Garcia and Fowler investigated the application of metallic standoff and RSI TPS's for the space shuttle [18]. They found that for temperatures less than 1,420 K (2,100 °F) the metallic standoff system had a lower mass than RSI. This is indicated in figure 2-16 [18]. Unfortunately, most aerobrake applications would exceed this temperature, so reusable surface insulation will be required. One possible method for decreasing the thermal load on an aerobrake is to decrease the ballistic coefficient of the vehicle by increasing the diameter of the aerobrake [16]. Figure 2-17 [6] shows that if ballistic coefficient is reduced to extremely low values, a metallic TPS could be used.

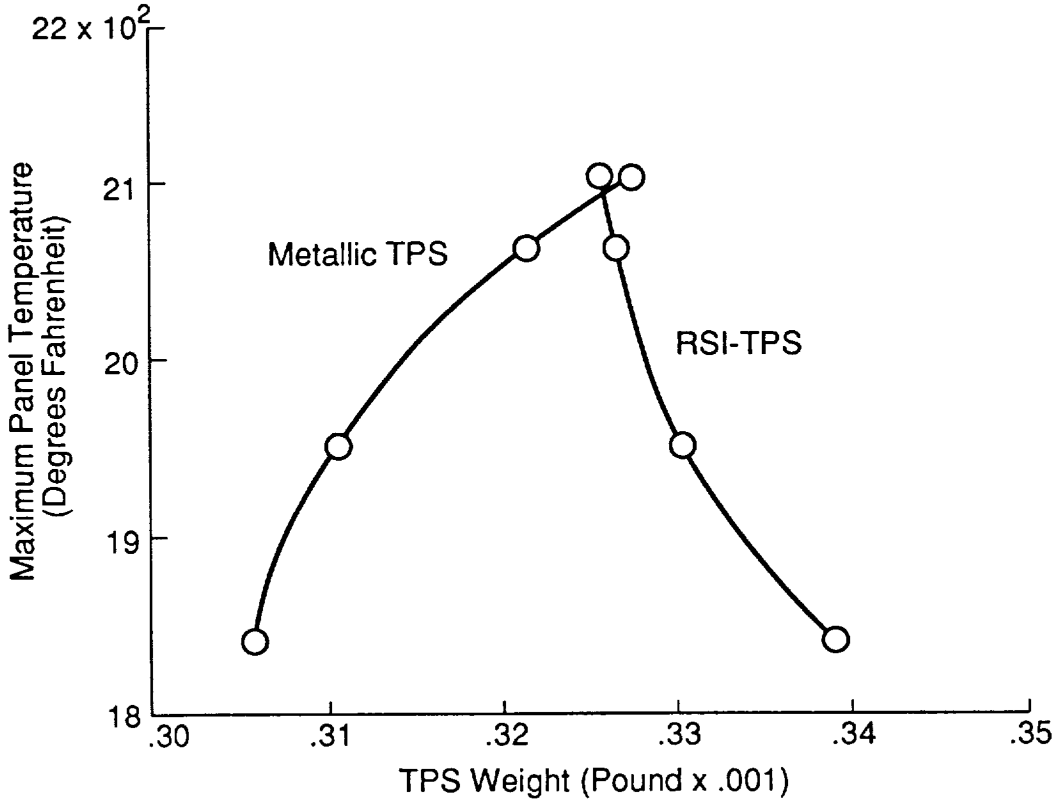

Figure 2-16. TPS weights for space shuttle entry [18].

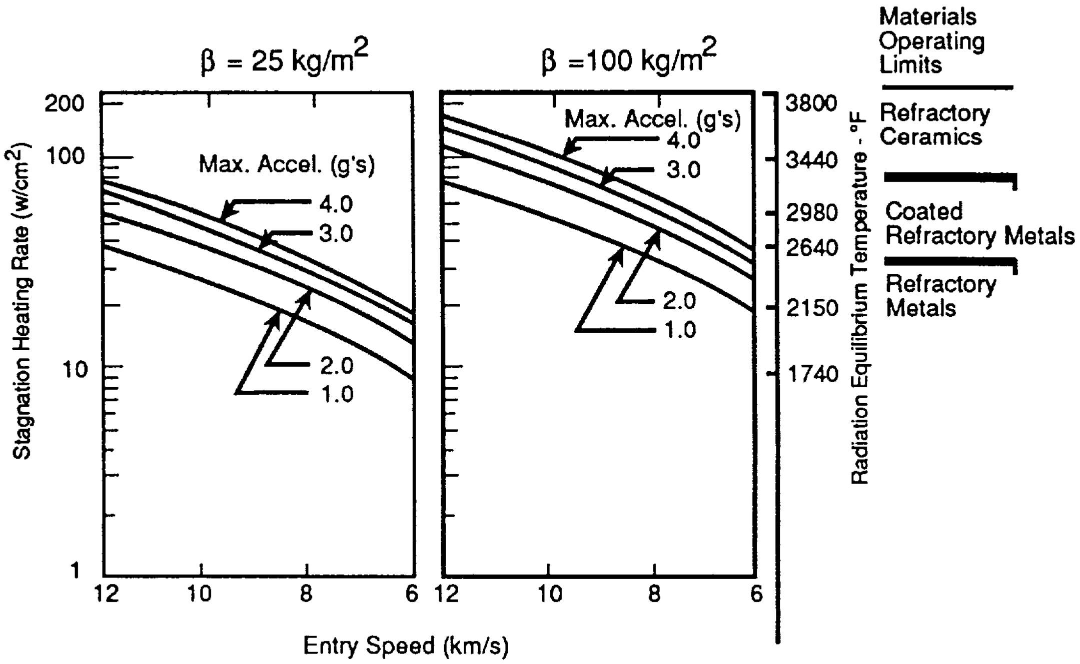

Figure 2-17. Sensitivity of thermal loads to ballistic coefficient [6].

The benefits of using the lighter TPS would have to be traded against the mass penalties of a larger aerobrake. Wurster and Eldred [1] found that a hybrid system that uses both types of TPS may provide benefits in reducing the mass and increasing the durability of the aerobrake.

2. Aerobrake Sizing

All of the design considerations that have been described influence the sizing of the aerobrake. Many tradeoffs are required to achieve the best aerobrake design for a particular mission. The ultimate goal in sizing an aerobrake is to minimize the mass. Figure 2-18 [5] shows the aerobrake specific mass as a function of accumulated heat load for an aerobrake. The structure mass includes the aluminum skin, stiffeners, and frame. The remainder of the mass is the TPS, which consists of the tiles, coating, strain isolation pad, and adhesive [5]. Since the mass of the aerobrake depends more on the supporting structure than on the insulation, it is advantageous to minimize the diameter of the aerobrake.

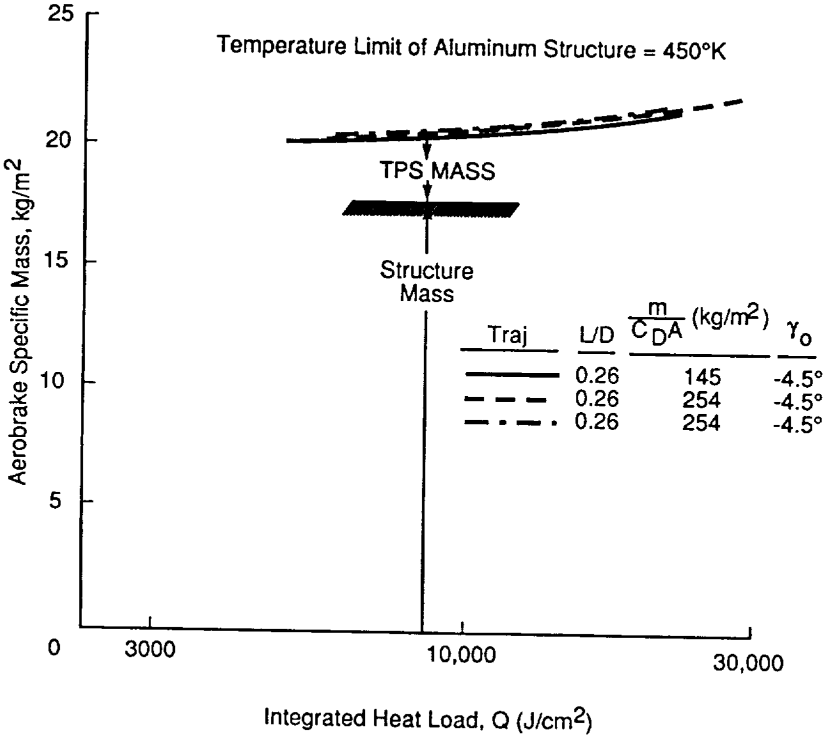

Figure 2-18. Specific mass of LI-900 TPS on aluminum structure aerobrake [5].

In most cases, the minimum diameter is determined by the heating rate constraint of the insulation material. The aerobrake must be sized to have a sufficiently low ballistic coefficient such that the maximum heating rate will not exceed the limit of the TPS. Figure 2-19 [5] shows the relationship between aerobrake diameter, payload mass, and maximum heating rate for a GEO to LEO transfer. The specific mass ratio, ρ_B/C_D, corresponds to a value similar to the space shuttle. The factor f represents the deviation of the aerobrake heating rate from a reference sphere. It includes the effects of nonequilibrium flow, catalysis, low atmospheric density, and the vehicle shape. The value of f for a spherical aerobrake was derived from data in reference 27. As the payload increases, aerobraking becomes more efficient as indicated by a decrease in the aerobrake mass

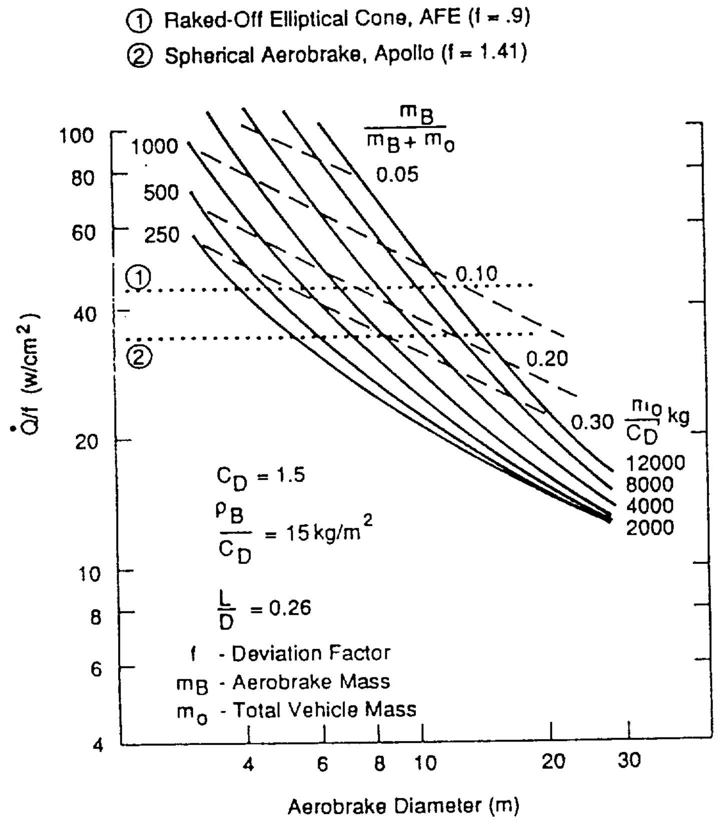

Figure 2-19. Vehicle sizing curve based on convective heat flux [5].

fraction. Also, if the maximum heating rate for an aerobrake could be increased, the diameter could be decreased for a given payload. This, too, would result in a lower mass fraction which would increase the efficiency.

Similar aerobrake sizing data was developed for a lunar transfer vehicle by Dickerson [19]. These data were used to construct figure 2-20, which shows several aerobrake parameters as a function of the aerobrake payload mass. The aerobrake sizing is based on a maximum heating rate of 51 W/cm^2. The values of ballistic coefficient and diameter represent the minimum values that will ensure that the heating rate constraint is not exceeded for an aeroassisted return from lunar orbit. In some cases, the diameter may need to be increased to prevent flow impingement on the payload. Increasing the diameter of the aerobrake decreases the ballistic coefficient and the thermal loads, therefore, some of the mass penalty could be reduced by decreasing the insulation thickness.

The size of the aerobrake appears to depend on two factors, aerodynamic heating and flow impingement on the payload. In general, higher L/D and lower ballistic coefficients reduce the vehicle loads. Ordinarily, reducing the loads on a vehicle results in a decrease in mass, but this is not always the case with aerobrakes. Decreasing the loads may result in a larger than necessary aerobrake, a more complex shape, or worse flow impingement (due to a higher angle of attack) [14]. The process of sizing an aerobrake and estimating its mass involves a number of trade-offs and iterations in which all the design considerations that have been described must be included. Figure 2-21 [14] shows a schematic of the process used to size an aerobrake. The process can be summarized by the criteria listed in table 2-3. In the next section, it will be seen that this aerobrake design process must also include careful design of the atmospheric trajectories that will be flown. The vehicle design must be closely coordinated with the trajectory design.

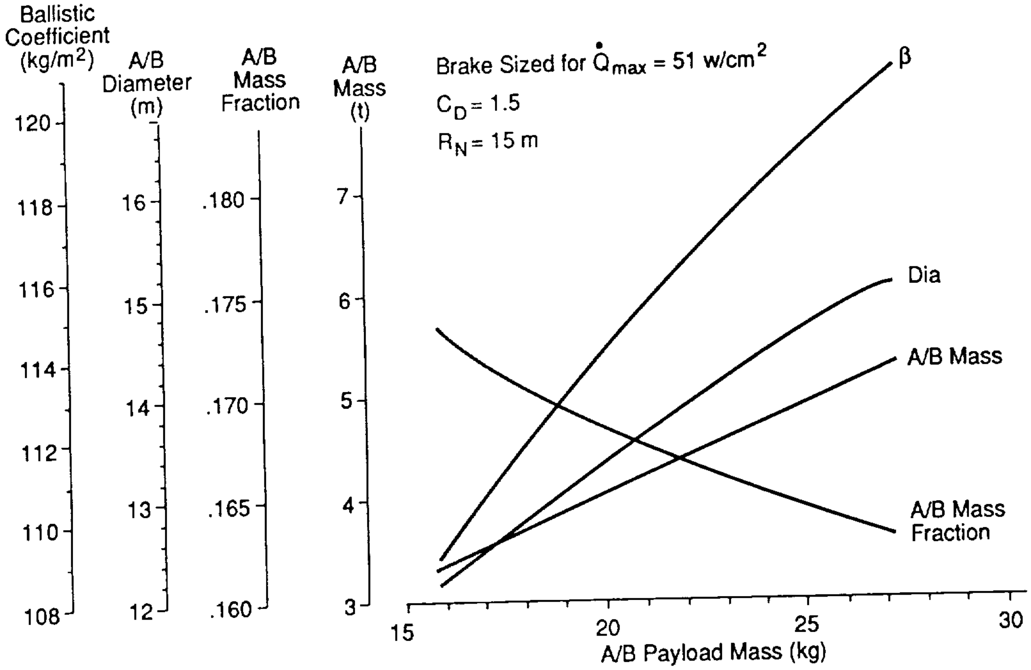

Figure 2-20. Lunar return aerobrake sizing.

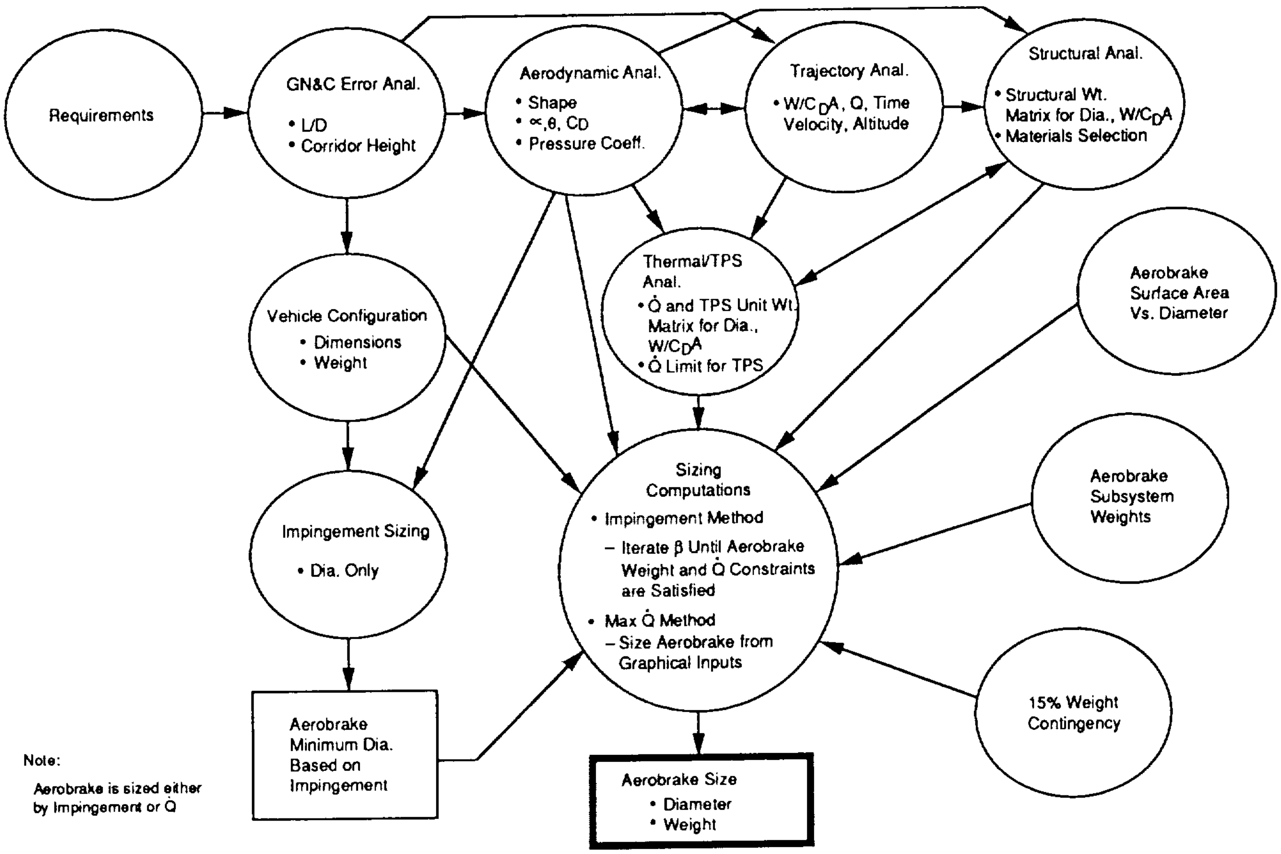

Figure 2-21. Aerobrake sizing approach schematic [14].

Table 2-3. Aerobrake sizing criteria.

- GN&C determines L/D requirement
- L/D determines angle of attack requirement
- Angle of attack determines impingement angle
- Ballistic coefficient determines:
    - Maximum heating rate
    - Maximum dynamic pressure
    - Maximum acceleration
- Thermal protection system determines maximum allowable heating rates
- Dynamic pressure and acceleration load sizes aerobrake structure
- Heating rate and impingement angle sizes aerobrake diameter

III. AEROBRAKE TRAJECTORY OPTIMIZATION

A. Formulation of the Optimization Problem

This discussion of trajectory optimization will begin with a description of the equations of motion which govern a trajectory and the formulation of the optimizing technique which can be applied to aerobrake trajectories. This will be followed by an investigation of candidate measures of aerobrake performance. Next, a detailed description of the process of finding the optimal angle of attack control function will be presented. Finally, several vehicle control strategies which could be used in aerobrake applications will be discussed. This section will lead to the variable angle of attack strategy used in section IV.

The motion of an aerobraked vehicle can be described by seven differential equations which apply during both the space portion and atmospheric portion of a trajectory. These equations are written below in vector form [1]:

$$\dot{\mathbf{r}} = \mathbf{V} , \tag{3-1}$$

$$\dot{\mathbf{V}} = (\mathbf{T}+\mathbf{A})/m + \mathbf{g}(\mathbf{r},\mathbf{t}) , \tag{3-2}$$

$$\dot{m} = T/g_0 I_{sp} , \tag{3-3}$$

where

$$\mathbf{g} = -\mu\mathbf{r}/r^3 . \tag{3-4}$$

From these equations it can be seen that during the space portion of the trajectory the motion is described by basic Keplerian orbital mechanics since $|\mathbf{T}| = |\mathbf{A}| = 0$. The vectors **T** and **A** (thrust and aerodynamic forces) are used as controls to achieve a desired transfer from one orbit to another. The initial and final orbits are represented by the boundary conditions:

$$\mathbf{r}(t_0) = \mathbf{r}_0 , \tag{3-5}$$

$$\mathbf{V}(t_0) = \mathbf{V}_0 , \tag{3-6}$$

$$m(t_0) = m_0 , \tag{3-7}$$

and,

$$\mathbf{G}[\mathbf{r}(t_f), \mathbf{V}(t_f)] = 0 . \tag{3-8}$$

G is a vector-valued function, such as the set of orbital elements at atmospheric exit which describe the final orbit. The orbit transfer is described by defining the functions **T**(t) and **A**(t) during the time interval $t_0 < t < t_f$ that transfer the vehicle from its initial state, equations (3-5) to (3-7), to the desired final state, equation (3-8) [1].

The function **T**(t) represents the thrust level during propulsive burns. As the number and duration of the burns increase, the propellant consumption increases according to equation (3-3). An alternative measure of propellant consumption can be derived from equation (3-2). This measure is called the characteristic velocity, C, and is defined by integrating the thrust acceleration over the entire transfer [1]:

$$\Gamma = \mathbf{T}/m , \tag{3-9}$$

$$C = \int_{t_0}^{t_f} dV\,dt \int_{t_0}^{t_f} |\Gamma|\,dt , \tag{3-10}$$

The characteristic velocity is the sum of all of the propulsive velocity changes. It provides a more general measure of propellant consumption since it does not depend on specific impulse [1]. For this reason, the characteristic velocity has been a popular performance index for evaluating aerobraked orbital transfers.

It was stated earlier that the control functions **T**(t) and **A**(t) are chosen to achieve a desired orbital transfer. In most cases, there are many functions which will result in the same transfer. The analysis of aerobrake trajectories then must include an evaluation of which functions provide the best transfer as indicated by some performance criteria. In order to select the best control functions, an optimization process is required. The optimization techniques applied to aerobrake trajectories make use of the equations of motion and a performance index to formulate an optimal control problem.

The selection of the optimization formulation depends somewhat on the performance index. Previously, the characteristic velocity was mentioned as a possible performance index. Other potential performance indices include aerodynamic heating rate, acceleration load, dynamic pressure, or altitude drop. If the performance index is a parameter which must be integrated over the duration of the aeropass, it is convenient to write the variational formulation using the Bolza form of the functional J [1]:

$$J = S[\mathbf{r}(t_f), \mathbf{V}(t_f), m(t_f)] + \int_{t_0}^{t_f} F[\mathbf{r}(t), \mathbf{V}(t), m(t)]\, dt\,. \tag{3-11}$$

The function S represents the final boundary conditions that are possible from the allowable trajectories. The function F is the trajectory or vehicle parameter which is to be integrated over the aeropass. F is a function of position, velocity, and mass which in turn are functions of the general control function $\mathbf{u}(t)$. The allowable trajectories are determined from two sets of auxiliary equations [20]:

$$\dot{x}_i = 0 \quad \text{and} \quad k_i = 0\,. \tag{3-12}$$

The equations $\dot{x}_i$ represent the governing equations for the system. In this case, these are the equations of motion, equations (3-1) to (3-3). The equations k_i represent boundary constraints such as the maximum acceleration or heating rate that is permissible for the trajectory. In some formulations [1], this is written as an inequality constraint;

$$k_i[\mathbf{r}(t), \mathbf{v}(t)] \leq 0\,. \tag{3-13}$$

This makes it easier to undertand the role of this function. As long as the value of k_i is below the maximum value, k_i plays no part in determining the optimal trajectory [1], but at the maximum value, k_i acts as a constraint on the trajectory.

The goal of the optimization is to determine the control functions $\mathbf{T}(t)$ and $\mathbf{A}(t)$ and the corresponding trajectory which will minimize J. This is accomplished by defining a Hamiltonian in the following form [20]:

$$H = F + \sum p_i \dot{x}_i\,. \tag{3-14}$$

The p_i are adjoint functions for each degree of freedom. They can be components of an adjoint vector or adjoint scalars. They serve the same purpose as Lagrange multipliers in an Eigenvalue problem except that they are functions of time rather than constants [20]. Using equations (3-1) to (3-3) and equation (3-11) the Hamiltonian can be written as [1]:

$$H = F(\mathbf{r},\mathbf{V},m) + \underset{\substack{|\\(3\text{-}1)}}{\mathbf{p}_r \cdot V} + \underset{\substack{|\\(3\text{-}2)}}{\mathbf{p}_v \cdot [(\mathbf{T}+\mathbf{A})/m+\mathbf{g}]} - \underset{\substack{|\\(3\text{-}3)}}{p_m\, T/g_0\, I_{sp}} = C = 0\,. \tag{3-15}$$

Since time does not appear explicitly, the Hamiltonian is equal to zero [1]. In the above formulation, $\mathbf{p}_r$ and $\mathbf{p}_v$ are adjoint vectors (each with three components), and p_m is a scalar. The functional J is minimized by minimizing the value of H at each point on the trajectory. In this case, the minimum value is equal to zero. The Hamiltonian is minimized by satisfying the Euler-Lagrange equations which relate H to the adjoint functions [20].

$$\left\{\frac{\partial H}{\partial x_i} - \frac{\partial}{\partial x_i}\left(\frac{\partial H}{\partial \dot{x}_i}\right) = 0 \quad i = 1,n\,.\right\} \tag{3-16}$$

The x_i represent the generalized coordinates (dependent variables) of the problem (r_x, r_y, r_z, v_x, v_y, v_z, m). Since the entry and exit conditions for the aeropass may be variable, the transversality condition shown below must also be satisfied [20]:

$$\left[\left(H - \sum_{i=1}^{n} \dot{x}_i \frac{\partial H}{\partial \dot{x}_i}\right) dt + \sum_{i=1}^{n} \frac{\partial H}{\partial \dot{x}_i} dx_i\right] + dt = 0\,. \tag{3-17}$$

Equations (3-16) and (3-17) and equations of motion y_i are solved using the control functions as independent variables for all of the unknowns, $x_j(t)$ and $\mathbf{p}_i(t)$.

If the performance index represents a parameter for which a peak value is to be minimized (regardless of where in the trajectory the peak occurs), the functional is written in a "nonclassical" form as a "minimax" or "Chebyshev" optimal control problem [21]:

$$J = S[\mathbf{r}(t_f), \mathbf{V}(t_f), m(t_f)] + \max F[\mathbf{r}(t), \mathbf{V}(t), m(t)]\,. \tag{3-18}$$

To simplify the notation, this can be rewritten as:

$$J(\mathbf{u}) = S(\mathbf{x}(t_f)) + \max F(\mathbf{x},\mathbf{u})\,, \tag{3-19}$$

where $\mathbf{u}$ is the control function ($\mathbf{u}$ replaces $\mathbf{T}$ and $\mathbf{A}$), and $\mathbf{x}$ is the set of state vectors. Using this notation, the equations of motion can be abbreviated by:

$$\dot{\mathbf{x}} = \mathbf{f}(\mathbf{x},\mathbf{u})\,. \tag{3-20}$$

The functional is minimized by satisfying a number of necessary conditions during the trajectory. The Hamiltonian is defined as [22]:

$$H(\mathbf{x},\mathbf{p},\mathbf{u}) = \mathbf{p}^T \mathbf{f}(\mathbf{x},\mathbf{u})\,. \tag{3-21}$$

The **p** represents adjoint functions similar to those used in the Bolza form.

The necessary conditions for an optimal trajectory can be described by a set of equations that must be satisfied at different times during the aeropass depending on whether the performance index is at its peak value. One condition that must be satisfied at all points on the trajectory regardless of the value of the performance index is the condition for the Hamiltonian [22]:

$$H(\mathbf{x},\mathbf{p},\mathbf{u}) = c \,, \tag{3-22}$$

(if time is not specified explicitly, $H = 0$).

If the performance index, F, is below its peak value, the following condition must be satisfied [22]:

$$\dot{\mathbf{p}}(t) = -\frac{\partial H}{\partial \mathbf{x}} \,. \tag{3-23}$$

At points in the trajectory where F hits peak values (assuming it is possible to have multiple peaks at $t_1, t_2, \ldots t_k$), another equation must be satisfied [22]:

$$\mathbf{p}(t^+) = \mathbf{p}(t^-) + \mu_i \frac{\partial F}{\partial \mathbf{x}}(\mathbf{x}(t_i)), \quad i = 1,2,\ldots,k \,, \tag{3-24}$$

where

$$\sum_{i=1}^{k} \mu = 1 \,, \quad \mu \geq 0 \,.$$

This condition relates the value of **p** just prior to the peak to the value just after the peak, and it is used to account for the discontinuity in $\mathbf{p}(t)$ at the peaks. If the value of F remains at the peak value for some finite time interval (t_i, t'_i), the trajectory has a "flat maximum" [22]. During this time interval two other equations must be satisfied [22]:

$$\dot{\mathbf{p}}(t) = -\frac{\partial H}{\partial \mathbf{x}} + \delta_i \frac{\partial \dot{F}(\mathbf{x},\mathbf{u})}{\partial \mathbf{x}} \,, \tag{3-25}$$

where $\delta_i(t)$ is a scalar function satisfying:

$$\frac{\partial H}{\partial \mathbf{u}} = \delta_i(t) \frac{\partial \dot{F}}{\partial \mathbf{u}} \,. \tag{3-26}$$

Finally, there is a necessary condition that must be satisfied at atmospheric exit [22]:

$$\mathbf{p}(t_f) = -\alpha \frac{\partial S(\mathbf{x}_f)}{\partial \mathbf{x}_f} \tag{3-27}$$

where α is a set of multipliers. A summary of which equations must be satisfied at various times to obtain an optimal trajectory using the Chebyshev formulation is shown in table 3-1.

Table 3-1. Necessary conditions for a Chebyshev optimal control problem.

PERFORMANCE INDEX VALUE	EQUATIONS TO SATISFY
F< MAXIMUM VALUE	(3-22), (3-23)
F REACHES MAXIMUM	(3-22), (3-24)
F IS AT A FLAT MAXIMUM	(3-22), (3-25), (3-26)
AT ATMOSPHERIC EXIT	(3-22), (3-27)

B. Performance Indices

The optimum trajectories that are found using the formulations that have been described provide the best performance as defined by the selected performance index [1]. Recent work has examined a number of performance indices and the implications they have on the resulting optimal trajectories [3]. It is possible that two performance indices will yield completely different "optimal" trajectories. A list of possible aerobrake trajectory performance indices is shown in table 3-2. The choice of a performance index often depends on specific mission or vehicle requirements. An aerobrake that is designed to perform a plane change usually flies deeper into the atmosphere than an aerobrake designed only to decrease velocity. Since the trajectories for these two purposes are inherently different, it would probably be necessary to use different performance indices to optimize each type of mission. The choice of a performance index must be made carefully. It is possible that if a trajectory is optimized to satisfy one criteria, the vehicle may be penalized in another aspect. The choice of a performance index often involves a compromise of several vehicle and trajectory constraints.

The most obvious performance index for an aerobrake trajectory is the characteristic velocity, *C*. It was defined earlier by equation (3-10). An alternative definition replaces the integral in equation (3-10) with a simple summation of the delta velocities [3]:

$$C = \Delta V_{\text{total}} = \Delta V_1 + \Delta V_2 + \Delta V_3 + \dots \, . \tag{3-28}$$

In the optimization formulation, equations (3-10) or (3-28) are substituted for *F* into the functional.

Table 3-2. Aerobrake performance indices.

1. Characteristic velocity (or propellant mass)
2. Payload mass fraction
3. Integrated convective heating rate
4. Peak convective heating rate
5. Peak acceleration
6. Peak dynamic pressure
7. Time integral of flight path angle squared
8. Peak altitude drop

Minimizing the characteristic velocity is in many cases equivalent to minimizing the propellant usage [1] or vehicle mass. This implies the minimum mission cost since cost is often proportional to vehicle mass [1]. Since the characteristic velocity is primarily a measure of propellant requirements, it overlooks two other factors that comprise the vehicle mass: the payload mass and the vehicle inert mass. The payload is the cargo or instrument that is carried by the veicle. The inert mass consists of the vehicle structure, subsystems, and aerobrake. Using the above three factors, the total vehicle mass can be written as [1]:

$$m_{\text{vehicle}} = m_{\text{propellant}} + m_{\text{payload}} + m_{\text{inert}} \, . \tag{3-29}$$

If an aerobrake mission is to be advantageous, the decrease in propellant mass must be greater than the increase in inert mass due to the addition of the aerobrake [1].

The balance between propellant savings and aerobrake mass is more obvious if another performance index is used. The payload mass fraction sometimes provides a better measure of aerobrake performance than the characteristic velocity [1]. It is defined as:

$$M = m_{\text{payload}}/m_{\text{vehicle}} \, . \tag{3-30}$$

This ratio automatically allows for the trade-off between propellant mass and aerobrake mass. The optimum trajectory, defined by the maximum value of M, would provide the best combination of energy requirements (delta velocity) and aerobrake requirements (TPS). The payload ratio implies that there is an inherent relationship between the vehicle design (specifically aerobrake TPS mass) and the trajectory design.

The coupling between TPS mass and trajectory design has been considered in many studies [1]. Performance indices which characterize this relationship more precisely than payload ratio have been investigated. In most cases, the relationship is not direct but in terms of some measurable trajectory parameter. Some of these alternative performance indices are listed in table 3-2. The peak heating rate ($\dot{Q}_{\max}$) and the total heat load (Q) are the most common indices used as an indication of TPS system requirements.

The peak heating rate is computed at the vehicle stagnation point [1] and is defined by the relation [1]:

$$\dot{Q} = c\,\rho^{0.5}\,V^{3.08}\ \mathrm{W/cm^2}\,, \tag{3-31}$$

where

$c = 1.83 \times 10^{-8}\, r_n^{-0.5}\,(1-g_w)$

r_n = nose radius (m)

g_w = wall enthalpy/total enthalpy

ρ = density (kg/m^3)

V = velocity (m/s) .

In many cases c is dropped from the functional, so the performance index has the form [3]:

$$F = \rho^{0.5} V^{3.08}\,. \tag{3-32}$$

The integrated heat load is simply the heating rate integrated over the duration of the aeropass [1]:

$$Q = \int_{t_0}^{t_f} \dot{Q}\,dt\,. \tag{3-33}$$

Two other performance indices which serve as indicators of vehicle structural requirements are the vehicle acceleration ($\dot{\mathbf{V}}$) and the dynamic pressure. The dynamic pressure gives a measure of aerodynamic loads. It is defined as:

$$q = \frac{1}{2}\rho\,V^2\,. \tag{3-34}$$

The four performance indices just described give a more precise indication of aerobrake or vehicle requirements than the payload ratio, but they do not necessarily lead to the best "overall" compromise between vehicle and trajectory design factors. The last two performance indices listed in table 3-2 were proposed as indices which could be used to obtain optimal trajectories in which the conflicting aerobrake mission and vehicle requirements could be effectively balanced.

The time integral of the flight path angle squared was proposed as a performance index by Miele [1]. It leads to a "nearly grazing trajectory" which will be discussed later. This performance index is defined by the integral [3]:

$$F = \int_{t_0}^{t_f} \tau \gamma^2 \, dt , \tag{3-35}$$

where τ is the normalized time in the atmosphere (= 0 at entry, = 1 at exit). The nearly grazing trajectory seeks to barely skim the top of the atmosphere. Miele has shown that this type of trajectory has several advantages [3]. Vinh and Lu [22] proposed the minimum peak altitude drop as a performance index which achieves the same goal as the integrated square of the flight path angle. The peak altitude drop refers to the depth of penetration into the atmosphere. This performance index yields trajectories that are similar to the "nearly grazing" solutions.

Miele and his colleagues [1] have conducted an extensive investigation of a number of performance indices in order to determine which leads to the most favorable flight path along with having favorable propellant requirements for the overall orbit transfer [1]. The indices that were evaluated are listed below [1].

1. Characteristic velocity (or propellant mass)
2. Integrated heating rate
3. Peak heating rate
4. Time integral of the flight path angle squared.

The trajectory that results in the minimum characteristic velocity is called the grazing trajectory [1]. It is an idealized trajectory which is not really possible, in which the vehicle travels along the edge of the atmosphere until just enough energy is dissipated to reach the final target orbit (fig. 3-1). The idealized "grazing" trajectory gives a good approximation for propellant requirements if the initial orbit is high or the entry angle is small and the exit flight path angle is near zero [1]. This type of trajectory is useful in many aerobrake performance analyses and will be discussed further in section IV.

The second performance index, the integrated heating rate, is minimized by penetrating deeper into the atmosphere and dissipating the energy as quickly as possible [1]. This is opposite to the strategy used to minimize the characteristic velocity (grazing trajectory). However, even in this case, where the deepest penetration into the atmosphere is desired, the propellant requirement is only 1 percent greater [1]. The disadvantage of this performance index is that it leads to optimal trajectories with very high peak heating rates. This implies greater TPS requirements, thus minimizing the "integrated" heating rate, and the "peak" heating rate yield conflicting requirements. The proper compromise depends on the type of TPS [1].

The third index, peak heating rate, is a function of density (altitude) and speed. The speed goes through the same range of values for any allowable trajectory, therefore the peak heating rate is minimized by minimizing the density during the aeropass [1]. This can be accomplished by flying as close to the atmospheric boundary as possible. As a result, the idealized or "grazing" trajectory

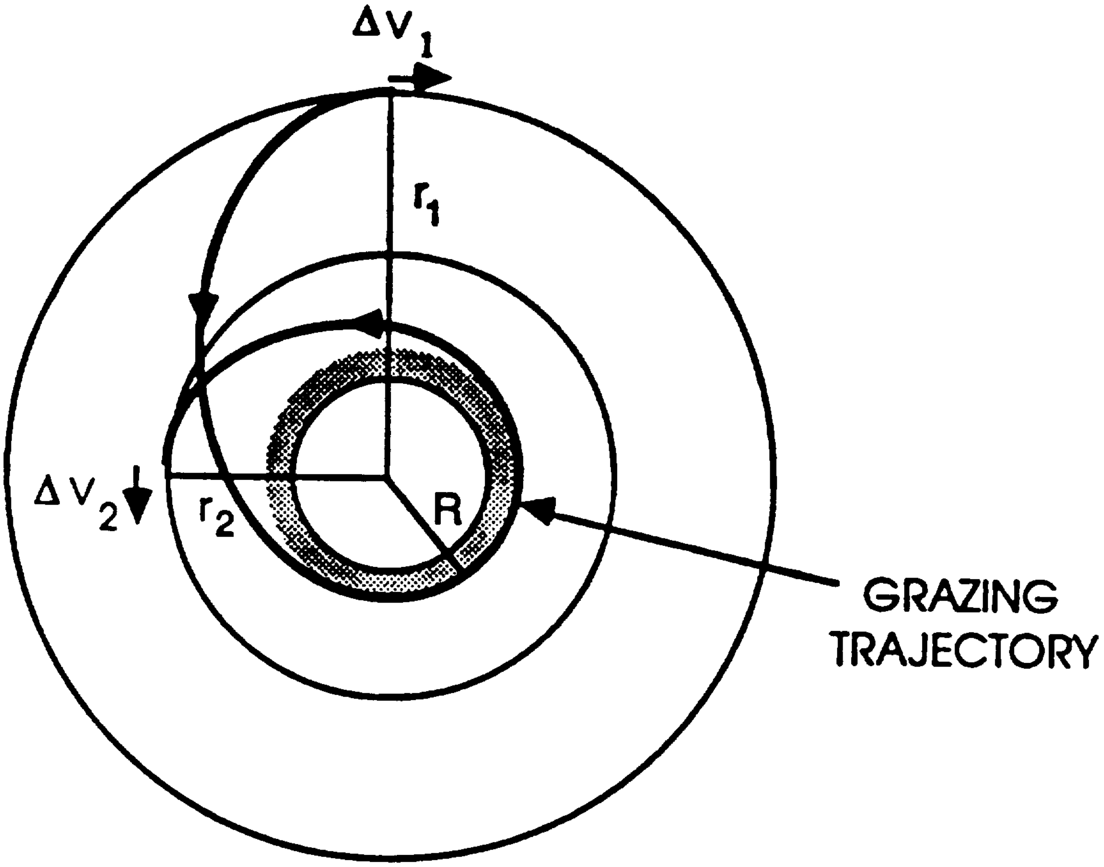

Figure 3-1. Idealized aeroassisted transfer.

minimizes both the propellant consumption and the peak heating rate [1]. Unfortunately, it is impossible to fly a grazing trajectory if realistic control bounds are applied to the optimization. The grazing trajectory is useful because it provides an ideal or goal for which actual trajectories can be designed to approximate. To achieve the best possible approximation, another performance index was needed.

The desire to approximate the idealized optimal trajectory led Miele to formulate the fourth performance index and to name the resulting optimal trajectory the "nearly grazing trajectory" [1]. By minimizing the flight path angle at each point in the trajectory, the penetration into the atmosphere is minimized. The actual altitude profile for the nearly grazing trajectory is determined by the trajectory boundary conditions and the vehicle control capabilities. A comparison of several trajectory parameters for transfers from GEO to LEO that result from the different performance indices is shown in figure 3-2 [3].

An interesting result of Miele's work is that performance indices 1, 3, and 4 yield almost identical trajectories and trajectory control functions. Miele expresses this result with the statement, "In the coplanar case, what is good for peak heat rate is good for the energy." From the data shown in figure 3-2, it appears that the nearly grazing solution provides an excellent compromise between energy requirements and aerodynamic heating requirements for GEO to LEO transfers [3]. The nearly grazing solution requires about 3.1 percent more energy than the minimum energy trajectory but reduces peak heating by 27.1 percent, dynamic pressure by 42 percent, and peak acceleration by 31.6 percent [3]. Miele also has shown that the nearly grazing solution is the best compromise for other types of transfers as well [3].

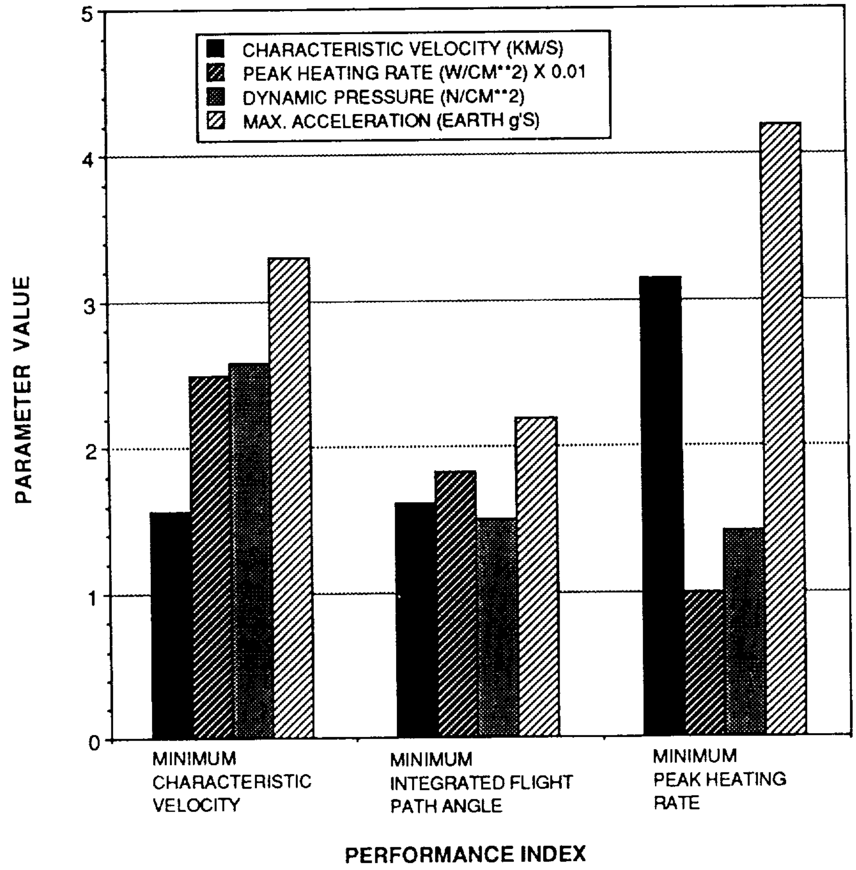

Figure 3-2. Relationship between performance index and trajectory parameters.

Vinh and Lu have arrived at results similar to Miele using the minimum peak altitude drop as a performance index [22]. The minimum peak altitude drop is defined as the minimum altitude during the aeropass (periapsis). In their analysis, Vinh and Lu use the Chebyshev minimax problem to prove that the heating rate and dynamic pressure pass through their respective maximum values along the descending portion of the aeropass, and that these parameters can be reduced by minimizing the peak altitude drop. They also derive the necessary control function $\mathbf{u}(t)$ needed to achieve the optimal (nearly grazing) trajectory. The near optimal trajectories that will be analyzed in the following section will be based on the results of Vinh and Lu, therefore an overview of their analysis will be presented.

C. Lift Control Function for Optimum Trajectories

The first step of the analysis was to describe the motion of the aerobraked vehicle in terms of dimensionless equations of motion. The use of modified Chapman's variables allows the problem to be formulated such that the only vehicle parameters are the maximum L/D and maximum lift coefficient. The modified Chapman's variables are defined as [23]:

$$z = \frac{\rho S C_L^*}{2m}\sqrt{\frac{r}{B}}\,, \qquad (3\text{-}36)$$

$$v = \frac{V^2}{gr}, \tag{3-37}$$

$$s = \int_{t_0}^{t_f} \frac{V}{r} \cos\gamma \, dt . \tag{3-38}$$

The atmospheric density is assumed to be inversely proportional to the scale height B,

$$d\rho = -B\rho \, dr . \tag{3-39}$$

The variable z is the altitude drop. It increases as altitude decreases and can be regarded as a replacement for altitude. The variable v is the dimensionless kinetic energy which is a measure of speed. Finally, the variable s is the dimensionless arc length of the atmospheric trajectory. It is the independent variable [22].

The vehicle parameters that will be used in the nondimensionalized equations of motion are derived from an assumed parabolic drag polar for the vehicle [22]:

$$C_D = C_{D_0} + K\, C_L^2 , \tag{3-40}$$

at the maximum L/D, E^*:

$$C_L{}^* = \sqrt{\frac{C_{D_0}}{K}} \qquad \text{and} \qquad C_D{}^* = 2\, C_{D_0} , \tag{3-41}$$

therefore:

$$E^* = \left(\frac{L}{D}\right) = \frac{1}{2\sqrt{KC_{D_0}}} , \tag{3-42}$$

the normalized lift coefficient, which is the control and is defined as:

$$\lambda = \frac{C_L}{C_L{}^*} , \quad C_1 \leq C_{L_{\max}} . \tag{3-43}$$

Using the above definitions, the dimensionless equations of motion for the nonthrusting vehicle considered as a point mass were written as [22]:

$$\frac{dz}{ds} = -k^2 z \tan \gamma \, , \tag{3-44}$$

$$\frac{dv}{ds} = \frac{-kzv(1+\lambda^2)}{E^* \cos \gamma} - (2-v) \tan \gamma \, , \tag{3-45}$$

$$\frac{d\gamma}{ds} = \frac{kz \lambda \cos \sigma}{\cos \gamma} + \left(1 - \frac{1}{v}\right) , \tag{3-46}$$

$$\frac{d\theta}{ds} = \frac{\cos \psi}{\cos \phi} \, , \tag{3-47}$$

$$\frac{d\phi}{ds} = \sin \psi \, , \tag{3-48}$$

$$\frac{d\psi}{ds} = \frac{kz \lambda \sin \sigma}{\cos^2 \gamma} - \cos \psi \tan \phi \, , \tag{3-49}$$

where:

γ = flight path angle

θ = longitude

φ = heading angle

λ = normalized lift coefficient

σ = bank angle.

The quantity $k^2 = Br$ is treated as a constant with a value of 900 for Earth's atmosphere [22].

Vinh and Lu chose three trajectory parameters as possible performance indices. The first was the stagnation point heating rate, defined as:

$$\dot{Q} = \rho^{0.5} \, V^{3.08} \, . \tag{3-50}$$

The second performance index was the dynamic pressure, defined as:

$$q = \frac{1}{2} \rho V^2 . \tag{3-51}$$

The third performance index was the peak altitude drop, z, which was defined earlier by equation (3-36). By substituting the Chapman variables into equations (3-50) and (3-51) and rescaling the formulas, all three performance indices can be put into the form [22]:

$$F = K z v^n , \tag{3-52}$$

where k is a constant. If $n = 3.08$, F represents peak heating rate; if $n = 1$, F represents dynamic pressure; and if $n = 0$, F represents peak altitude drop.

Using the derivative of F with respect to time, it is possible to determine that the maximum value of F for any value of n, $n > 0$, occurs during the descending part of the trajectory.

$$\frac{dF}{dt} = \frac{dF}{ds}\frac{ds}{dt} = K\, v^{n-1} \left(v \frac{dz}{ds} + n\, z \frac{dv}{ds} \right) \frac{ds}{dt} , \tag{3-53}$$

from the definition of s, (equation (3-38))

$$\frac{ds}{dt} > 0 , \tag{3-54}$$

also, at atmospheric entry:

$$z \approx 0 , \tag{3-55}$$

$$\frac{dz}{ds} > 0 , \tag{3-56}$$

(z increases as altitude decreases). Due to the conditions of equations (3-54) to (3-56), it can be concluded that at atmospheric entry [22]:

$$\frac{dF}{dt} > 0 . \tag{3-57}$$

At the lowest point of the trajectory, since the flight path angle is zero:

$$\frac{dz}{ds} = 0 . \tag{3-58}$$

Since the speed is always decreasing:

$$\frac{dv}{ds} < 0 , \tag{3-59}$$

therefore at periapsis, equation (3-53) will result in:

$$\frac{dF}{dt} < 0 . \tag{3-60}$$

Since the time derivative of F is positive at atmospheric entry and negative at periapsis, it must pass through zero somewhere on the descending path. This point corresponds to a maximum value of F. From equation (3-53), it can also be concluded that the location of the maximum value of F depends on the value of the exponent n [22]. Vinh and Lu have proven that the peak heating rate always occurs first, followed by the peak dynamic pressure, then the peak altitude drop [22]. From the trajectory properties just described, it can be inferred that by minimizing the peak altitude drop, the peak heating rate and peak dynamic pressure are also reduced [22].

The process of finding the control function which yields the minimum peak altitude drop begins with the formulation of the optimization problem. If only coplanar aeroassisted transfers are considered, the dimensionless equations of motion, equations (3-44) to (3-49), reduce to [22]:

$$\frac{dz}{ds} = -k^2 z \tan \gamma , \tag{3-61}$$

$$\frac{dv}{ds} = \frac{-kzv\ (1+\lambda^2)}{E^* \cos \lambda} - (2-v) \tan \gamma , \tag{3-62}$$

$$\frac{d\gamma}{ds} = \frac{kz\,\lambda}{\cos \gamma} + \left(1 - \frac{1}{v}\right) . \tag{3-63}$$

The aerodynamic control is the normalized lift coefficient defined by equation (3-43). The performance index in its most general form is given by equation (3-52). The Hamiltonian is defined using equations (3-61) to (3-63) [22]:

$$H = -p_z\, k^2 z \tan \gamma - p_v\left(\frac{kzv\ (1+\lambda^2)}{E^* \cos \gamma} + (2-v) \tan \gamma\right) + p_\gamma\left(\frac{kz\,\lambda}{\cos \gamma} + \left(1 - \frac{1}{v}\right)\right) = 0 . \tag{3-64}$$

Subject to the necessary conditions that are outlined in equations (3-22) to (3-27), the optimal lift control can be determined. For an isolated maximum, the lift control is defined by the following relation [22]:

$$\lambda = \begin{cases} \dfrac{E^* p_\gamma}{2 v p_v} \ , & \text{if } |\lambda| \le \lambda_{\max} \\ \lambda_{\max} \operatorname{sign}(p_\gamma) \ , & \text{otherwise} \end{cases} \tag{3-65}$$

At each point in the trajectory, the adjoint variables must satisfy the following equations [22]:

$$\dot{p}_z = -\frac{\partial H}{\partial z} = p_z k^2 \tan \gamma + \frac{p_v kv\,(1+\lambda^2)}{E^* \cos \gamma} - \frac{p_\gamma k \lambda}{\cos \gamma}, \tag{3-66}$$

$$\dot{p}_v = -\frac{\partial H}{\partial v} = \frac{p_v kz\,(1+\lambda^2)}{E^* \cos \gamma} - p_v \tan \gamma - \frac{p_\gamma}{v^2}, \tag{3-67}$$

$$\dot{p}_\gamma = -\frac{\partial H}{\partial \gamma} = \left(p_z K^2 z + \frac{p_v kzv\,(1+\lambda^2) \sin \gamma}{E^*}\right) \frac{1}{\cos^2 \gamma} + (p_v(2-v) - p_\gamma kz \lambda \sin \gamma) \frac{1}{\cos^2 \gamma}. \tag{3-68}$$

The optimal trajectory is defined by integrating the system of equations (3-58) to (3-60) and (3-66) to (3-68) using equation (3-65) [22].

If the performance index has a flat maximum, then during the time at the maximum equation (3-65) is replaced by [22]:

$$\lambda^2 = \frac{-E^* \sin \gamma\,(m(2-v) + k^2 v)}{m\, kzv} - 1, \tag{3-69}$$

and the adjoint variables must satisfy the following equations instead of equations (3-66) to (3-68) [22]:

$$\dot{p}_z = -\frac{\partial H}{\partial z} + \delta \frac{\partial \dot{F}}{\partial z}, \tag{3-70}$$

$$\dot{p}_v = -\frac{\partial H}{\partial v} + \delta \frac{\partial \dot{F}}{\partial v}, \qquad (3\text{-}71)$$

$$\dot{p}_\gamma = -\frac{\partial H}{\partial \gamma} + \delta \frac{\partial \dot{F}}{\partial \gamma}, \qquad (3\text{-}72)$$

$$\delta = \frac{2\, p_v\, v\, \lambda - E^*\, p_\gamma}{2\, n\, k\, z\, v^{nT}\, \lambda}, \qquad (3\text{-}73)$$

$$\dot{F} = \frac{dF}{ds} = -\,kz\; v^{n-1}\left(\frac{nkzv\;(1+\lambda^2)}{E^*\cos\gamma} + ((k^2-n)v+2n)\tan\gamma\right). \qquad (3\text{-}74)$$

It was mentioned earlier that by minimizing the peak altitude drop it is possible to reduce both the peak heating rate and the peak dynamic pressure. This assertion enables the formulation to be simplified by allowing the value of n to be set to zero to obtain the best overall optimal trajectory. The performance index is simplified to [22]:

$$F = kz\,. \qquad (3\text{-}75)$$

The use of peak altitude drop as the performance index also significantly simplifies the Hamiltonian and adjoint functions. Vinh and Lu have applied numerical methods to solving the Chebyshev problem that has just been described, and they have defined the optimal lift control functions for several sets of atmospheric entry and exit conditions using the peak altitude drop as the performance index. The lift control function that they have defined for coplanar aeroassisted transfers from high altitude orbits to low altitude orbits will be the basis for the angle of attack profiles used for the trajectories in section IV.

The lift control profile and the resulting altitude profile for the optimal trajectory defined by Vinh and Lu are shown in figures 3-3 and 3-4. This specific trajectory was calculated using the following values for the maximum normalized lift coefficient and maximum L/D [22]:

$$\lambda = 2.0 \text{ and } E^* = 0.5\,.$$

At atmospheric entry, the lift coefficient is at its maximum positive value (lift up). It remains at this value until shortly before the peak altitude drop (periapsis). This allows the vehicle to fly at the highest altitude possible during the descending portion of the trajectory. Since the peak heating rate and peak dynamic pressure occur during the descending leg of the trajectory, it is beneficial to fly at the highest possible altitude where the density is less. Shortly before periapsis, the lift control begins a continuous transition toward the maximum negative value of lift coefficient (lift down). The lift coefficient has a value of zero at periapsis [22]. During the ascending leg of the trajectory, the lift

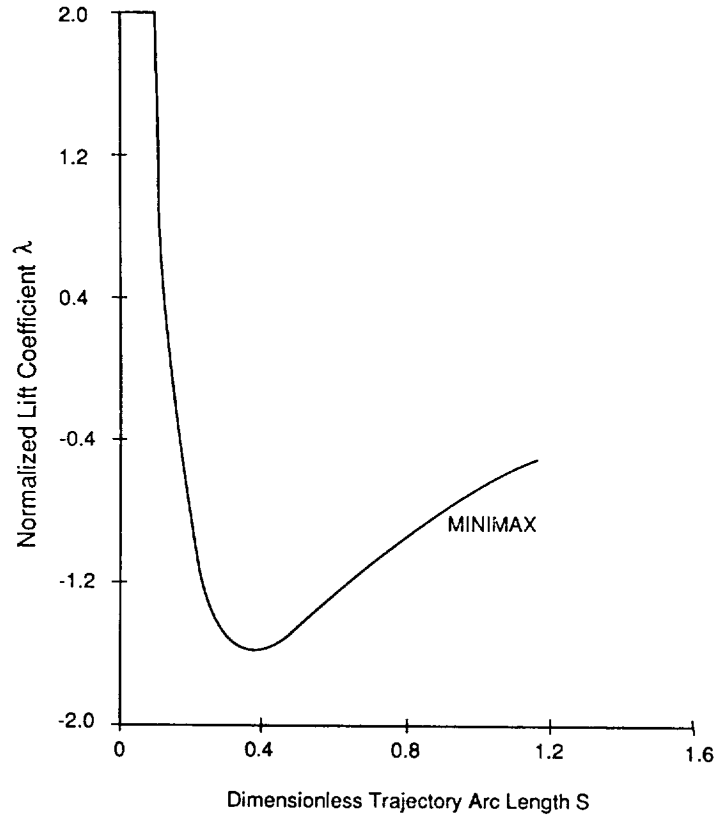

Figure 3-3. Variation of lift control for a minimax aerobrake trajectory [22].

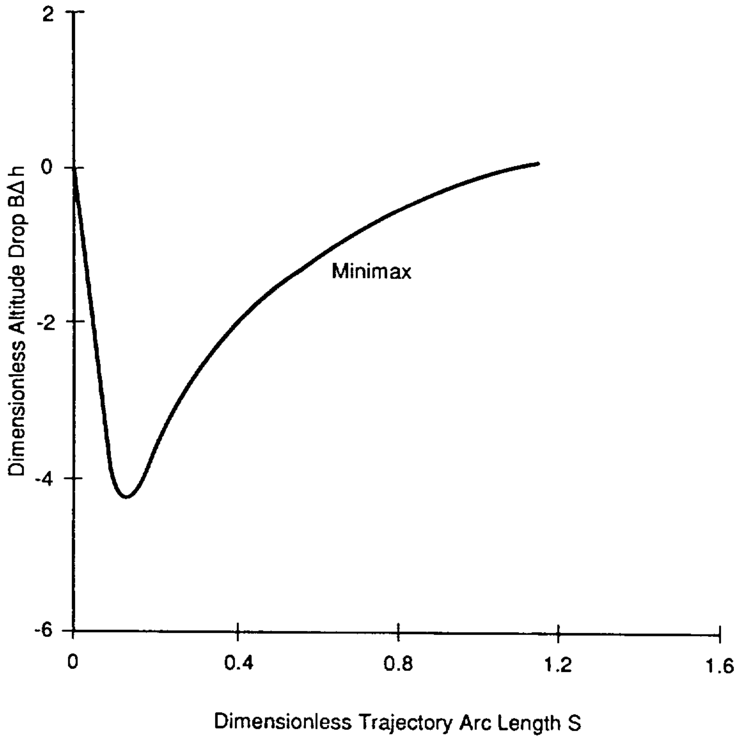

Figure 3-4. Altitude drop for minimax trajectory [22].

control remains negative but decreases in magnitude. The negative lift allows the vehicle to remain in the atmosphere as long as possible and also have a small flight path angle at atmospheric exit. The decrease in magnitude of the lift coefficient results in an increase in the drag coefficient so the maximum velocity change can be achieved.

D. Control Strategies

Based on the results of Miele, Vinh, and Lu, it appears that the nearly grazing solution is the best "overall" optimum aerobrake trajectory. The aerodynamic control function can be obtained using the integral of the flight path angle squared [1] or the minimum peak altitude drop [22] as the performance index in the optimization formulation. The aerodynamic control functions are usually specified by the magnitude and direction of the lift force and the magnitude of the drag force. In order to describe these functions in terms of vehicle characteristics and attitude conditions, it is necessary to choose a vehicle control strategy. There are three possible control strategies that can be used for aerobrakes. They are roll control, pitch control, and drag control (sometimes called drag modulation). In theory, they could be used separately or in combination).

Roll control uses a rotation of the vehicle about its roll-axis (bank angle) to control the direction of the lift vector. By rotating the lift vector out of the orbital plane, the vertical component of lift is used to control the rate of altitude change, and the lateral component of lift is used to control the rate of heading change (plane change). The bank angle profile for an aeropass for a GEO to LEO transfer is shown in figure 3-5 [3]. This profile shows the bank angle is varied and below 90°. This results in a 22.8° plane change in the atmosphere. If no plane change is desired, the bank angle is alternated from side to side such that the time spent banked to each side is balanced so there is no net heading change. One method for doing this is to perform a series of S-turns during the aeropass. Another method is to continuously roll the vehicle at varying rates during the aeropass [24]. The two strategies for roll control are illustrated in figure 3-6. In both strategies, the rotation of the vehicle would be achieved using the reaction control system (RCS) thrusters on the vehicle.

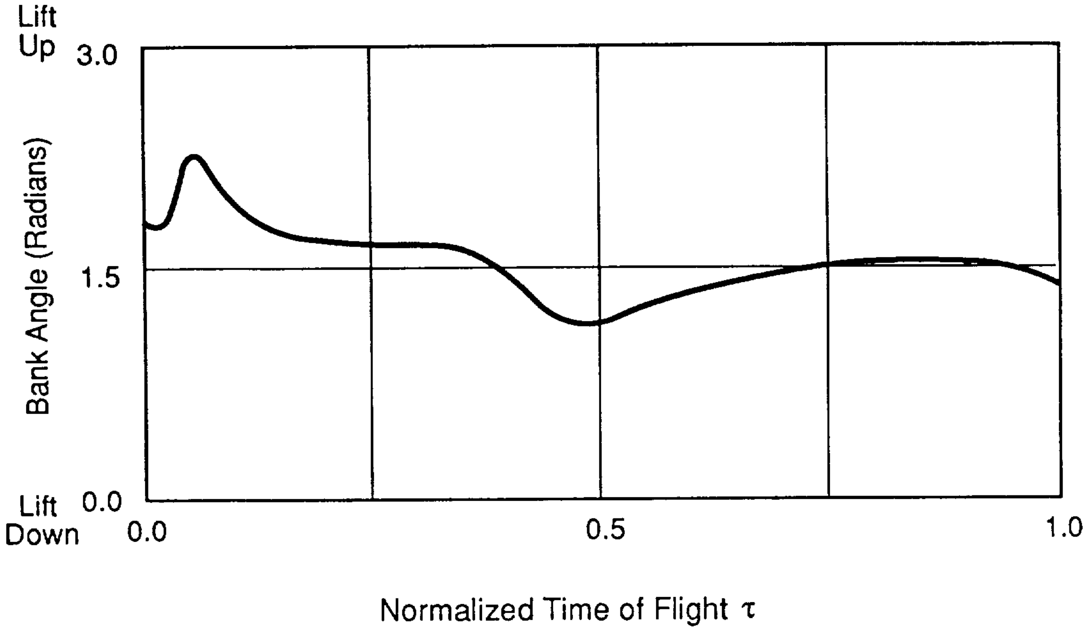

Figure 3-5. Bank angle profile for a GEO to LEO transfer [3].

S-TURNS

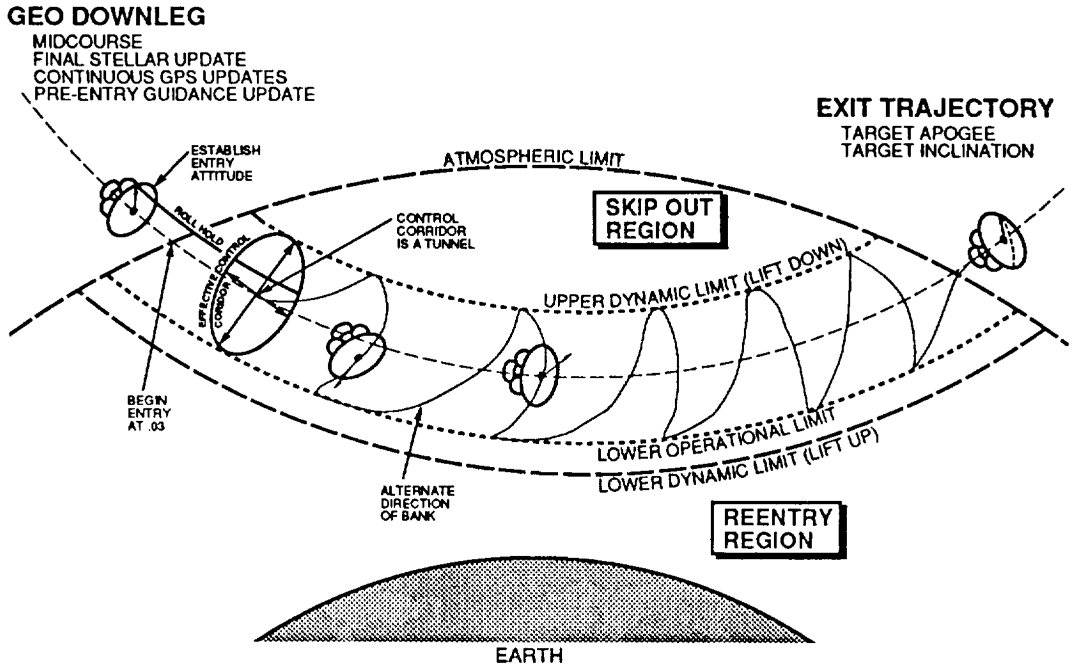

CONTINUOUS ROLL

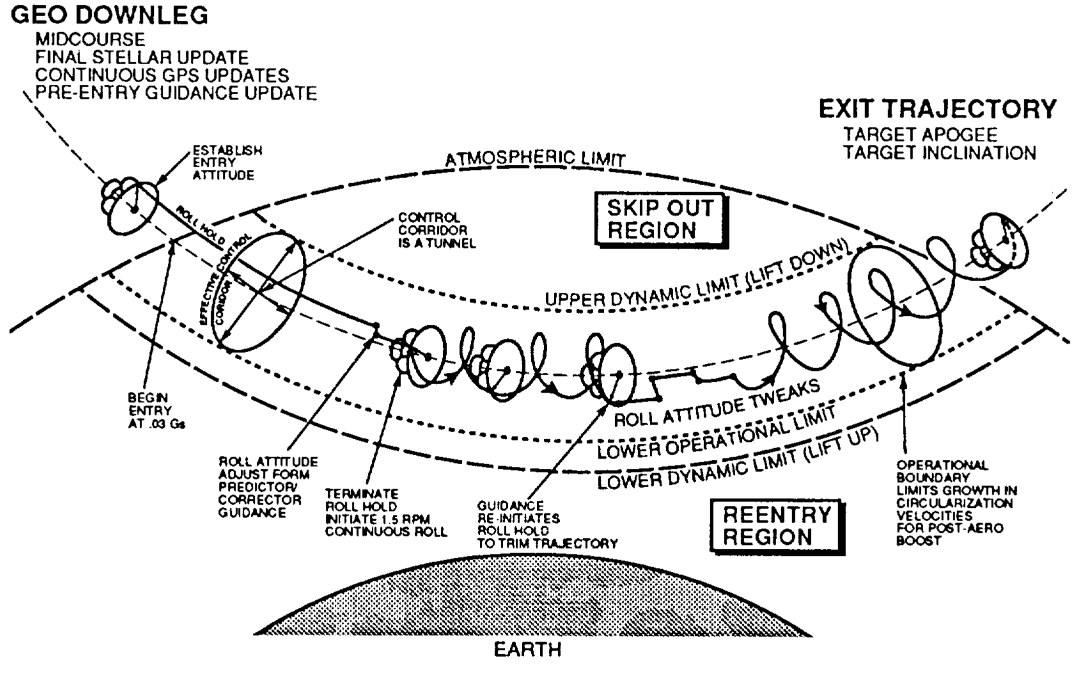

Figure 3-6. Roll control strategies.

Roll control requires a very responsive control system. The RCS system will need roll acceleration rates of about $10°/s^2$ [14]. The thrust required to achieve this level of angular acceleration is shown in figure 3-7. The thrust level depends on the vehicle inertia in the roll axis and the moment arm of the thrusters. The propellant required by the RCS system is shown in figure 3-8. The data shown is for a return from lunar orbit and assumes 12 roll maneuvers at an L/D of 0.15 during the aeropass [14].

Pitch control uses a rotation of the vehicle about its pitch axis (angle of attack) to control the magnitude of the lift and drag forces. There are no lateral forces associated with pitch control, therefore, pitch control cannot be used for atmospheric plane changes unless it is used in combination with roll control. The angle of attack for an aerobraked vehicle could be controlled by mechanically shifting the vehicle center of mass such that the vehicle would "trim" at the desired angle of attack. Two strategies for changing the vehicle center of mass are shown in figure 3-9. One strategy would use tracks or sliding mechanisms to shift the position of certain vehicle elements. The other strategy proposed by Tom Goodrick of Marshall Space Flight Center (MSFC) is to rotate the aerobrake payload with respect to the aerobrake using a pivot mechanism. This strategy has the advantage that the payload is kept further from the flow behind the aerobrake.

Pitch control may offer several advantages over roll control. It allows a continuous, smooth variation of the L/D from 0 to as much as 1.5, if flow impingement can be managed [13]. Another advantage is that all of the motion remains in the orbit plane, so many of the calculations are simplified [13]. Since the vehicle does not require S-turns or a continuous roll, the vehicle motion is reduced. This may simplify the guidance scheme and reduce the requirements on the RCS system.

The third aerobrake control strategy is drag control. It uses a change in the surface area or shape of the aerobrake to control the magnitude of the lift and drag forces. As was the case with pitch control, there are no lateral forces generated so drag control cannot be used for atmospheric plane changes unless roll control is also used. The primary difference in control authority between pitch control and drag control can be seen in the equations for lift and drag:

$$\mathbf{L} = \frac{1}{2} \rho V^2 C_L A \qquad \mathbf{D} = \frac{1}{2} \rho V^2 C_D A \, . \tag{3-76}$$

Pitch control uses angle of attack to vary the lift and drag coefficients. Drag control changes the vehicle reference area without necessarily changing the aerodynamic coefficients. The effectiveness of one strategy compared to the other depends on the relationship between the aerodynamic coefficients and angle of attack and the feasibility of changing the aerobrake surface area. One concept that has been proposed for controlling the aerobrake area is to use an inflatable elastic aerobrake (called a ballute). An illustration of a ballute aerobrake is shown in figure 3-10 [25].

Each of the three control strategies has advantages and disadvantages. The ideal control strategy would probably make use of all three types of control, but when realistic vehicle considerations are imposed this may not be possible. There has been considerable study of aerobrake trajectories which use only roll control. One possible reason is that roll control has been used almost exclusively for atmospheric reentry vehicles dating back to Project Mercury. Many of the computer programs used for reentry analysis can be modified to study aerobraking to orbit. A possible reason that pitch control has not received a high level of study in recent years could be the fact that the planned AFE will use only roll control. Pitch control also has the design problems posed by the

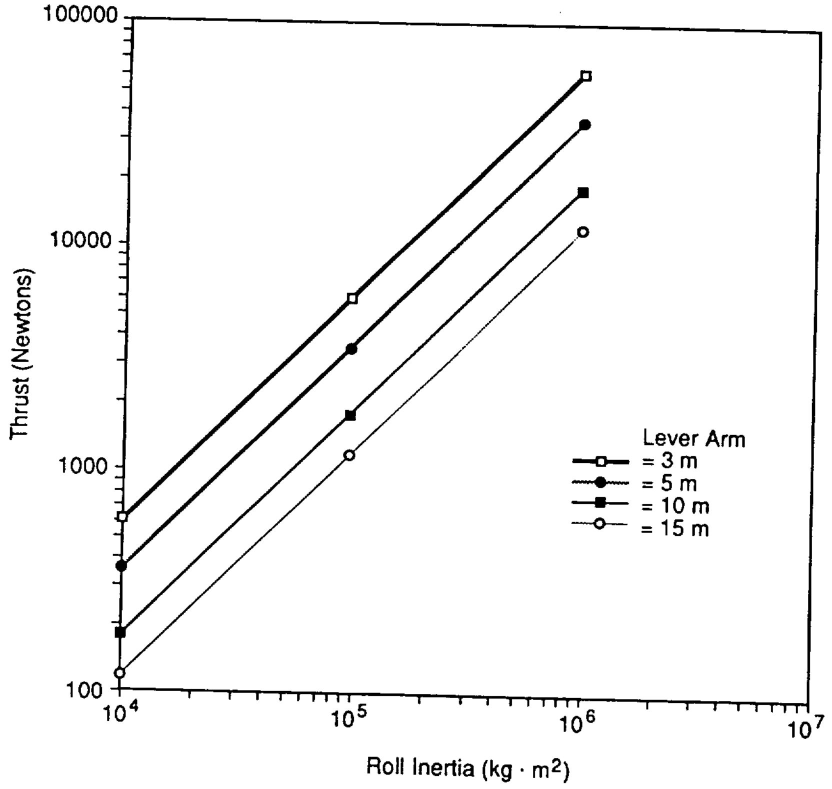

Figure 3-7. Required roll thrust for roll control [14].

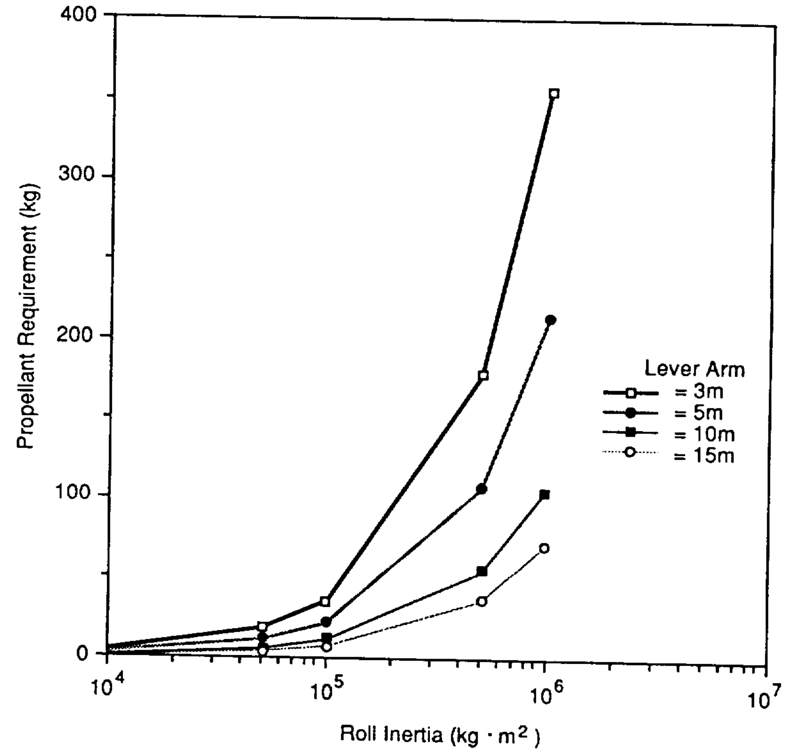

Figure 3-8. Propellant requirement for roll control [14].

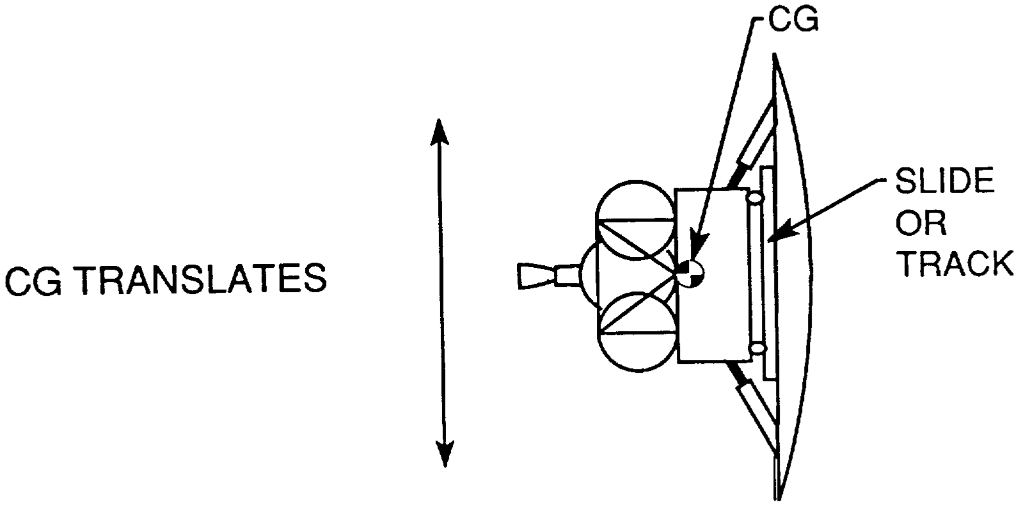

CG TRANSLATION

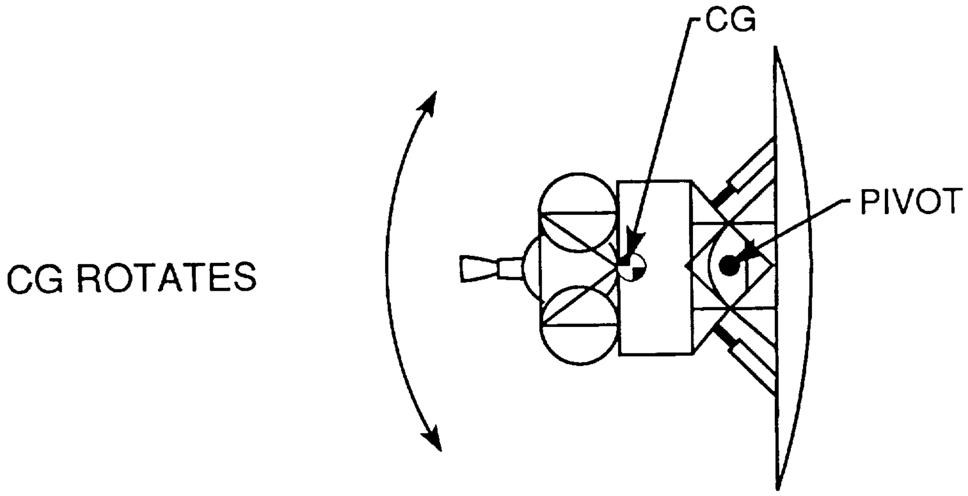

TILT CONTROL

Figure 3-9. Pitch control strategies.

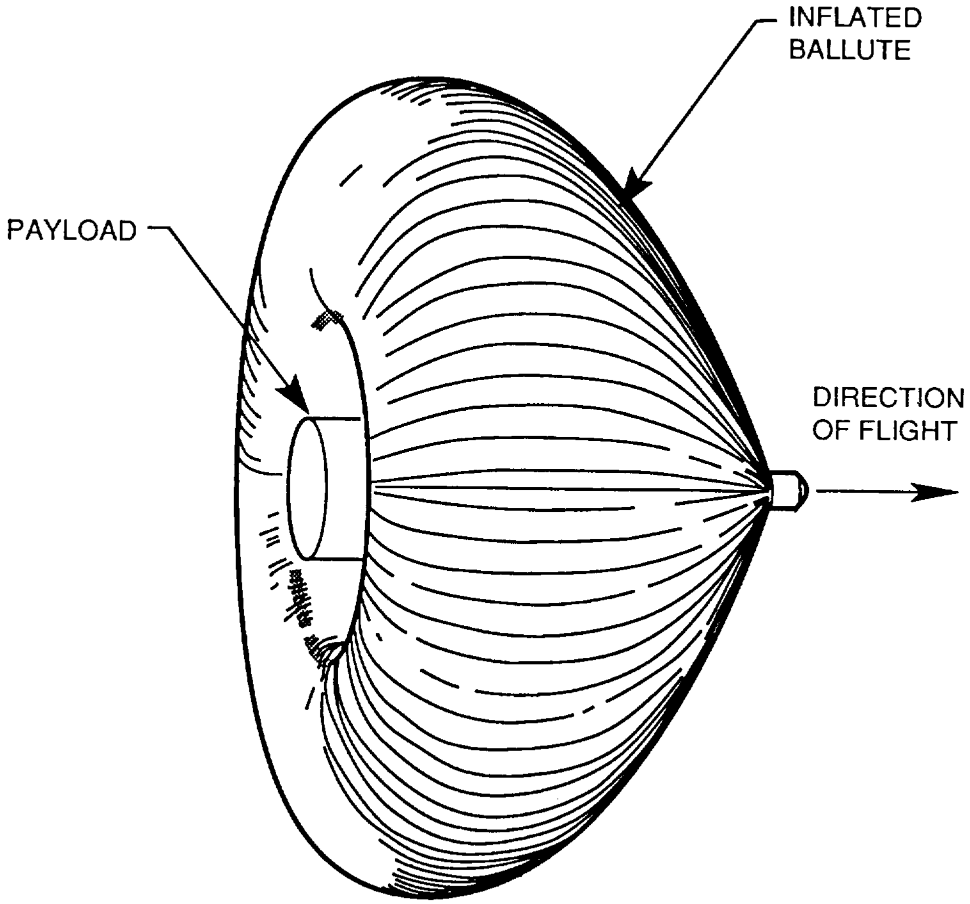

Figure 3-10. Ballute aerobrake [25].

control mechanisms which have hindered its popularity. Drag control was studied during the early 1980's in NASA's Space Transfer Vehicle studies, but the technological problems of the ballute have diminished its popularity.

Despite the fact that pitch control has not been as popular as roll control in recent aerobrake studies, there are several reasons that it may be more effective. These reasons can be illustrated by examining the differences between aerobraking to the surface (reentry) and aerobraking to orbit. These differences are summarized in figure 3-11. The most obvious difference is in the trajectory paths. In aerobraking to the surface, the trajectory becomes steeper during the reentry, while in aerobraking to orbit the trajectory remains almost parallel to the surface. Probably the most significant difference is in the velocities. In aerobraking to the surface, the velocity quickly decreases to suborbital speed, but in aerobraking to orbit, the velocity is always above orbital velocity. The target condition for a reentry trajectory is usually a specified landing site. Since the trajectory is always becoming more vertical, the reentry trajectory becomes less sensitive to velocity errors as long as the vehicle maintains the proper path. The target condition for an aerobraking to orbit is usually a specified apoapsis altitude at atmospheric exit. This altitude is very sensitive to both exit velocity and exit flight path angle. A small error in velocity due to guidance errors or atmospheric density variations results in a greatly amplified error in final apoapsis altitude.

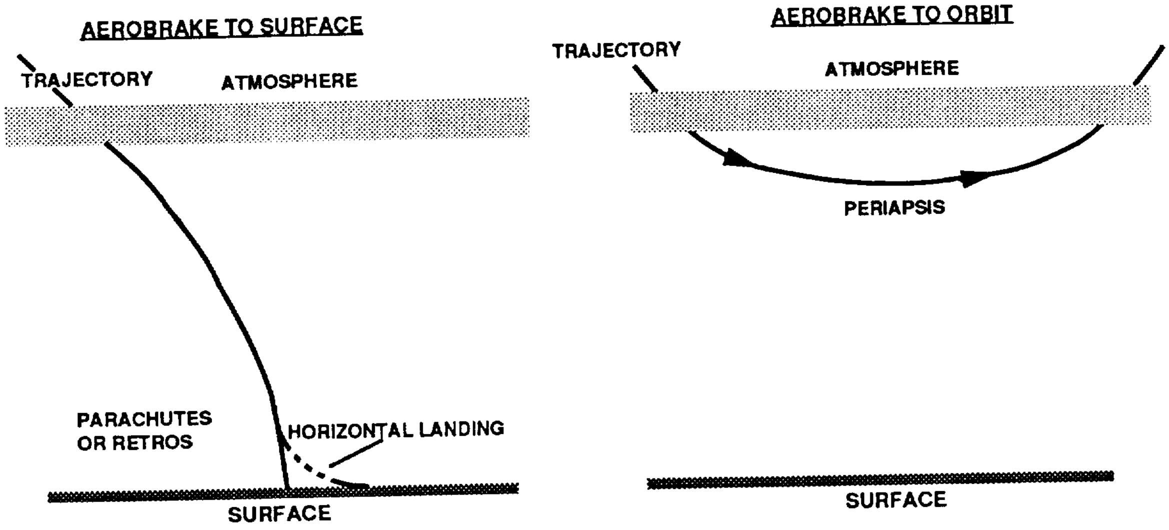

AEROBRAKE TO SURFACE	AEROBRAKE TO ORBIT
● TRAJECTORY APPROACHES VERTICAL	● TRAJECTORY IS ALMOST PARALLEL TO SURFACE
● VELOCITY RAPIDLY BECOMES SUB-ORBITAL	● VELOCITIES REMAIN ABOVE ORBITAL SPEED
● LANDING LOCATION LESS SENSITIVE TO VELOCITY ERRORS	● EXIT APOAPSIS HIGHLY SENSITIVE TO VELOCITY ERRORS
● ROLL CONTROL AT CONSTANT ANGLE OF ATTACK PROVIDES SUFFICIENT RESPONSE TIMES	● ROLL CONTROL AT CONSTANT ANGLE OF ATTACK MAY NOT PROVIDE ADEQUATE RESPONSE TIME FOR ATMOSPHERE UNCERTAINTIES
● HIGH ANGLE OF ATTACK FOR AEROBODY (LIFTING BODY) PROVIDES MORE DRAG, LESS AIR TIME	● HIGH ANGLE OF ATTACK FOR AEROBODY (LIFTING BODY) PROVIDES MORE DRAG. MORE AIR TIME
● LOW ANGLE OF ATTACK FOR AEROBRAKE PROVIDES MORE DRAG, LESS AIR TIME	● LOW ANGLE OF ATTACK FOR AEROBRAKE PROVIDES MORE DRAG, MORE AIR TIME

Figure 3-11. Differences between aerobraking to the surface and aerobraking to orbit.

The differences in sensitivity to velocity errors between reentry trajectories and aerobraking to orbit trajectories indicates the possibility that the two different types of aerobraking may require different guidance and control strategies. Trajectories for aerobraking to orbit appear to be much more sensitive to velocity errors. The control system needs fast response times. If roll control is used, the requirement to balance the lateral components of lift will add considerable complexity to the guidance strategy and increase the response time to compensate for trajectory errors. The factors that will have the greatest influence on the response time of a control strategy will be the aerodynamic properties of the aerobrake and the capabilities of the control mechanism (mechanical or RCS).

In the next section, the requirements of the aerobrake control system will be investigated. Several aerobrake trajectories will be modeled which will use variable angle of attack control strategies which approximate the optimum lift profile that has been described in this section.

IV. AEROBRAKE TRAJECTORY ANALYSIS

A. Trajectory Simulation (IMP Computer Program)

To investigate the relationships between aerobrake design factors and to develop approximations of the flight characteristics of aerobraked vehicles, it is necessary to mathematically model their trajectories through the atmosphere. The particular methods used to perform this modeling depend on the type of data that is desired and the level of accuracy needed. If the only data that is required is a reasonable approximation of propellant consumption, detailed trajectory data is not necessary, but, if vehicle loads or control requirements are being investigated, then an accurate trajectory must be calculated. This requires careful modeling of the forces on the vehicle and the atmosphere in which the vehicle flies.

The trajectory data that are included in this report were developed using numerical simulations of the aeropasses. The desired output consisted of vehicle loads and orbit conditions at atmospheric exit. Vehicle characteristics, entry conditions, and atmospheric density were varied in order to investigate the sensitivities of the trajectory and vehicle loads. The trajectory data that were developed will be described in detail later.

The computer program used to model the aerobrake trajectories is called IMP (Integrated Mission Program). It is a simulation language used to model orbital missions about Earth, Mars, or the Moon [26]. It was developed by Vince Dauro of MSFC and is used in many preliminary design studies. IMP uses a Fehlberg seventh-order, 13-evaluation Runge-Kutta integrator with error and step size control [27] to integrate the equations of motion of an orbital vehicle. The equations of motion include the accelerations listed below [26].

Earth:	Earth's gravity Sun's gravity Moon's gravity Atmosphere (aerodynamic forces) Solar pressure
Mars:	Mars' gravity Sun's gravity Atmosphere Solar pressure.

For aerobraking trajectories the acceleration due to solar pressure is not applicable.

The orbital parameters are computed as smoothed mean values using up to a sixth-order gravity model to simulate the Earth or Mars gravity field. Earth's gravitational potential field is computed with J through J4 constants. The Mars gravitational field is computed using the J and J2 constants [26].

B. Atmosphere Modeling

1. Atmosphere Models

In order to compute the atmospheric trajectories, it is necessary to use an atmosphere model in the program. There are several atmosphere models which can be used within the IMP program. These models provide a density profile as a function of altitude. Accurate modeling of the atmospheric density is of paramount importance in aerobrake analysis since the drag is proportional to the density [28]. The atmosphere models which can be selected for use by the program are listed below:

Earth:	U.S. 1962 Standard Atmosphere Jacchia
Mars:	COSPAR Mars cool-low (temperature-pressure) COSPAR Mars warm-high MSFC Mars Gram.

In each of the atmosphere models, the density altitudes are calculated spherically [26]. In this report, the U.S. 1962 Standard Atmosphere was used for Earth aerobraking missions, and the Mars cool-low atmosphere was used for the Mars aerobraking missions. The U.S. 1962 atmosphere is defined in terms of an ideal air, assumed to be devoid of moisture, water vapor, and dust [29]. The density profile shown in figure 4-1 was derived from the calculated values of pressure and molecular-scale temperature. The top of the Earth's atmosphere was assumed to be 121-km altitude. Above this altitude, the atmospheric drag force can be neglected for aerobrake missions.

The COSPAR Mars atmosphere models provide envelopes around the excursions of temperature and density measured by the Viking probes during aerobraking and descent. They represent the best knowledge of the range of temperature and density from near 100-km altitude down to the surface. The density of the upper atmosphere of Mars was calculated using an estimate of the ultraviolet radiation on the atmosphere since the ultraviolet insolation has a greater effect on the exospheric temperature and density than the surface pressure [28]. The density profile is shown in figure 4-2, which was constructed from data in reference 30.

2. Density Variations

The atmosphere models that were chosen provide nominal or baseline density profiles that can be used in determining the sensitivity of the trajectory to vehicle characteristics or entry conditions. The actual atmospheric densities vary widely due to factors such as time of day or year and solar activity. Figure 4-3 shows that density variations of up to ±50 percent from the nominal value are possible in the range of altitudes where aerobraking would take place in the Earth's atmosphere [2]. There is a similar range of atmospheric density variation in the Mars atmosphere. Aerobraked vehicles must be designed to operate over these wide ranges of atmospheric conditions.

The amount of departure from the nominal density profile is not constant with altitude. Data from space shuttle flights have indicated "potholes in the sky" as shown in figure 4-4. These diagrams show the amount of departure from the U.S. 1962 standard atmosphere density profile. The Viking entry measurements showed the same type of oscillatory density variations in the Mars atmosphere [28]. These variations are also shown in figure 4-4. These large density excursions,

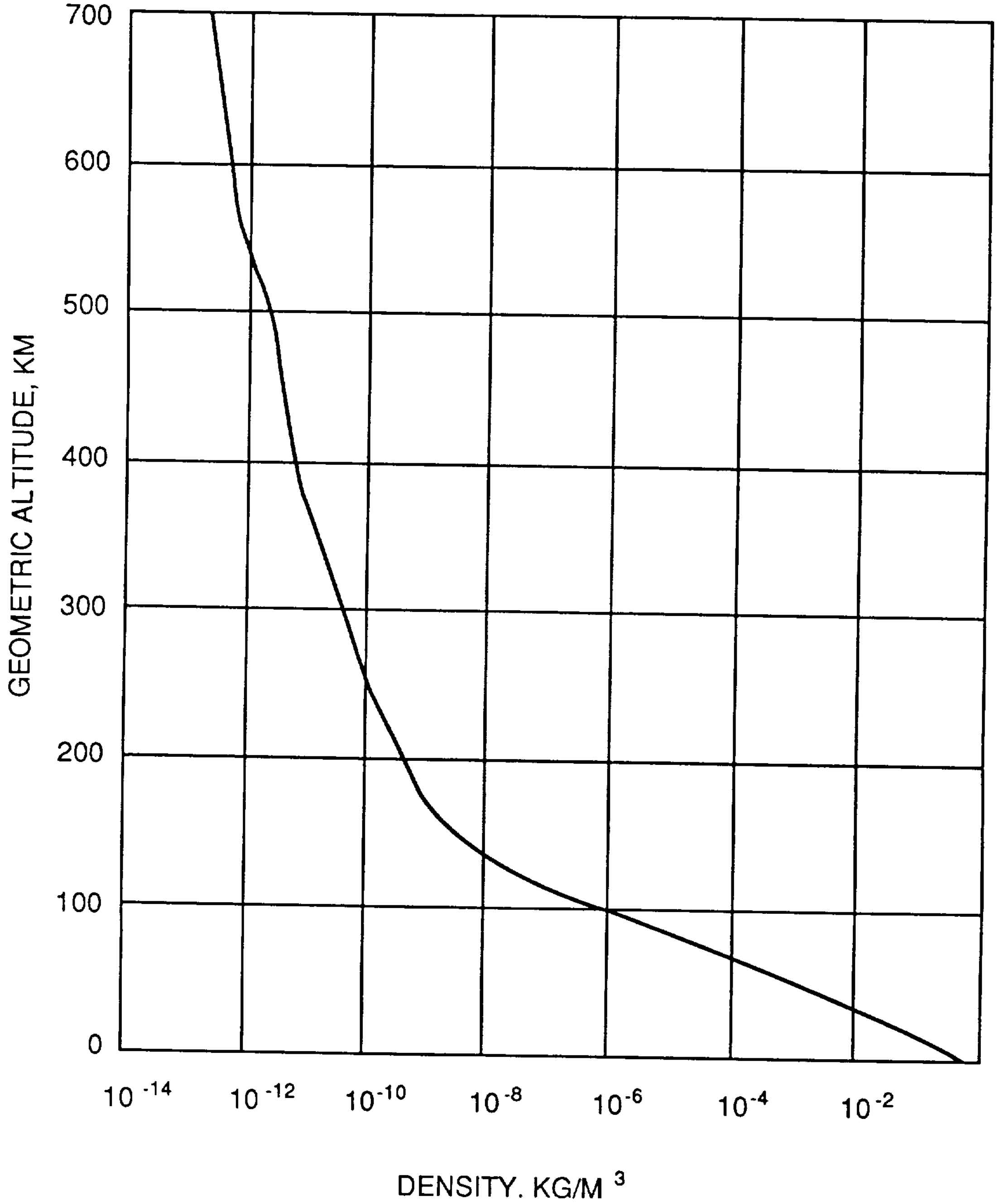

Figure 4-1. U.S. 1962 standard atmosphere density profile [29].

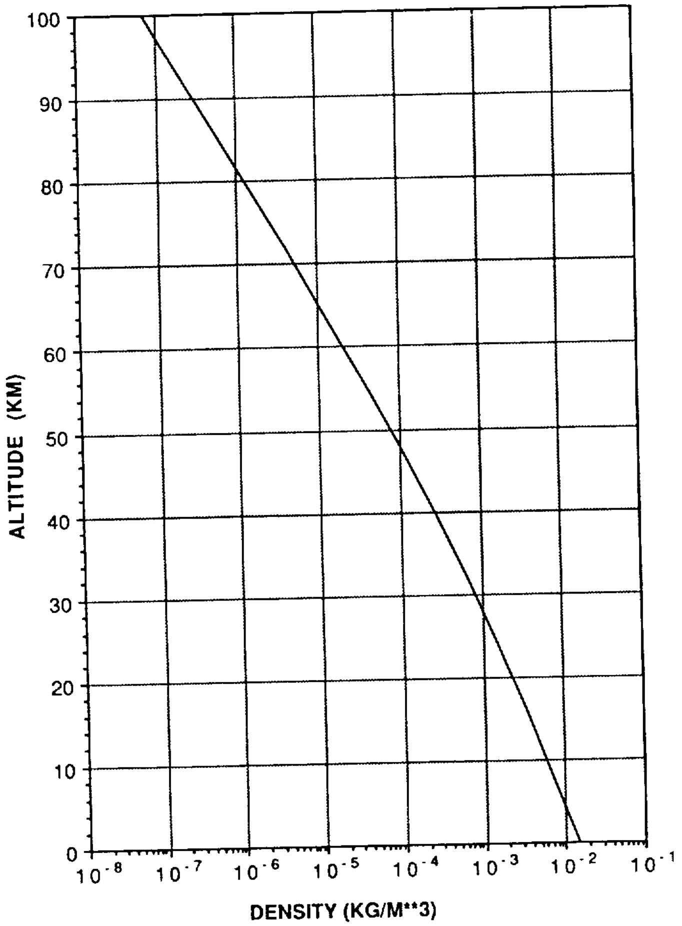

Figure 4-2. COSPAR Mars cool-low atmosphere density profile.

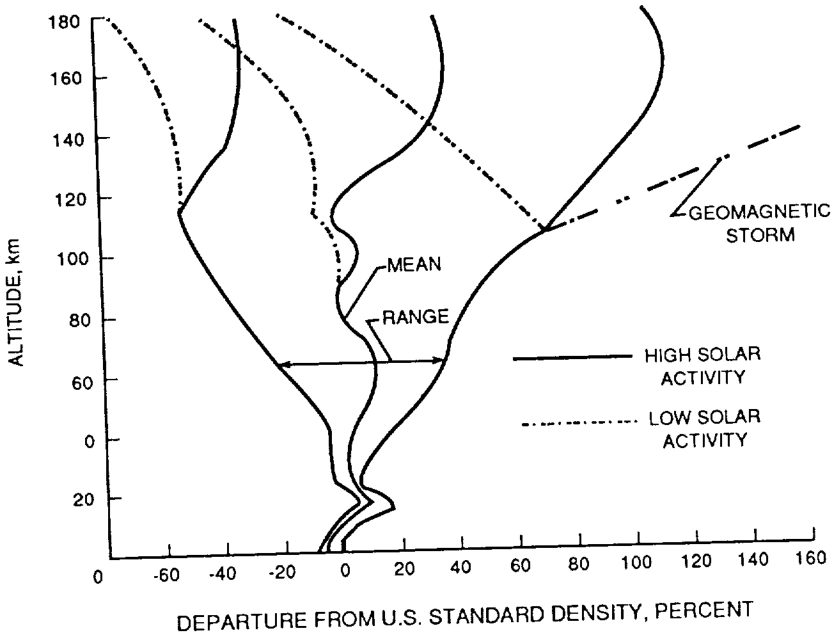

Figure 4-3. Range of Earth atmosphere density variations [2].

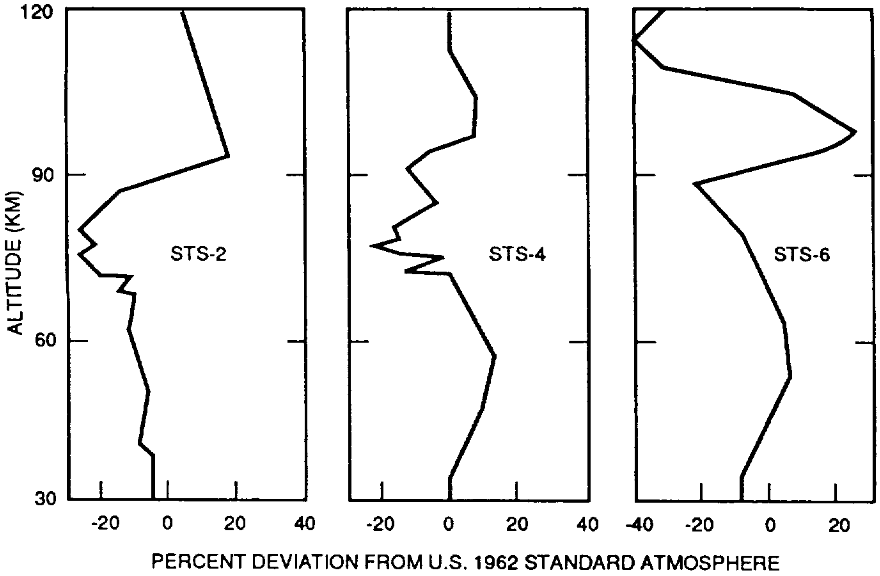

Shuttle Derived Density Variations During Reentry (Reference 2)

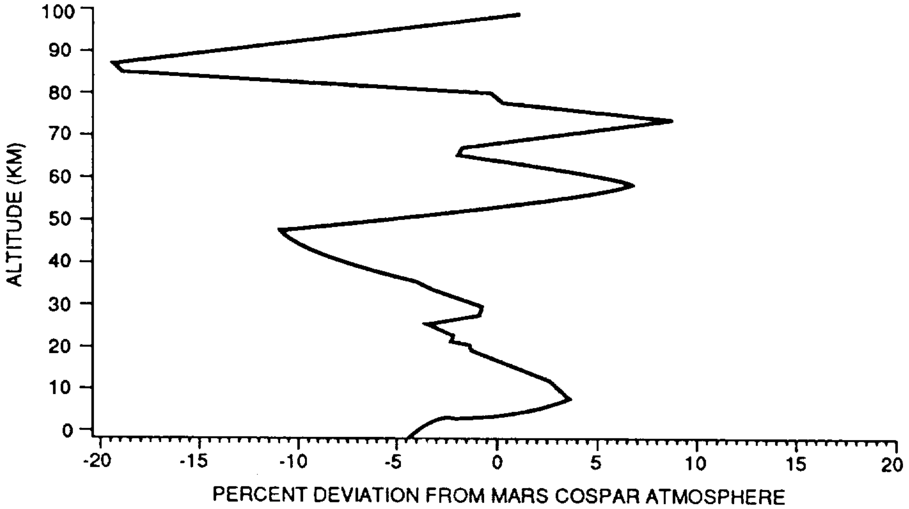

Viking 2 Derived Density Variations During Reentry (Reference 28)

Figure 4-4. Atmospheric density variations during reentry.

which occur over relatively narrow altitude ranges, pose a significant challenge in the design of aerobrake control systems [2]. Since it will be difficult to predict the atmospheric conditions ahead of the vehicle, sophisticated adaptive control laws may be required [2].

Recently, aerobrake guidance and control system design has received intensive study. The central issue in guidance and control system design is the amount of aerodynamic control authority required to contend with unpredictable variations in atmospheric density. This report will not attempt to define a guidance law that could be used in an actual aerobrake mission. Instead, only the bounds of the requirements for the control systems will be investigated. This will be accomplished by investigating the capabilities of low L/D aerobrakes for several aerobrake applicationns. As an initial step in this analysis, it is necessary to determine the sensitivity of aerobrake trajectories to entry conditions, vehicle characteristics, and atmospheric conditions. The following section will show trajectory data that were generated to investigate the relationships between several aerobrake parameters.

C. Aerobraking Trajectory Analysis

Numerical simulations of aerobrake trajectories were used to analyze four applications of aerobraking. These applications were return from geosynchronous orbit, return from lunar orbit, Earth aerocapture from a hyperbolic orbit, and Mars aerocapture from a hyperbolic orbit. The analysis consisted of identifying the sensitivity of the apoapsis altitude at atmospheric exit to the incoming target vacuum periapsis altitude and the vehicle angle of attack. The vacuum periapsis represents the periapsis altitude of the orbit if there was not an atmosphere present. The peak vehicle loads during the aeropass were also investigated. These loads included the peak acceleration load, the peak stagnation point temperature, the peak dynamic pressure, and the peak stagnation point convective heating rate. The sensitivity of these loads to entry conditions, ballistic coefficient, and angle of attack was investigated using a wide range of constant and variable angle of attack trajectories. The analysis was completed with an investigation of the effect of atmospheric density variations on the range of allowable target periapsis altitudes and the definition of a target vacuum periapsis tolerance to allow for these variations.

The data for return from geosynchronous orbit are representative of atmospheric entry from an elliptical transfer orbit with an apoapsis altitude of 35,876 km and a target vacuum periapsis inside the Earth's atmosphere. The data for return from lunar orbit is representative of atmospheric entry from a transfer orbit from the Moon, with an apoapsis altitude of 385,747 km. The data for Earth aerocapture covers the range of entry conditions for an atmospheric entry from a hyperbolic orbit representative of a return from Mars. Similarly, the Mars aerocapture data covers the range of entry conditions representative of a transfer from Earth.

Table 4-1 lists the orbital and vehicle characteristics that were used in the trajectory simulations. The range of ballistic coefficients and mission energies (represented by C_3's) were derived from studies performed at MSFC from 1983 to the present. The aerodynamic properties of the vehicle were based on the spherical, Apollo style aerobrake. The angle of attack range yields low L/D's between 0.0 and 0.25, with the lift directed upward or downward. The heating rate calculations are based on the stagnation point convective heating rate defined by equation (3-31). A nose radius of 15 m was used.

1. Sensitivity of Trajectory to Entry Conditions and Vehicle Characteristics

Figures 4-5 through 4-11 show the sensitivity of the orbit apoapsis altitude at atmospheric exit to target vacuum periapsis altitude for various ballistic coefficients and angles of attack for each of the aerobrake applications. These data were generated assuming a constant angle of attack for the entire aeropass. In reality, this would not be possible for reasons that will soon become obvious. The data for angles of attack of −15° (lift upward) clearly show that as the target vacuum periapsis increases, the exit apoapsis increases. Also, the exit apoapsis becomes much more sensitive to target periapsis as the periapsis altitude increases. It approaches a point where the exit apoapsis is so large that it is difficult to see a relation between target periapsis and exit apoapsis. This sensitivity increases as angle of attack becomes more positive. In most cases, the curves for angles of attack of 10° or 15° (lift down) are almost vertical lines.

The extreme sensitivity of exit apoapsis to target periapsis altitude indicates that it would not be realistic to use a constant angle of attack (constant L/D) trajectory. This is especially true in the case of aerobrake applications where the desired exit apoapsis altitude is high. In many aerocapture studies, it is assumed that the vehicle would aerobrake into a highly elliptical orbit with

Table 4-1. Trajectory analysis parameters.

MISSION	C3 (KM**2 /S**2)	BALLISTIC COEFFICIENT (KG/M**2)	ANGLES OF ATTACK (DEG)
GEO RETURN	N/A	50	-15,0,15
		100	-15,-10,-5,0,5,10,15
		200	-15,0,15
LUNAR RETURN	N/A	50	-15,0,15
		100	-15,-10,-5,0,5,10,15
		200	-15,0,15
EARTH AEROCAPTURE	10	50	-15,0,15
		100	-15,-10,-5,0,5,10,15
		200	-15,0,15
	50	50	-15,0,15
		100	-15,-10,-5,0,5,10,15
		200	-15,0,15
MARS AEROCAPTURE	10	50	-15,0,15
		100	-15,-10,-5,0,5,10,15
		200	-15,0,15
	25	50	-15,0,15
		100	-15,-10,-5,0,5,10,15
		200	-15,0,15
	40	50	-15,0,15
		100	-15,-10,-5,0,5,10,15
		200	-15,0,15

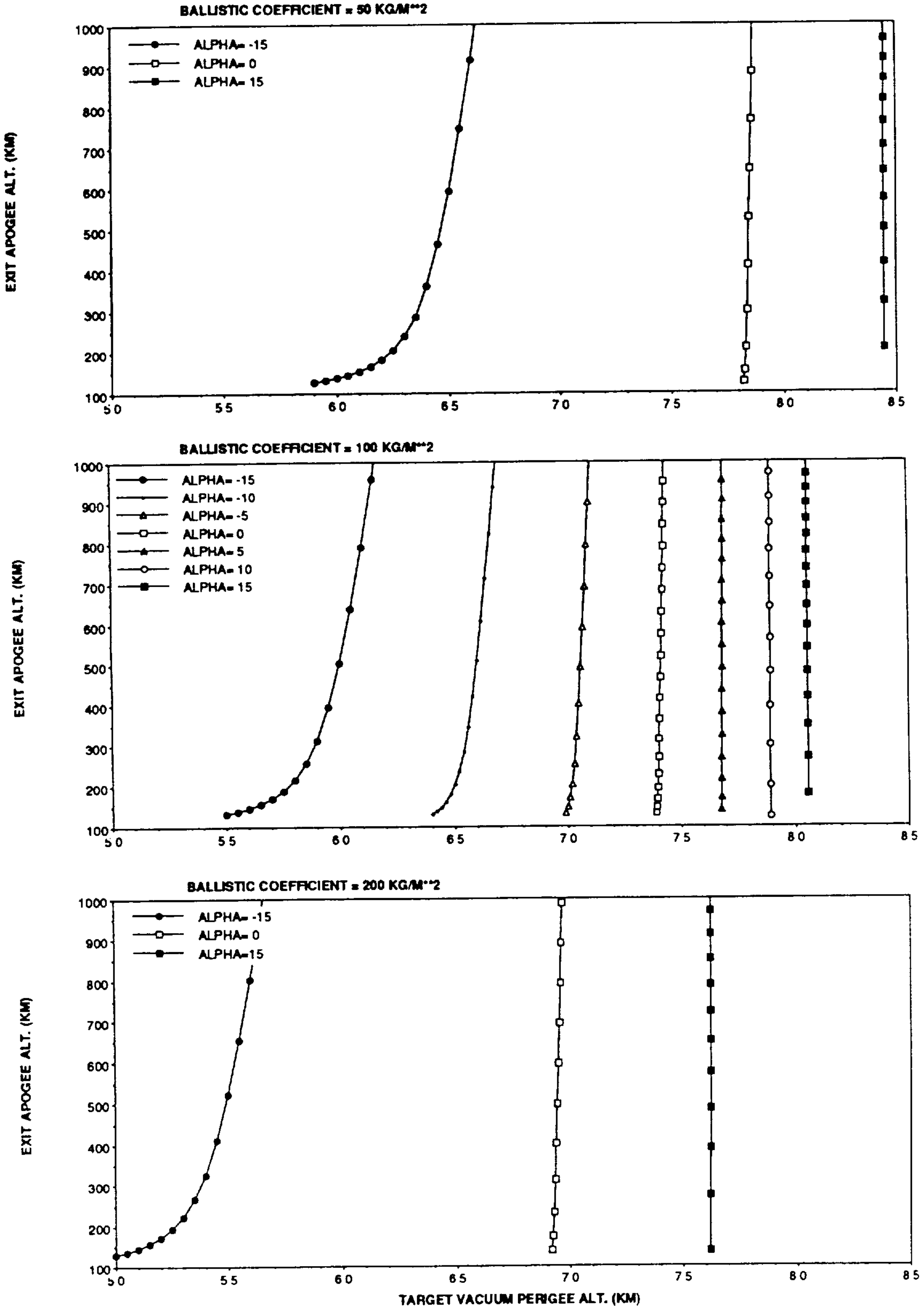

Figure 4-5. GEO return aerobraking—exit apoapsis as a function of target vacuum periapsis.

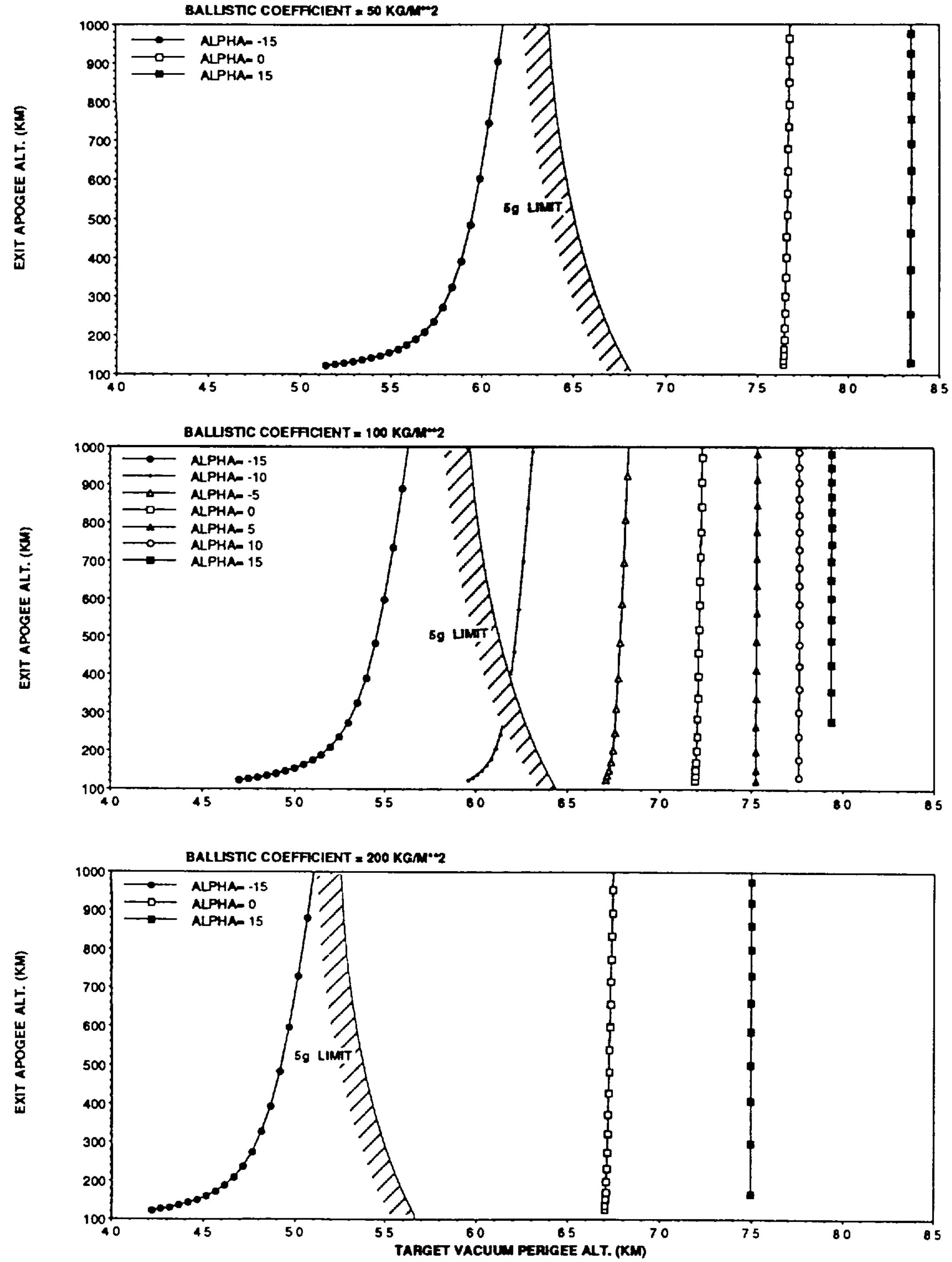

Figure 4-6. Lunar return aerobraking—exit apoapsis as a function of target vacuum periapsis.

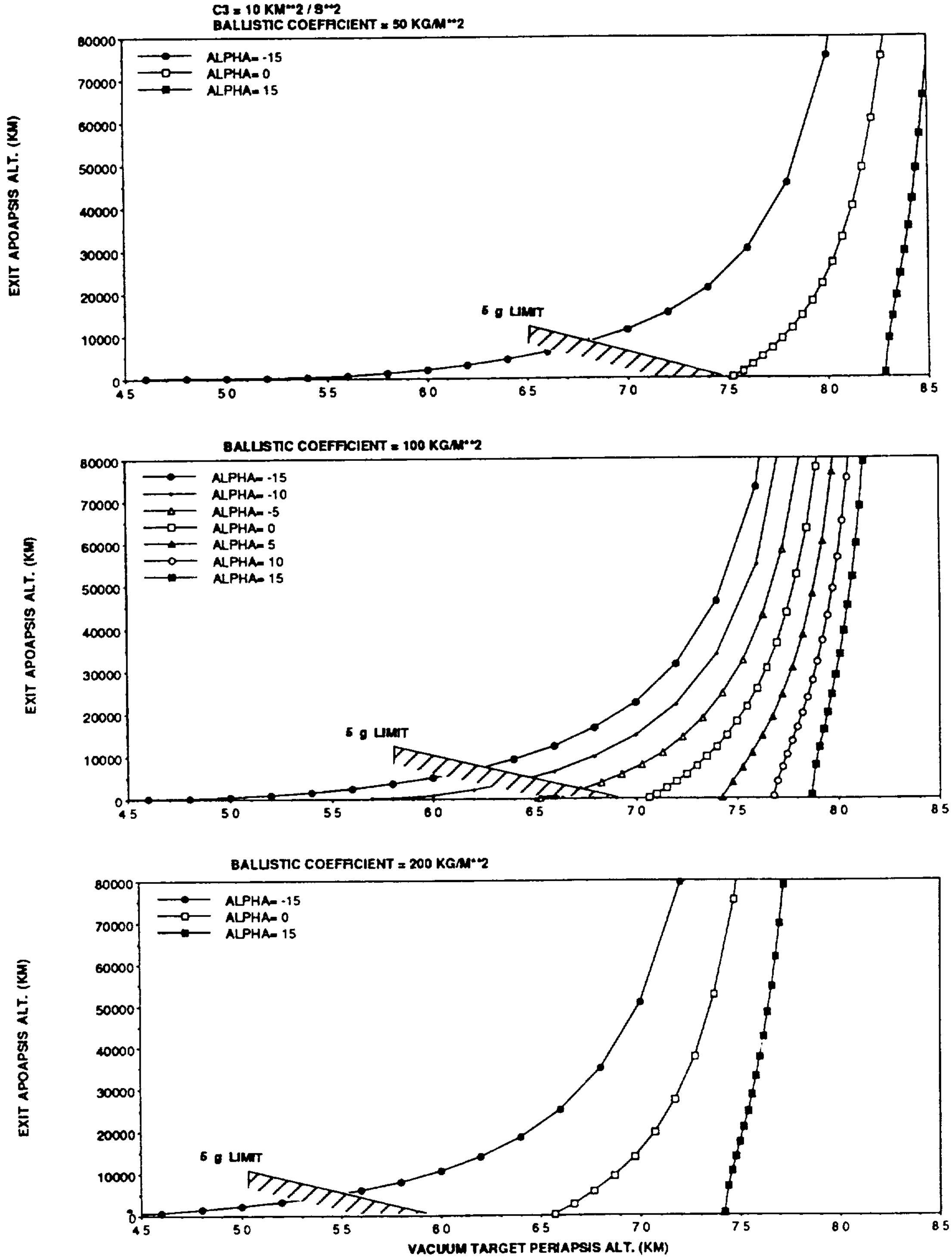

Figure 4-7. Earth aerocapture—exit apoapsis as a function of target vacuum periapsis at $C_3 = 10\ km^2/s^2$.

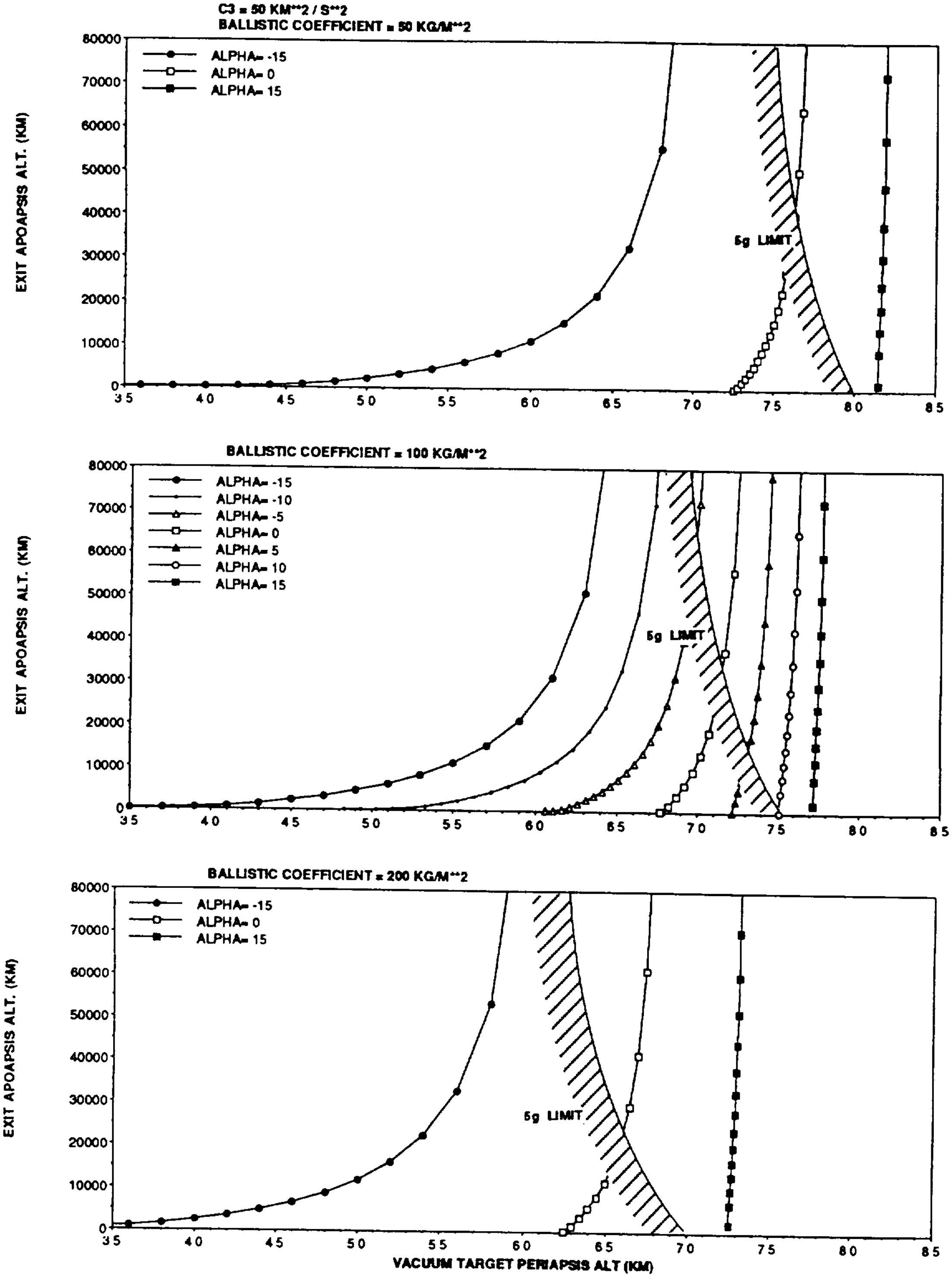

Figure 4-8. Earth aerocapture—exit apoapsis as a function of target vacuum periapsis at $C_3 = 50\ km^2/s^2$.

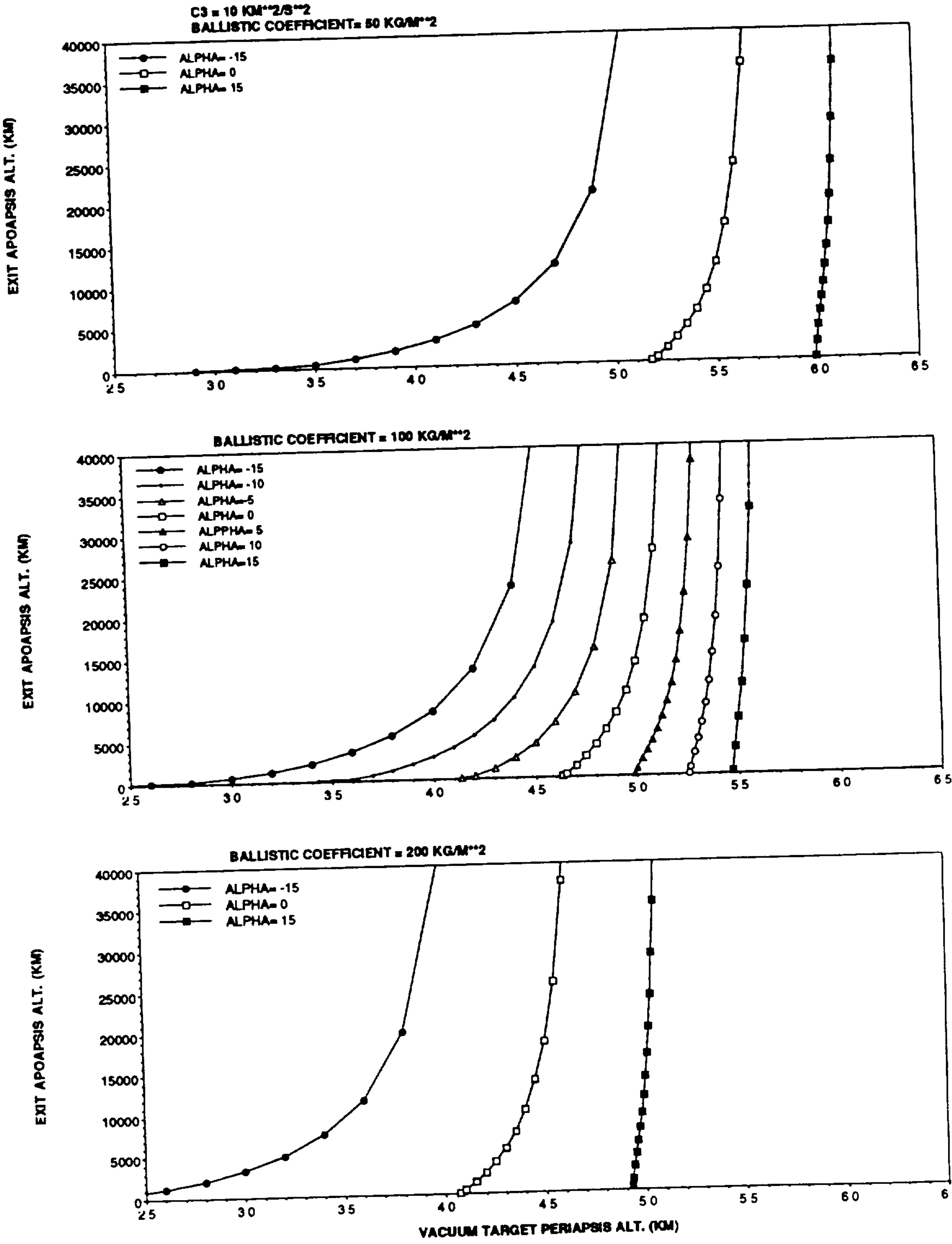

C3 = 10 KM**2/S**2
BALLISTIC COEFFICIENT= 50 KG/M**2

BALLISTIC COEFFICIENT = 100 KG/M**2

BALLISTIC COEFFICIENT = 200 KG/M**2

Figure 4-9. Mars aerocapture—exit apoapsis as a function of target vacuum periapsis at $C_3 = 10$ km^2/s^2.

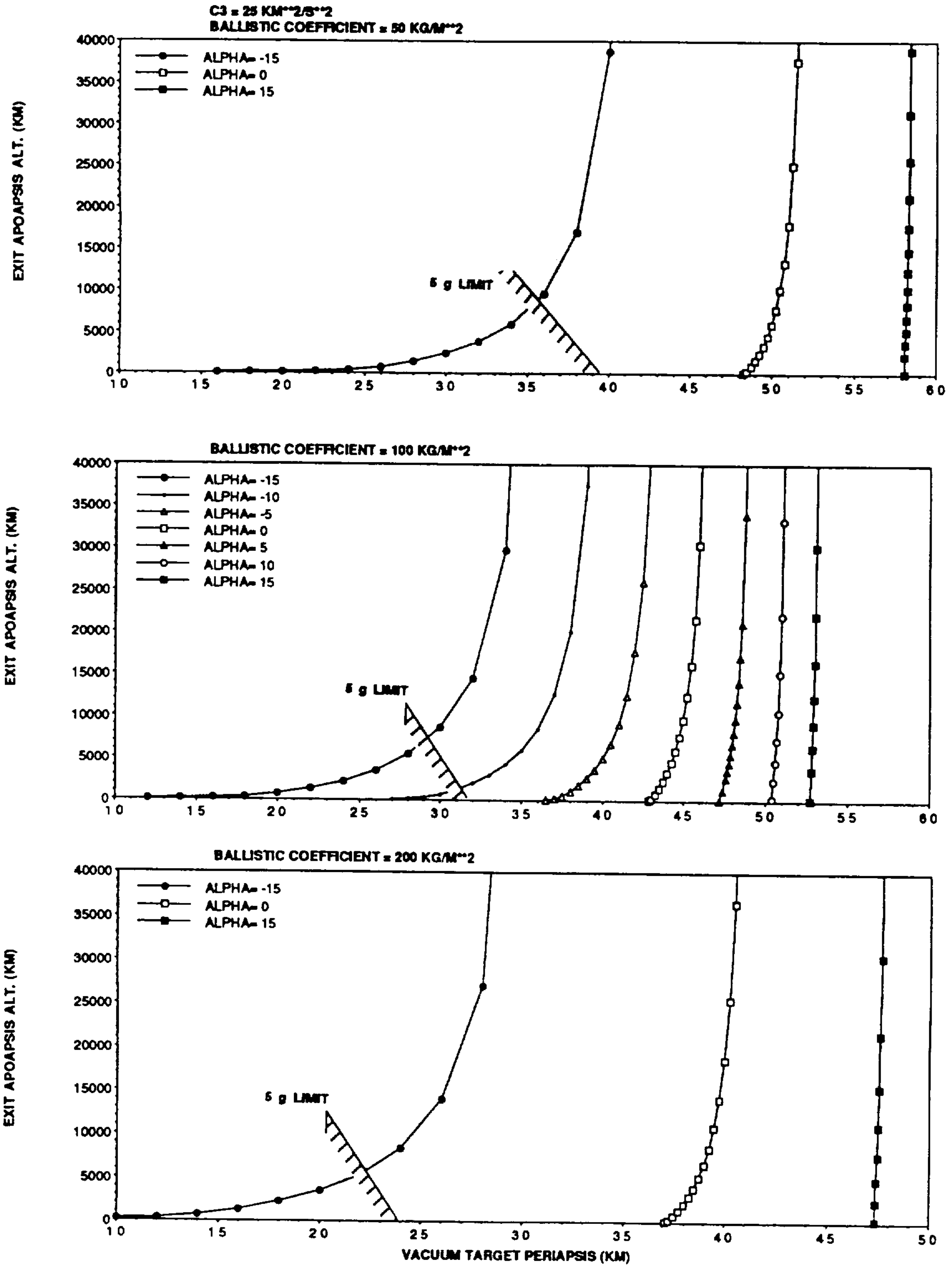

Figure 4-10. Mars aerocapture—exit apoapsis as a function of target vacuum periapsis at $C_3 = 25\ km^2/s^2$.

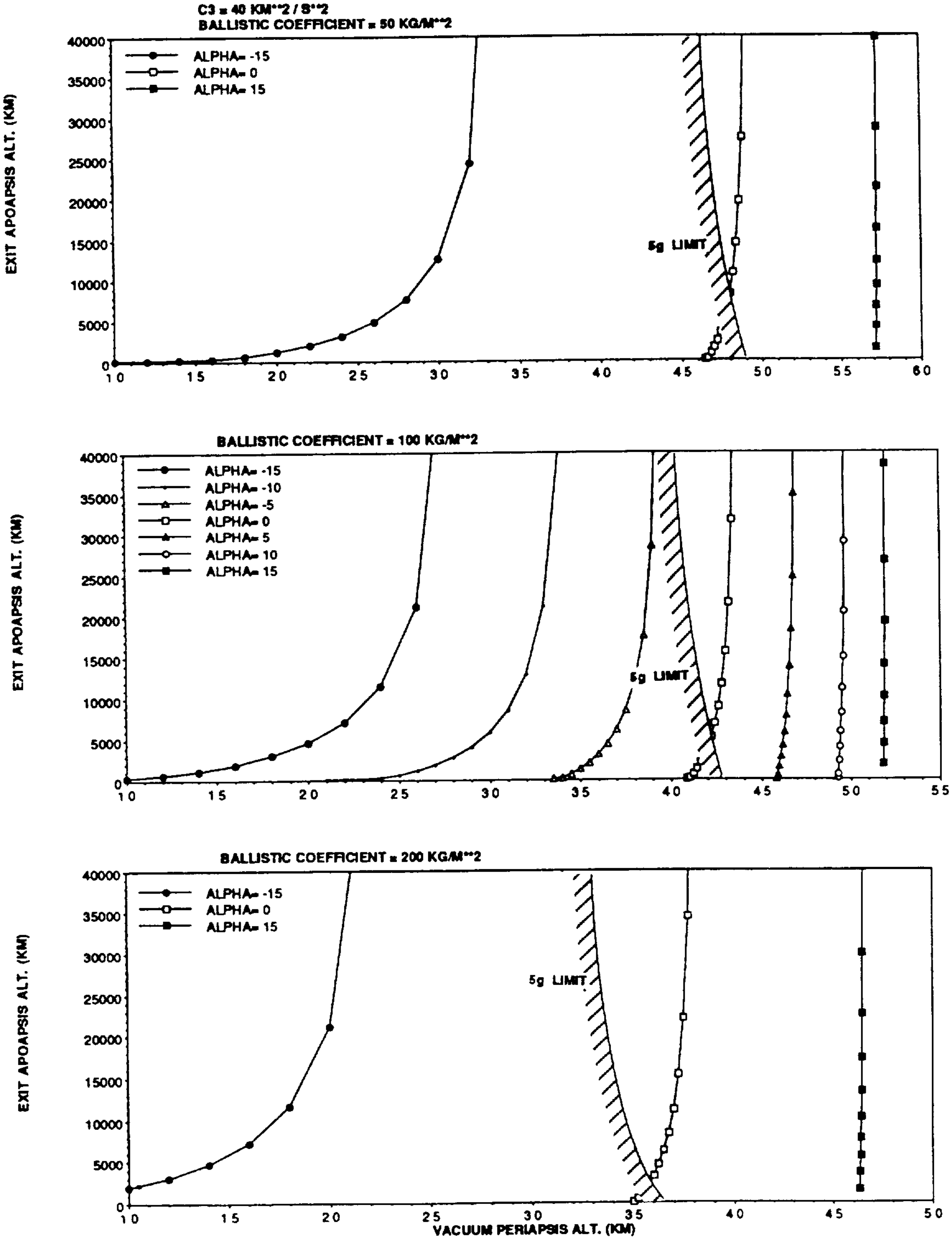

Figure 4-11. Mars aerocapture—exit apoapsis as a function of target vacuum periapsis at $C_3 = 40\ km^2/s^2$.

a period of 1 day. This would require an exit apoapsis altitude of 71,200 km for Earth aerocapture or an apoapsis altitude of 33,800 km for Mars aerocapture. The data do not provide any indication of what the guidance scheme would be, but they do indicate a bound for the amount of control that is required. If the target vacuum periapsis is in the range defined by the −15° and 15° angle of attack curves, then there is an angle of attack within that range which would yield any desired exit apoapsis altitude. A successful guidance scheme would have to vary the angle of attack to continually adjust the trajectory during the aeropass.

A constraint on the allowable range of target vacuum periapsis altitudes and angles of attack is the acceleration load experienced by the vehicle. The points at which the acceleration loads exceed five Earth "g's" (five times the acceleration due to gravity at the Earth's surface) are shown on the graphs where applicable. These g-limits decrease the range of target periapsis altitudes that can be used. These limits were plotted assuming constant angle of attack trajectories. In section III, it was shown that the peak acceleration load occurs just before the vehicle reaches periapsis. Therefore, it is possible to avoid exceeding the acceleration load limit by using a variable angle of attack trajectory which allows the use of a higher target periapsis altitude for the atmospheric entry. This was basically the approach used by Vinh and Lu that was described in section III.

Another factor that affects the range of allowable target vacuum periapsis altitudes is the vehicle ballistic coefficient. The data in figures 4-5 through 4-11 show that for a given angle of attack, it is necessary to decrease the target periapsis altitude as ballistic coefficient increases. An increase in the ballistic coefficient also results in a shift of the acceleration load limit boundary. This means that for a given target periapsis altitude, the peak acceleration load decreases as ballistic coefficient increases. Unfortunately, other vehicle loads increase as ballistic coefficient increases, so a tradeoff must be made in selecting a vehicle ballistic coefficient. The effect of ballistic coefficient on the vehicle loads was investigated and results are shown in the next set of figures.

2. Vehicle Loads

Figures 4-12 through 4-18 show the vehicle loads at various angles of attack and ballistic coefficients. As was the case for the previous set of data, these data were generated assuming constant angle of attack trajectories. The loads for variable angle of attack trajectories would usually be less. The vehicle loads that were investigated included the maximum acceleration load, $g_{\max}$; the maximum stagnation point temperature, $T_{0_{\max}}$; and the maximum dynamic pressure, $q_{\max}$. Where it is necessary, the 5-g acceleration limit and the maximum temperature limit of current reusable thermal protection systems (1,645 K) are indicated on the graphs. No limit for the maximum dynamic pressure is indicated since that is usually a function of vehicle design.

The loads in figures 4-12 and 4-13 are based on an assumed exit apoapsis altitude range from 120 to 1,000 km. In reality, the loads decrease as exit apoapsis altitude increases, but for the range of exit apoapsis altitudes considered, the decrease is usually not significant. The data for the aerocapture applications, figures 4-14 through 4-18, have a slightly different format. A range of vehicle loads are depicted for a range of exit apoapsis altitudes, from the top of the atmosphere to about 100,000 km. The loads are shown for three angles of attack and three ballistic coefficients. The maximum load indicated at the top of each bar corresponds to a low exit apoapsis altitude, and the maximum load indicated by the bottom of each bar corresponds to a high exit apoapsis altitude.

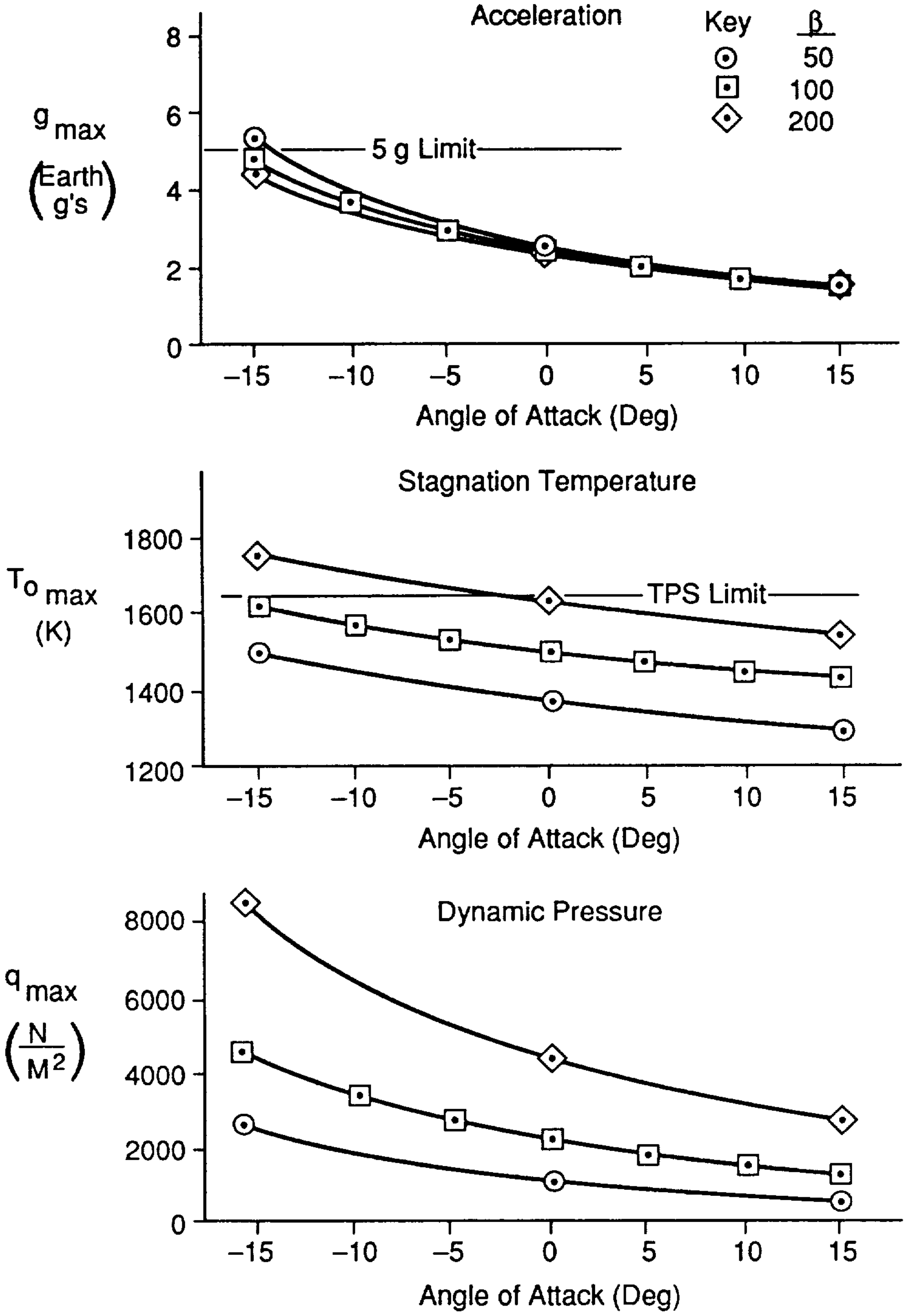

Figure 4-12. GEO return aerobraking vehicle loads.

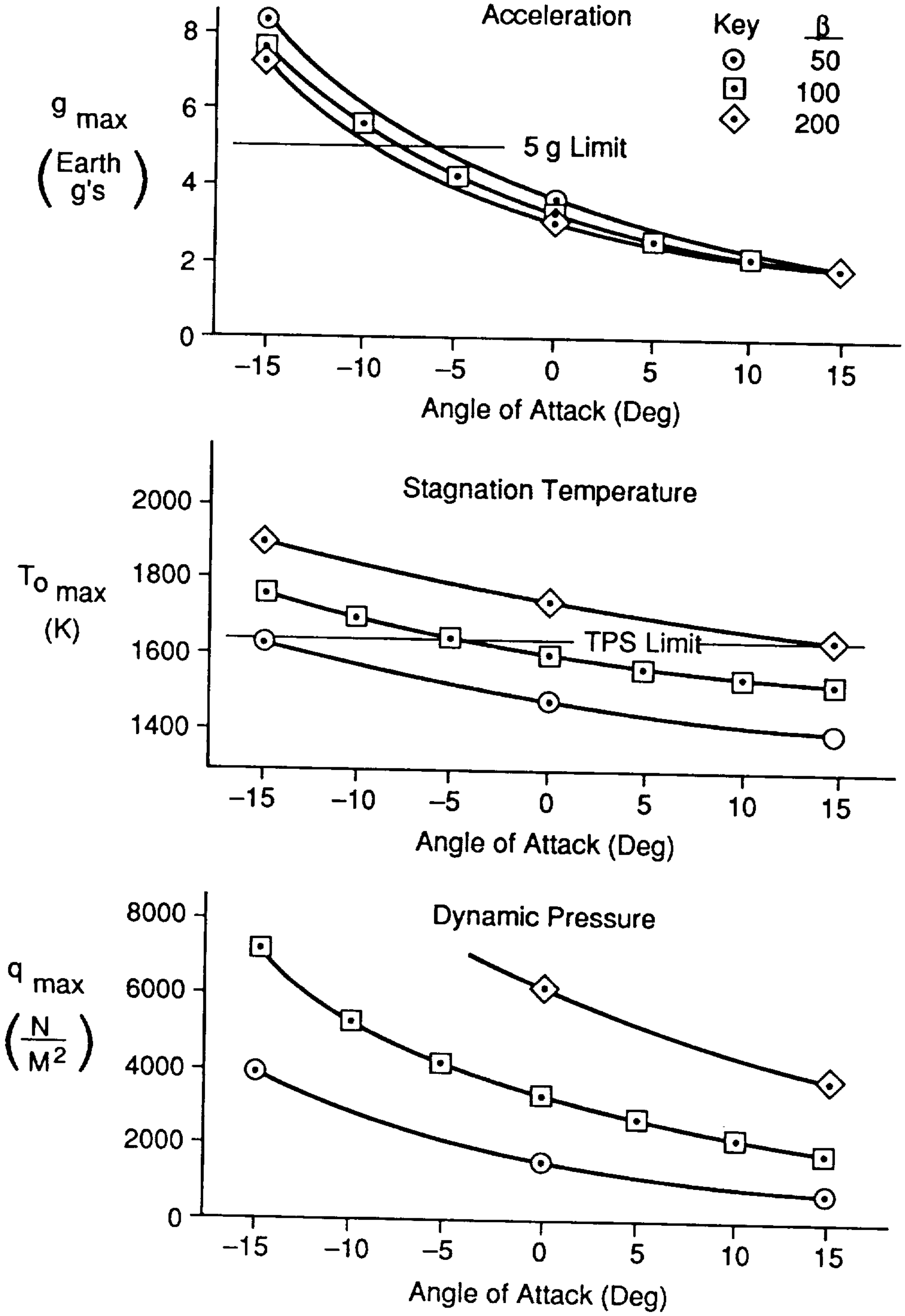

Figure 4-13. Lunar return aerobraking vehicle loads.

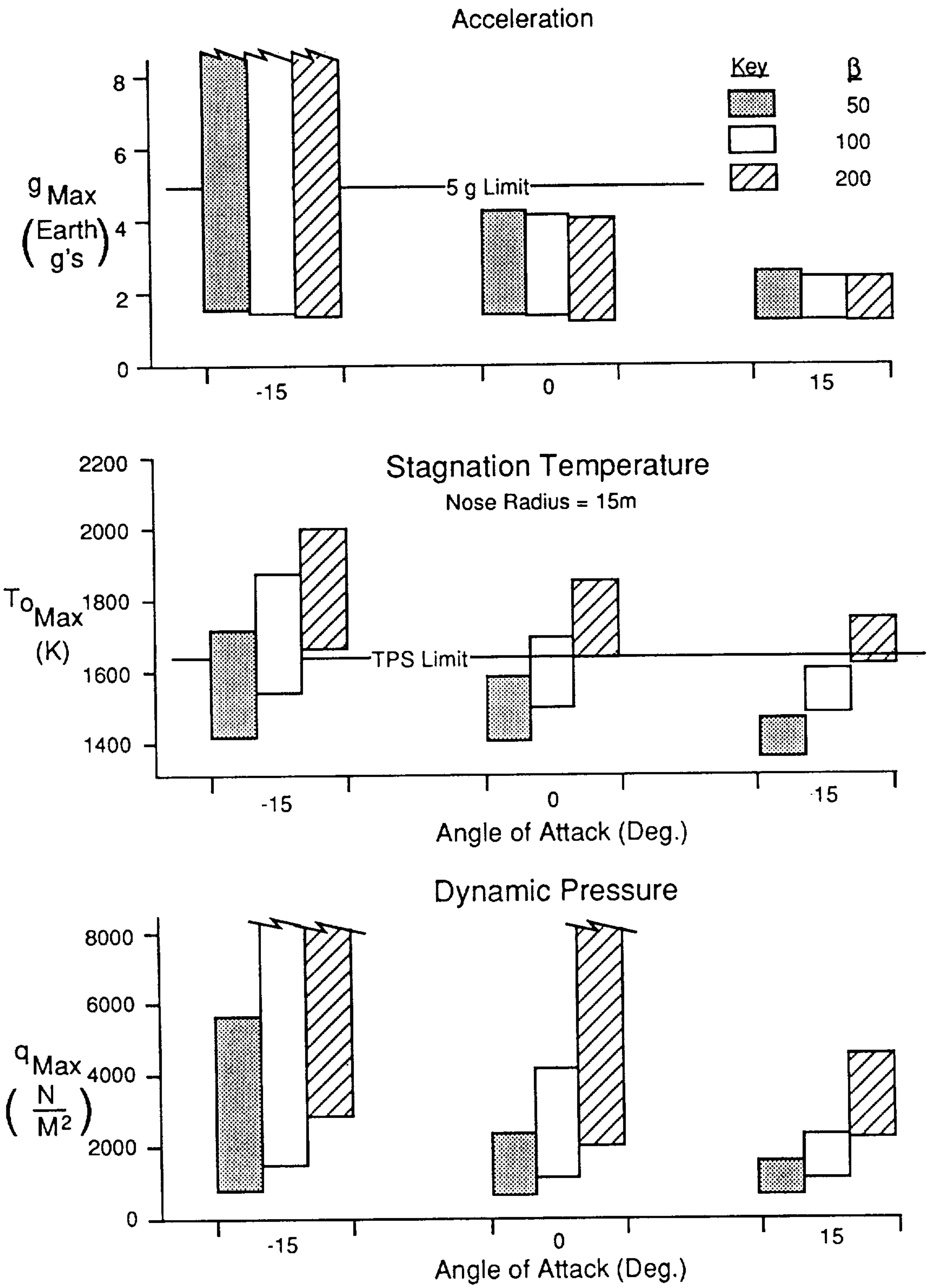

Figure 4-14. Earth aerocapture vehicle loads, $C_3 = 10\ km^2/s^2$.

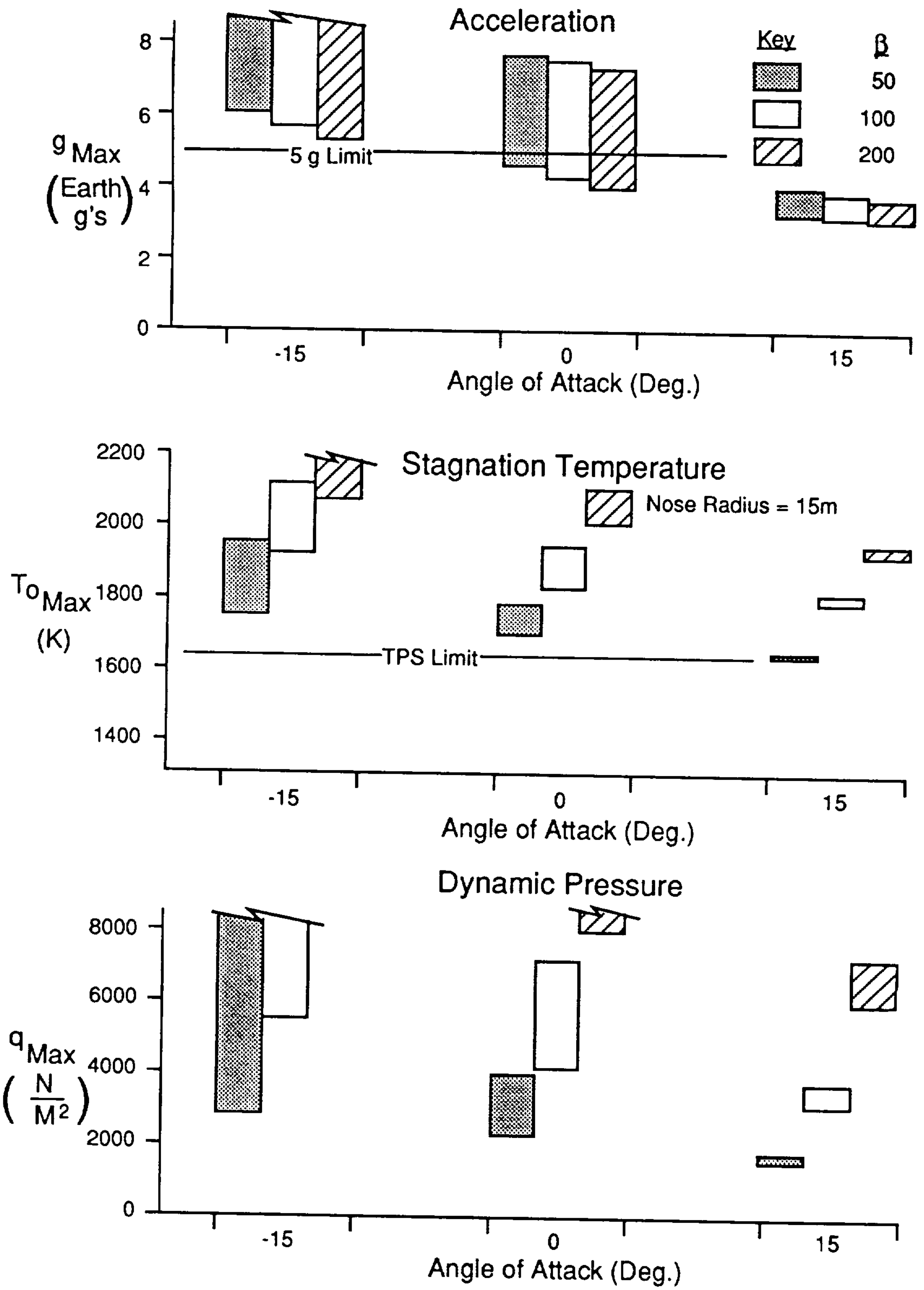

Figure 4-15. Earth aerocapture vehicle loads, $C_3 = 50\ km^2/s^2$.

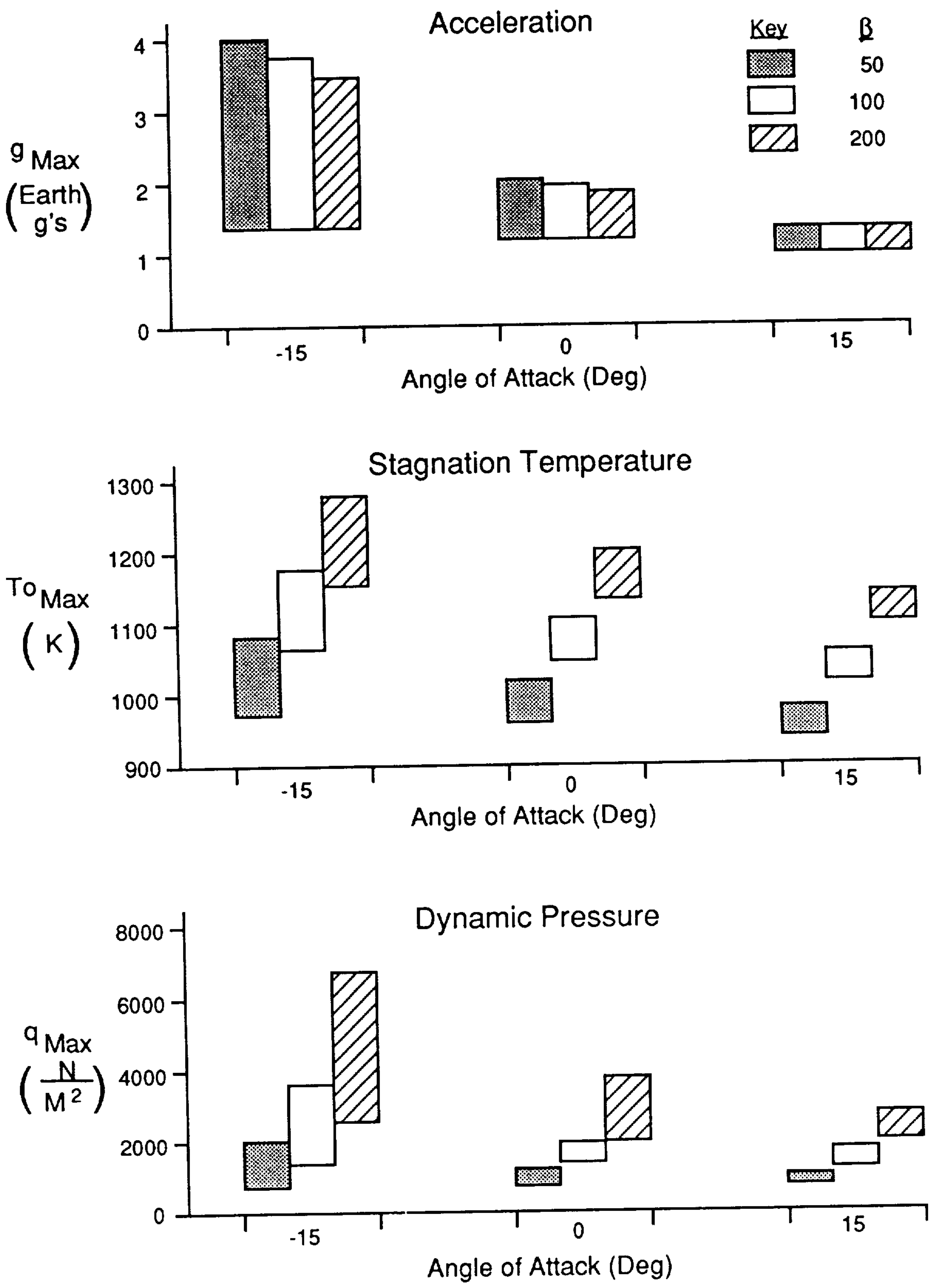

Figure 4-16. Mars aerocapture vehicle loads, $C_3 = 10\ km^2/s^2$.

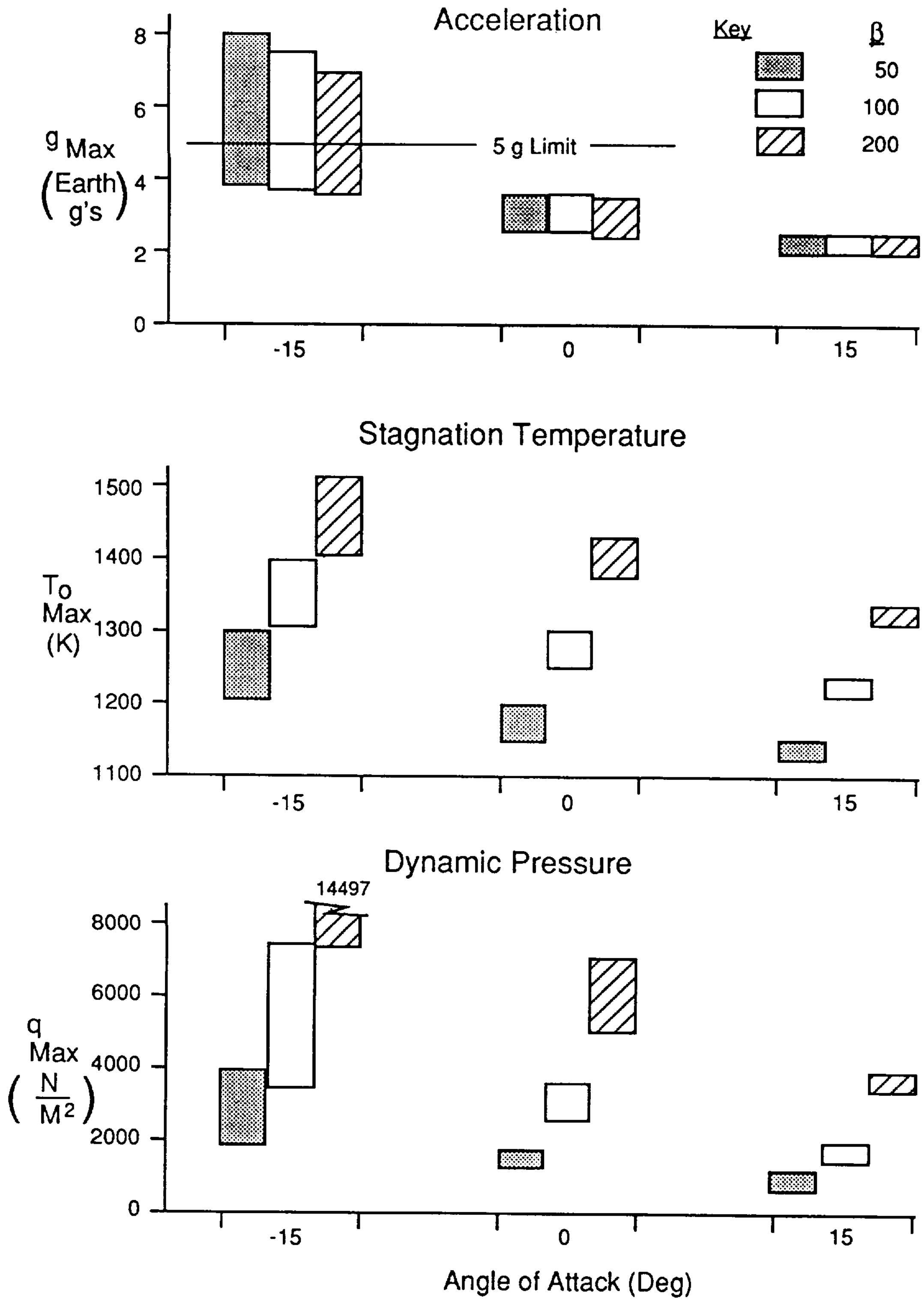

Figure 4-17. Mars aerocapture vehicle loads, $C_3 = 25\ km^2/s^2$.

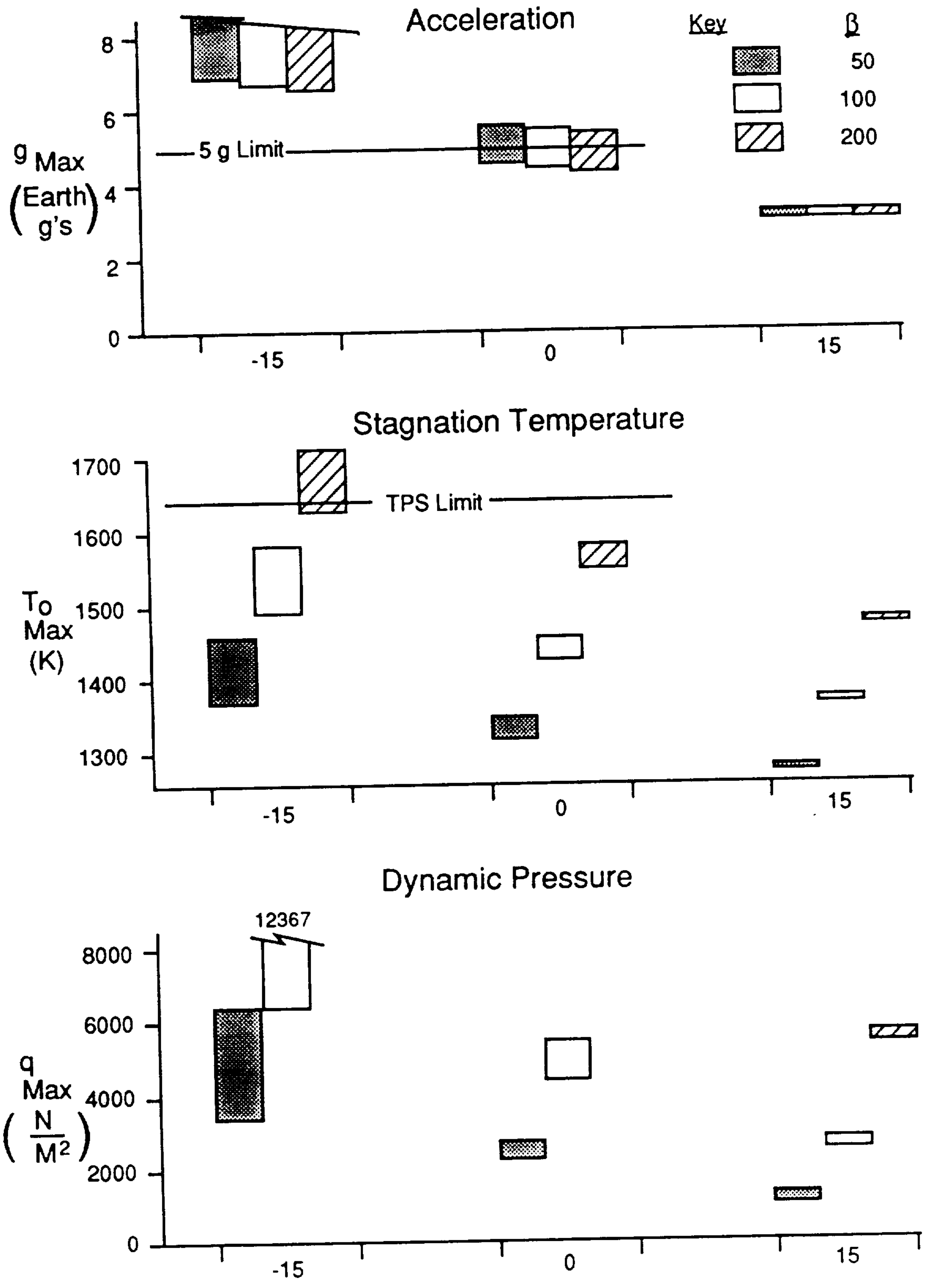

Figure 4-18. Mars aerocapture vehicle loads, $C_3 = 40\ km^2/s^2$.

The data in figures 4-12 through 4-18 show the importance of careful sizing of an aerobrake. The ballistic coefficient of the vehicle has a strong influence on the loads. As the ballistic coefficient increases (i.e., aerobrake diameter decreases), the maximum acceleration load decreases slightly, but the maximum stagnation point temperature and maximum dynamic pressure can increase significantly. The angle of attack can also have an impact on the vehicle loads. As the angle of attack becomes more positive (increasing lift downward) the maximum loads decrease. The sometimes counteracting effects of increasing ballistic coefficient and angle of attack on the vehicle loads show why it is necessary to consider both the vehicle design and the trajectory design in the process of sizing an aerobrake.

The two previous sets of data which were generated using constant angle of attack trajectories indicate that to minimize the vehicle loads it would be desirable to fly with lift directed downward at the highest possible L/D. This would result in the nearly grazing trajectory which was defined earlier [1]. Unfortunately, even at low L/D's, at positive angles of attack the exit apoapsis is too sensitive to the target vacuum periapsis. This is indicated by the almost vertical curves on the graphs in figures 4-5 through 4-11. One way to decrease the sensitivity to vacuum periapsis altitude and also reduce vehicle loads is to use a variable angle of attack trajectory with a lift profile similar to the one developed by Vinh and Lu [22].

3. Comparison of Constant and Variable Angle of Attack Trajectories

Comparisons of the trajectrories and maximum vehicle loads for constant and variable angle of attack trajectories are shown in figures 4-19 through 4-25. Due to the limitations of the computer programs that were available, it was not possible to find the optimum lift profile for each aerobrake mission, therefore, a lift profile that approximated the one developed by Vinh and Lu [22], and described in the previous section, was used. The variable lift profile used a simple two-step approximation to Vinh and Lu's solution. Maximum upward lift (negative angle of attack) was used for the descending leg of the aeropass, then maximum downward lift was used for the ascending leg of the aeropass. The switch from negative to positive angle of attack was performed at the minimum altitude of the trajectory and was assumed to be almost instantaneous.

Each of the figures in this set of data show the altitude profile during the aeropass as a function of time for three constant angle of attack trajectories and the variable angle of attack trajectory. The data listed with each figure show several trajectory parameters and the peak vehicle loads for each trajectory. The variable angle of attack trajectory is designated as "–/+15.0," which signifies an angle of attack of –15° during the descending leg of the aeropass and +15° during the ascending leg of the aeropass.

The trajectories are typical for each application. The exit apoapsis altitude for the GEO return and lunar return trajectories is representative of a return to an LEO space station orbit altitude. The exit apoapsis altitude for the Earth aerocapture missions represents the apoapsis altitude of an elliptical orbit with a period of 24 hours and a periapsis altitude of about 500 km. The exit apoapsis altitude of the Mars aerocapture missions represents the apoapsis altitude of an elliptical orbit with a period of one Mars solar day and a periapsis altitude of 250 km. The use of a high exit apoapsis for aerocapture missions reduces the peak vehicle loads.

A variable angle of attack lift profile provides a compromise between the disadvantages of constant upward and constant downward lift profiles. Trajectories flown with constant lift upward (negative angle of attack) are less sensitive to target vacuum periapsis altitude but can have high

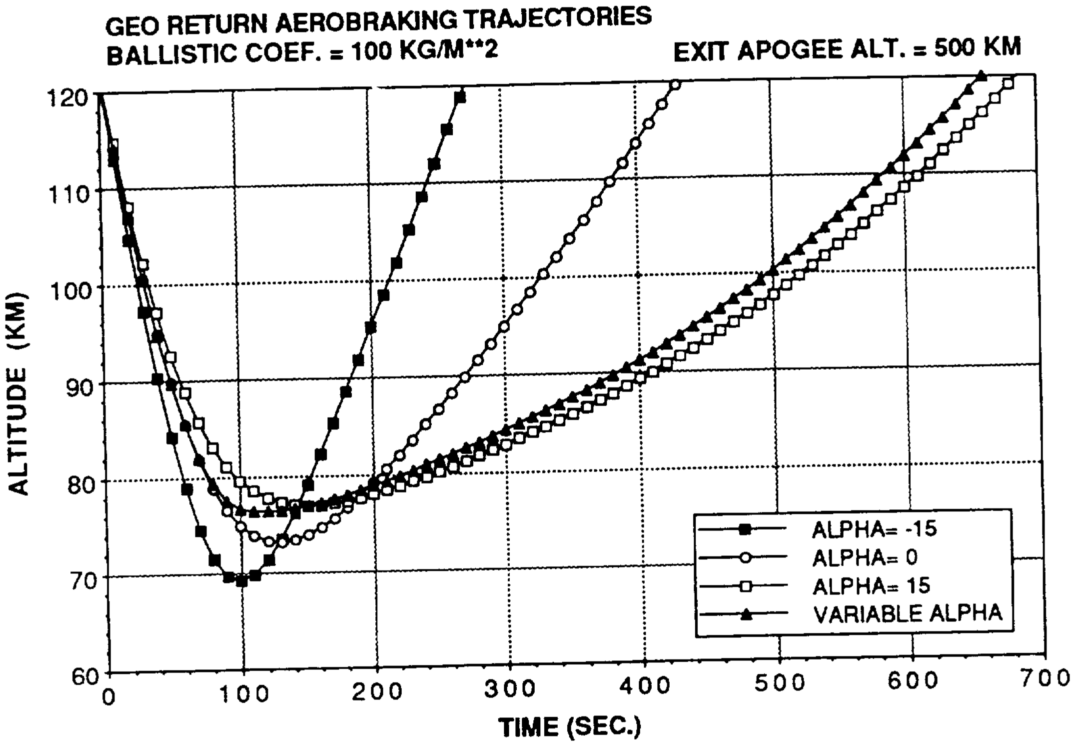

ALPHA (DEG)	TARGET PERIAPSIS (KM)	EXIT APOAPSIS (KM)	ENTRY VELOCITY (M/S)	MIN ALT (KM)	MAX G-LOAD (g)	MAX HEAT RATE (W/CM**2)	MAX DYN PRESS (N/M**2)
-15.0	59.9800	499.95	9899.85	69.21	3.91	37.20	3735.91
0.0	74.1400	499.90	9899.68	73.25	2.28	29.55	2231.11
15.0	80.5563	500.57	9899.60	77.01	1.40	23.78	1338.67
-/+ 15.0	73.9357	499.80	9899.68	76.45	1.58	26.13	1510.07

Figure 4-19. GEO return aerobrake trajectories.

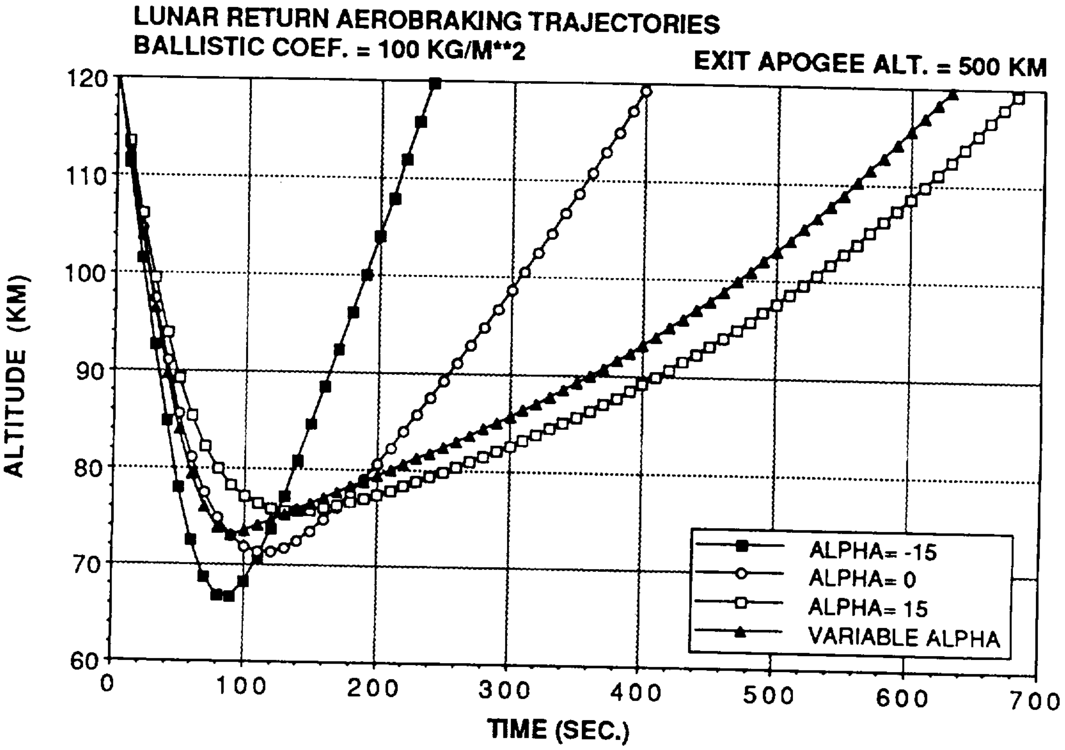

ALPHA (DEG)	TARGET PERIAPSIS (KM)	EXIT APOAPSIS (KM)	ENTRY VELOCITY (M/S)	MIN ALT (KM)	MAX G-LOAD (g)	MAX HEAT RATE (W/CM**2)	MAX DYN PRESS (N/M**2)
-15.0	54.5820	499.93	10574.89	66.79	5.99	51.68	5728.59
0.0	72.1521	500.08	10574.32	71.32	3.23	39.82	3170.00
15.0	79.3996	502.46	10574.08	75.59	1.92	31.48	1832.77
-/+ 15.0	68.5790	500.49	10574.43	73.05	2.89	39.31	2764.95

Figure 4-20. Lunar return aerobrake trajectories.

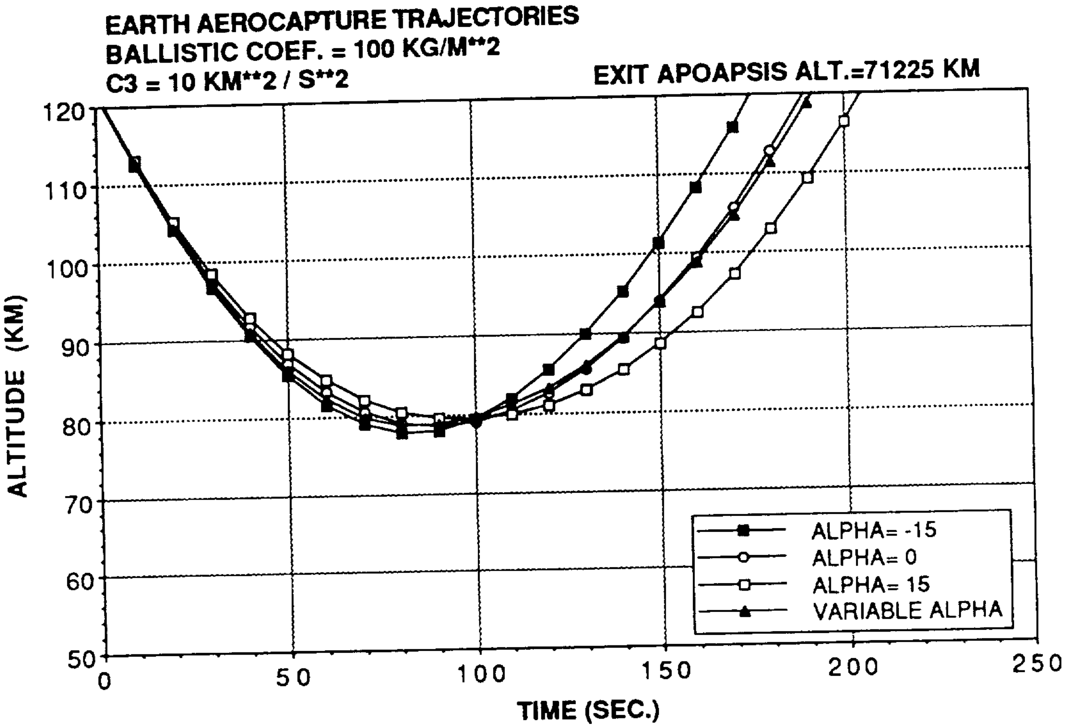

ALPHA (DEG)	TARGET PERIAPSIS (KM)	EXIT APOAPSIS (KM)	ENTRY VELOCITY (M/S)	MIN ALT (KM)	MAX G-LOAD (g)	MAX HEAT RATE (W/CM**2)	MAX DYN PRESS (N/M**2)
-15.0	75.8992	71225.75	11104.50	77.87	1.70	35.53	1625.45
0.0	78.7908	71227.04	11104.40	78.60	1.46	32.98	1432.51
15.0	81.1538	71226.40	11104.31	79.47	1.30	31.20	1240.04
-/+ 15.0	77.0565	71225.33	11104.46	78.74	1.49	33.61	1428.68

Figure 4-21. Earth aerocapture trajectories, $C_3 = 10\ km^2/s^2$.

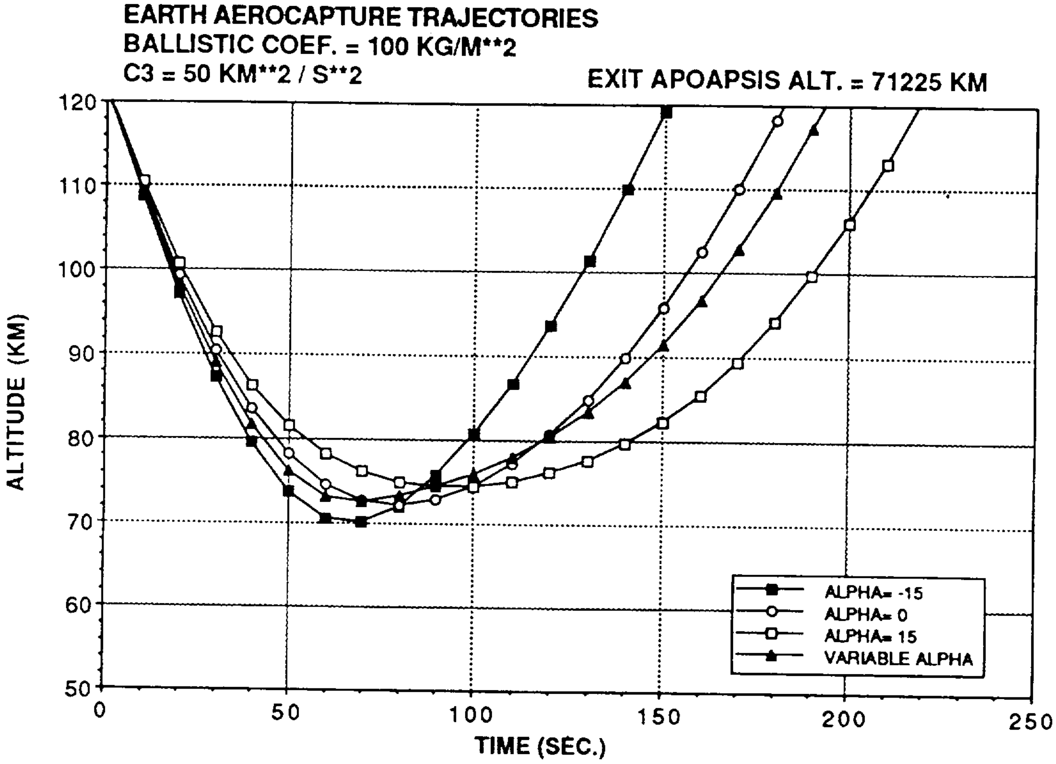

ALPHA (DEG)	TARGET PERIAPSIS (KM)	EXIT APOAPSIS (KM)	ENTRY VELOCITY (M/S)	MIN ALT (KM)	MAX G-LOAD (g)	MAX HEAT RATE (W/CM**2)	MAX DYN PRESS (N/M**2)
-15.0	64.0276	71225.80	12727.35	70.06	6.02	82.38	5752.05
0.0	72.4564	71226.57	12726.99	72.12	4.38	71.42	4290.82
15.0	77.7764	71214.72	12726.76	74.43	3.33	61.57	3179.57
-/+ 15.0	68.5179	71224.53	12727.16	72.55	4.41	73.45	4215.65

Figure 4-22. Earth aerocapture trajectories, C_3 = 50 km^2/s^2.

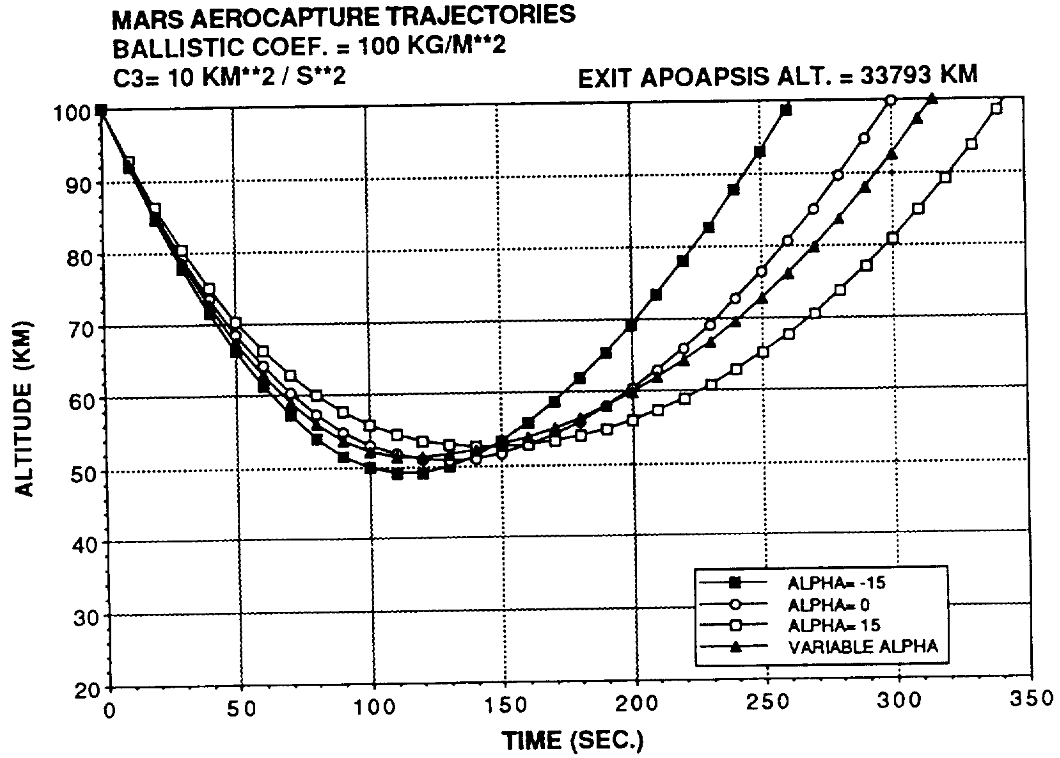

ALPHA (DEG)	TARGET PERIAPSIS (KM)	EXIT APOAPSIS (KM)	ENTRY VELOCITY (M/S)	MIN ALT (KM)	MAX G-LOAD (g)	MAX HEAT RATE (W/CM**2)	MAX DYN PRESS (N/M**2)
-15.0	45.0521	33793.52	6073.00	49.13	1.46	8.30	1397.08
0.0	51.2504	33793.43	6073.22	50.78	1.15	7.41	1128.48
15.0	55.8255	33791.74	6073.39	52.60	0.94	6.73	893.88
-/+ 15.0	48.3351	33793.65	6073.12	51.36	1.14	7.45	1093.53

Figure 4-23. Mars aerocapture trajectories, $C_3 = 10\ km^2/s^2$.

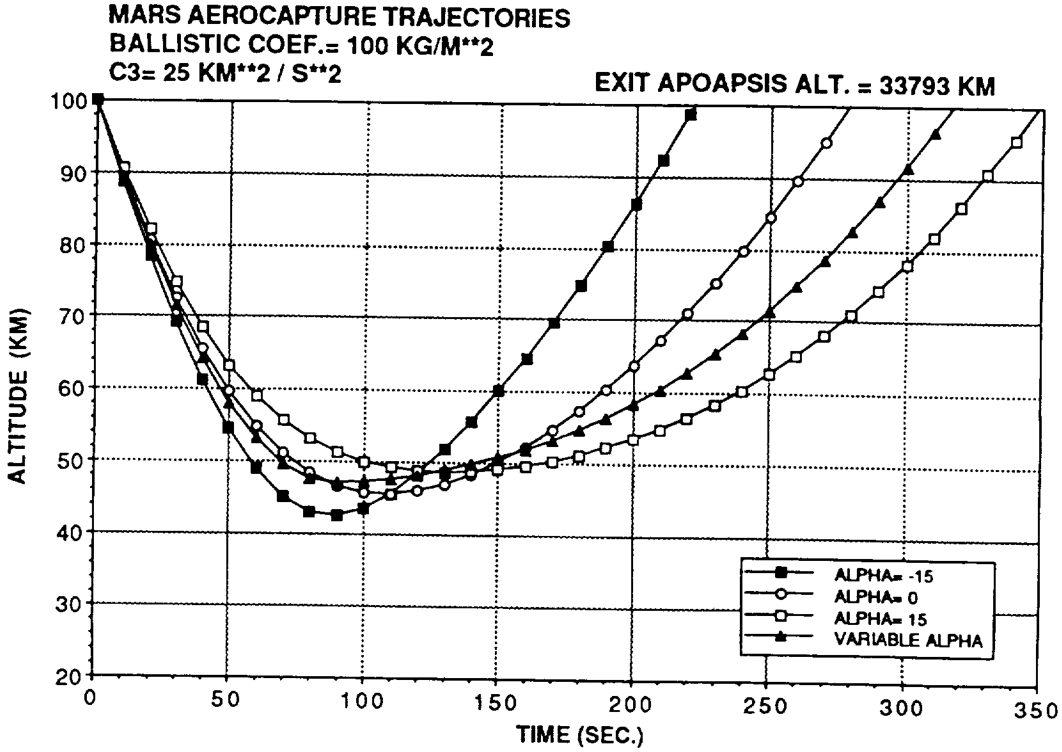

ALPHA (DEG)	TARGET PERIAPSIS (KM)	EXIT APOAPSIS (KM)	ENTRY VELOCITY (M/S)	MIN ALT (KM)	MAX G-LOAD (g)	MAX HEAT RATE (W/CM**2)	MAX DYN PRESS (N/M**2)
-15.0	34.2682	33792.97	7234.13	42.56	4.03	18.30	3850.82
0.0	46.0666	33793.06	7234.63	45.54	2.76	15.44	2706.06
15.0	53.1162	33788.04	7234.92	48.63	1.96	13.30	1869.15
-/+ 15.0	42.3419	33795.40	7234.47	46.98	2.55	15.55	2436.99

Figure 4-24. Mars aerocapture trajectories, $C_3 = 25\ km^2/s^2$.

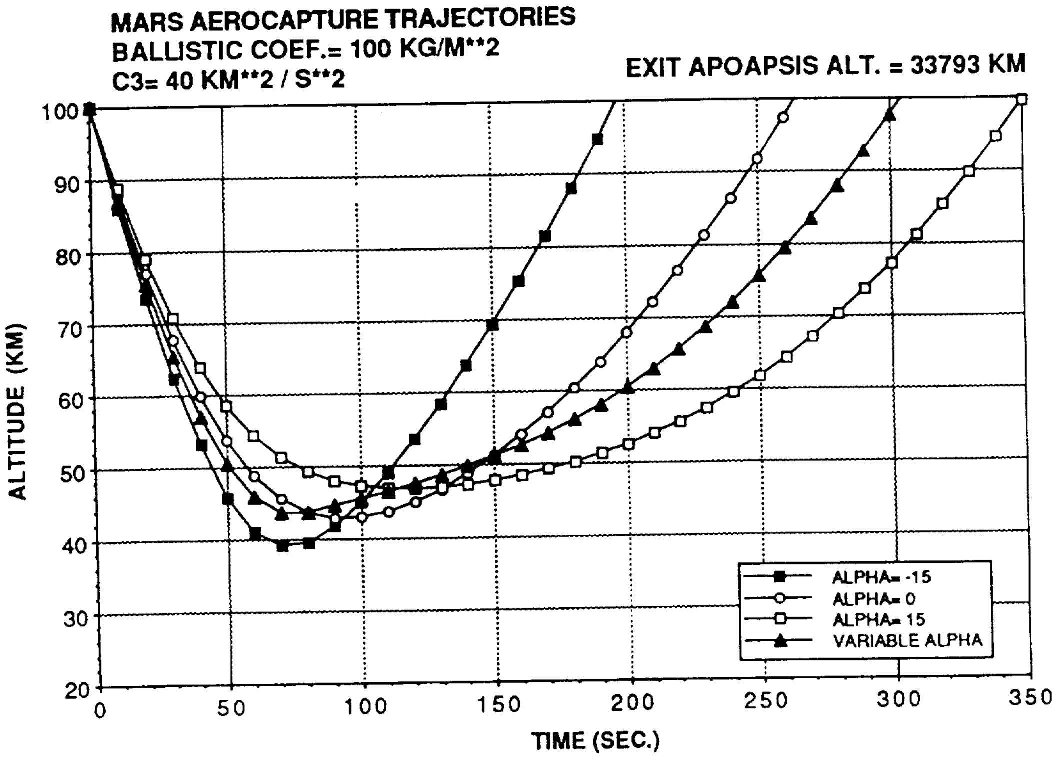

ALPHA (DEG)	TARGET PERIAPSIS (KM)	EXIT APOAPSIS (KM)	ENTRY VELOCITY (M/S)	MIN ALT (KM)	MAX G-LOAD (g)	MAX HEAT RATE (W/CM**2)	MAX DYN PRESS (N/M**2)
-15.0	27.0874	33793.22	8229.39	39.15	6.93	30.52	6628.69
0.0	43.4275	33791.81	8230.13	42.96	4.41	25.42	4320.50
15.0	51.9733	33810.53	8230.51	46.90	2.93	21.08	2800.86
-/+ 15.0	36.6991	33793.68	8229.82	43.74	4.71	26.74	4500.52

Figure 4-25. Mars aerocapture trajectories, $C_3 = 40\ km^2/s^2$.

peak loads. Trajectories flown with constant lift downward (positive angle of attack) have lower peak loads but are very sensitive to target vacuum periapsis altitude. The variable angle of attack profile results in a minimum altitude between that of a constant lift up or constant down profile. This results in peak loads which are between the two extremes but generally closer to the constant lift down trajectory and a sensitivity to target vacuum periapsis that is similar to a zero lift trajectory (constant angle of attack equal to zero).

All of the trajectories in figures 4-19 through 4-25 were generated using the standard atmosphere models described earlier. Since the density profiles were smooth functions of altitude, the lift profiles, whether constant or variable, represent "nominal" or baseline cases. In reality, the lift would have to vary from the nominal to correct for guidance errors and atmospheric variations. Varying the angle of attack allows the trajectory to be adjusted during the aeropass. The benefits of a variable angle of attack can be seen by looking at the effect of density variations on aerobrake trajectories and the range of allowable target vacuum periapsis altitudes.

4. Definition of Target Vacuum Periapsis Tolerance

As stated earlier, the actual guidance scheme that would allow a vehicle to achieve an exact exit condition was not investigated. Rather, given an assumed vehicle ballistic coefficient and angle of attack range, the limits within which the guidance scheme would operate were defined. Figures 4-26 through 4-28 show the range of allowable target vacuum periapsis altitudes for an aerobraked vehicle at various atmospheric densities for each aerobrake application. The vehicle was assumed to have a ballistic coefficient of 100 kg/m^2 and an angle of attack control range from –15° to +15°. Trajectories were analyzed using atmosphere models corresponding to the mean density profile, 20 percent above the mean and 20 percent below the mean. In reality the deviation of the density from the mean is not constant with altitude so this data provides conservative boundaries of the density variation.

Each bar in these figures represents a range of target vacuum periapsis altitudes which allow an exit apoapsis within the designated acceptable range without exceeding a maximum acceleration load of five Earth g's. For GEO and lunar return (fig. 4-26), the designated range of exit apoapsis altitudes is from 130 to 1,000 km. For the aerocapture applications (figs. 4-27 and 4-28), the range is from 500 to 100,000 km.

The range of altitude for which the three bars overlap define the target vacuum periapsis altitudes for which the vehicle could achieve a desired exit apoapsis as long as the density is within 20 percent of the mean. This range of altitudes will be defined as the target vacuum periapsis altitude tolerance. The size of this tolerance is shown for each aerobrake application. It defines the accuracy to which the vehicle must be targeted prior to atmospheric entry. Once the vehicle enters the atmosphere, the trajectory would be adjusted by varying the angle of attack within the control range.

To find the limits of the target vacuum periapsis altitude without defining a guidance scheme, a very conservative approach was used for adjusting the trajectory in the atmosphere. Only one angle of attack adjustment was used. The entry angle of attack was held constant until the vehicle reached minimum altitude, then the angle of attack was adjusted to either maximum lift down or maximum lift up for the ascending leg of the trajectory. This single large adjustment reveals the limits of what a real guidance scheme could achieve with many small adjustments.

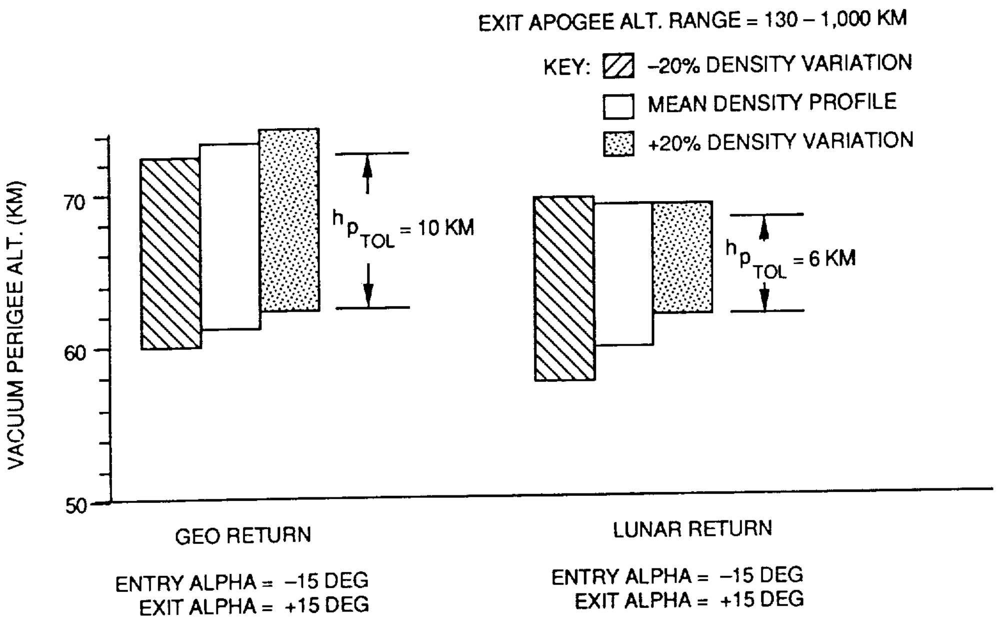

Figure 4-26. Effect of density variations on target vacuum periapsis tolerance for GEO and lunar return aerobraking.

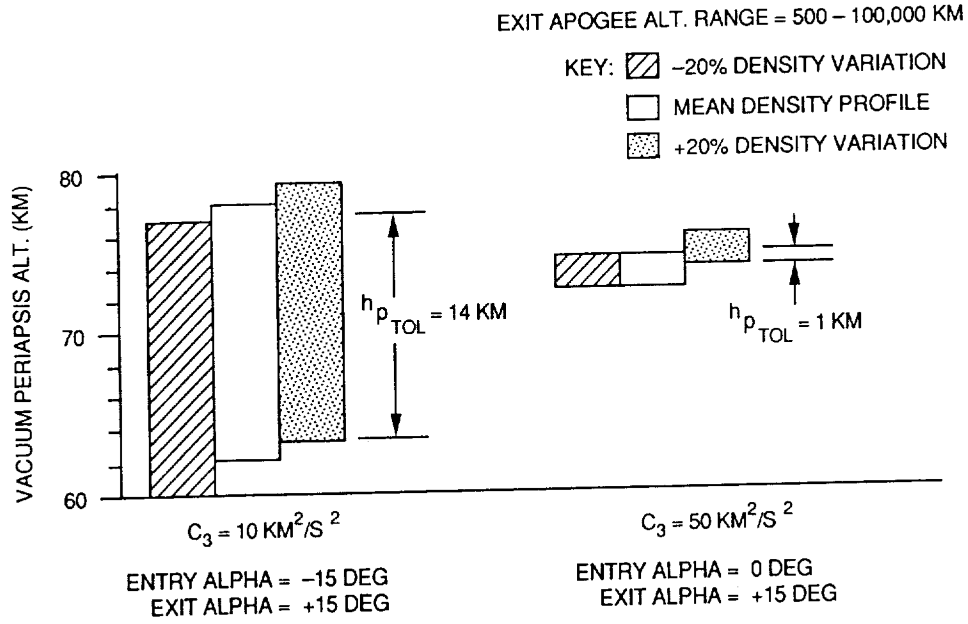

Figure 4-27. Effect of density variations on target vacuum periapsis tolerance for Earth aerocapture.

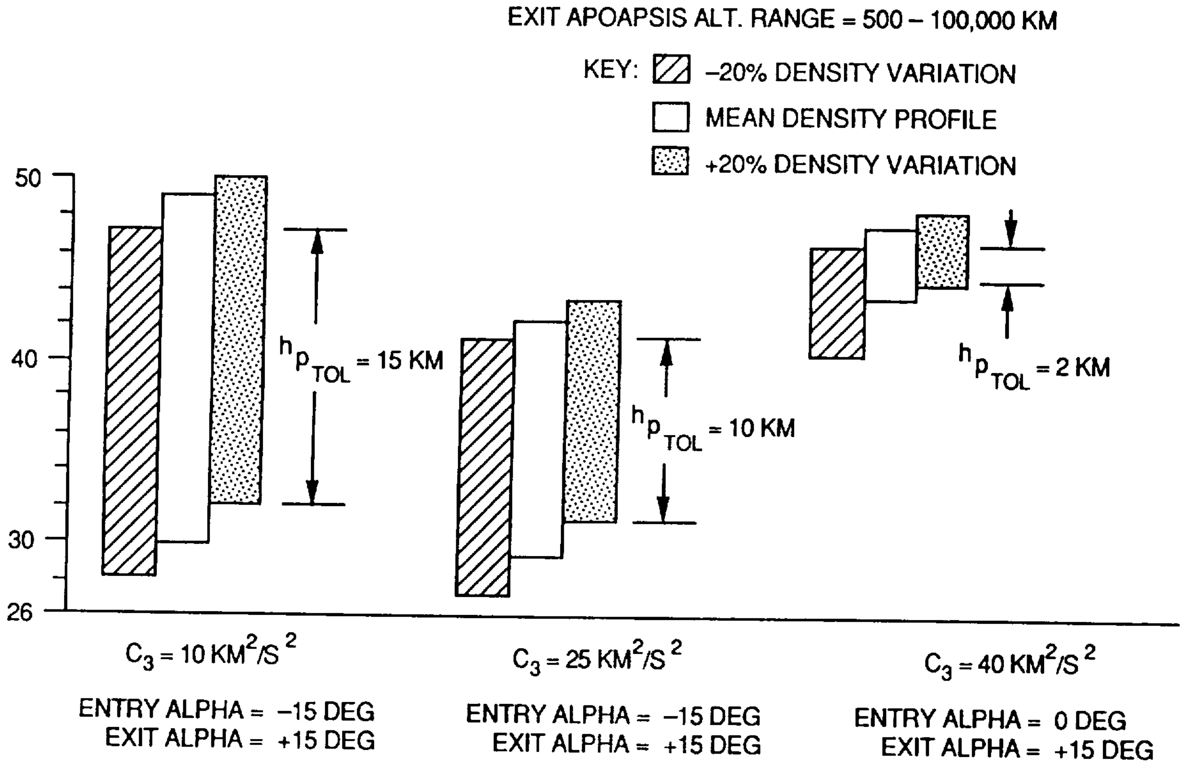

Figure 4-28. Effect of density variations on target vacuum periapsis tolerance for Mars aerocapture.

In agreement with the results of Vinh and Lu [22], it was found that the vehicle loads were reduced if maximum upward lift (angle of attack equal to –15°) was used during the descending leg of the trajectory. In most cases, this entry angle of attack also resulted in the largest target vacuum periapsis altitude tolerance. The exceptions were the aerocapture applications at high C_3's where it was found that a ballistic entry (angle of attack equal to 0°) yielded the largest target vacuum periapsis tolerance.

V. SUMMARY

This report has investigated the application of aerobraking for orbital transfers from geosynchronous and lunar orbit to low Earth orbit and aerocapture at Earth and Mars. The objective was to show that low L/D aerobrakes which use angle of attack variation for control could be used for each of these applications. The investigation began with a study of the design considerations that are necessary in the process of designing and sizing an aerobrake for a particular application. Since the aerobrake vehicle design process is interrelated to the trajectory design, a review of several formulations for obtaining optimum aerobrake trajectories was presented. Finally, the relationship between aerobrake design factors and trajectory characteristics was investigated further using numerical simulations to analyze aerobrake trajectories for each application.

The aerodynamic characteristics of aerobrakes are in many ways unique from most other atmospheric vehicles. The one characteristic that sets aerobrakes apart is that they are designed primarily to utilize the drag force rather than the lift force. Lift is used only as a control for changing the lateral direction of flight or the rate of altitude change. In many aerobrake applications, very little lift is needed. Each of the aerobrake applications that were investigated could be implemented with a maximum L/D of only 0.3 using a spherical aerobrake. It was shown that the L/D is closely related to the ballistic coefficient in determining the atmospheric trajectory of an aerobraked vehicle. The proper combination of L/D and ballistic coefficient allows the vehicle to achieve sufficient depth of penetration into the atmosphere for aerodynamic control. This combination is determined by the vehicle acceleration and heating load limits.

Due to the unique aerodynamic characteristics of aerobraked vehicles, special attention must be paid to the aerodynamic stability of the vehicle. The conditions for static longitudinal stability were investigated. It was shown that the location of the vehicle center of mass must be in front of the neutral point so that C_{m_α} is less than zero. The neutral point was defined as the point on the vehicle trim line where C_{m_α} equals zero. The location of the neutral point depends on the aerodynamic coefficients and the diameter of the aerobrake. For a spherical aerobrake, the distance from the front of the aerobrake to the neutral point increases as the angle of attack decreases or the aerobrake diameter increases.

Several other aerobrake design factors were also described. One of the most important design considerations is the flow behind the aerobrake. The aerobrake must be sized so that flow does not impinge on the vehicle behind the aerobrake. For angles of attack between 5° and 15°, the flow impingement angle ranges from 20° to 35° of inward deflection behind the aerobrake. The flow impingement places limits on the size of the aerobrake payload since the aerobrake diameter must often be balanced against the capabilities of the vehicle to withstand thermal and aerodynamic loads. As indicated previously, the effect of aerobrake diameter on the vehicle design must be carefully considered since the ballistic coefficient of the vehicle has a large influence on the atmospheric trajectory, which in turn determines the magnitudes of the loads.

One of the most critical vehicle loads that influences the design of an aerobrake is the aerodynamic heating. The heating loads determine to a large extent the size of the aerobrake. The magnitude of the heating loads that are allowed is determined primarily by the capabilities of the TPS. Several types of TPS's were reviewed, but due to the large heat loads that can be experienced, it appears that reusable surface insulation is the best choice. The aerodynamic heating environment for an aerobrake is not yet clearly understood. There is considerable uncertainty concerning the existence and effects of nonequilibrium aerodynamic heating during an aerobraking maneuver. One of the primary objectives of the planned AFE is to investigate this phenomenon.

The optimization of aerobrake trajectories depends largely on how optimum is defined. There are many performance indices that can be used as criteria for defining an optimum trajectory. In many cases the optimum trajectories, as measured by different performance indices, are very different. It was found that performance indices which result in "nearly grazing" optimal trajectories provided the best compromise between the often conflicting goals of minimizing the vehicle propulsive requirements and minimizing the aerodynamic heating. To implement an optimum aerobraking trajectory, it is necessary to select a vehicle control strategy. The performance indices and allowable trajectory controls are closely related to or constrained by the vehicle design. This indicates that there is an interrelationship between vehicle design and trajectory design. Roll control, pitch control (angle of attack variation), and drag control were discussed.

The investigation of the relationship between vehicle and trajectory design and the potential for using angle of attack variation for control was continued using numerical simulations to analyze trajectories for each aerobrake application. The data that were presented showed the sensitivity of the trajectory to vehicle angle of attack, ballistic coefficient, and entry conditions. A conservative approach was used in modeling the atmospheric density variations and aerobrake angle of attack control profile. This provided a representative boundary of the effects of atmospheric density variations on the trajectories and the capabilities of low L/D aerobrakes across a wide range of trajectory conditions.

The data that were developed showed that aerobrake trajectories are very sensitive to the atmospheric entry conditions and the density variations within the atmosphere. This implies that a very responsive control scheme is required. One potential advantage in the responsiveness of pitch control over roll control is that there is no lateral component of the lift force to be balanced in order to maintain a particular orbital plane. Data were also developed to illustrate the relationship between vehicle design and trajectory design. The sensitivity of several vehicle loads to angle of attack and ballistic coefficient was investigated. The data showed that in some applications the acceleration and heating constraints may limit the range of allowable aerodynamic controls. To reduce the peak loads, it may be necessary to constrain the magnitude and direction of the lift force to limit the depth of penetration into the atmosphere.

The feasibility of using low lift to drag aerobrakes for the selected applications was investigated further by determining the range of target vacuum periapsis altitudes for which an aerobraked vehicle could achieve desired atmospheric conditions. A simple two-phase angle of attack control profile was used to provide an approximation of the optimum lift profile to reduce vehicle loads and provide an approximation of the control limits for low L/D aerobrakes. The target vacuum periapsis tolerances that were defined indicate that low L/D aerobrakes have sufficient control capability to perform each of the aerobrake applications.

The aerobrake trajectory analysis that was performed for this report provides only a shallow penetration (aerobrake pun) into some of many problems that will require thorough investigation if aerobraking is to become a useful operation for space transportation vehicles. Nevertheless, the results in this report have shown that a wide range of aerobrake applications are feasible for vehicles with low L/D aerobrakes using angle of attack variation for control.

REFERENCES

1. Mease, K.D.: "Optimization of Aeroassisted Orbital Transfer: Current Status," Journal of the Astronautical Sciences, vol. 36, No. 1/2, January–June 1988, pp. 7–34.

2. Walberg, G.D.: "A Survey of Aeroassisted Orbital Transfer," Journal of Spacecraft and Rockets, vol. 22, No. 1, January–February 1985, pp. 3–18.

3. Miele, A., Lee, W.Y., and Mease, K.D.: "Nearly Grazing Optimal Trajectories for Aeroassisted Noncoplanar Orbital Transfer," Journal of the Astronautical Sciences, vol. 36, No. 1/2, January–June 1988, pp. 139–158.

4. Hanson, J.M.: "Combining Space-Based Propulsive Maneuvers and Aerodynamic Maneuvers To Achieve Optimal Transfer," AIAA Paper 87-2567, August 1987.

5. Scott, D.C., Reid, R.C., Maraia, R.J., Liu, C.P., and Derry, S.M.: "An AOTV Aeroheating and Thermal Protection Study," AIAA Paper 84-1710, June 1984.

6. Austin, R.E., Cruz, M.I., and French, J.R.: "System Design Concepts and Requirements for Orbital Transfer Vehicles," AIAA Paper 82-1379, August 1982.

7. Mayo, E.E., Lamb, R.H., and Romere, P.O.: "Newtonian Aerodynamics for Blunted Raked-Off Circular Cones and Raked-Off Elliptical Cones," NASA TN-D-2624, May 1965.

8. Goodrick, T.F., Data Provided in a Personal Interview, NASA, Marshall Space Flight Center, August 1990.

9. Gentry, A.E., Smyth, D.N., and Oliver, W.R.: "The Mark IV Supersonic-Hypersonic Arbitrary-Body Program, Volume I Users Manual," Air Force Flight Dynamics Laboratory Technical Report AFFDL-TR-73-199, vol. I, November 1973.

10. Hair, L.M., Engel, C.D., Shih, P., Bithell, R., and Bowman, M.: "Aerothermal Test Data of Low L/D Aerobraking Orbital Transfer Vehicle at Mach 10, NASA LaRC Test 117," Remtech Inc., Huntsville, Alabama, RTR 069-1, April 1983.

11. Dauro, V.A.: "A Tutorial on Aerobraking," NASA, Marshall Space Flight Center, December 1988 (Unpublished).

12. NASA, Marshall Space Flight Center, "Mars Exploration Mission and System Analysis of the Split Sprint Mission," Program Development, December 1988.

13. Goodrick, T.F.: "Tilt-Trim for Aerobrakes," Data provided in a personal interview, NASA, Marshall Space Flight Center, March 1990.

14. NASA, Marshall Space Flight Center, "LTV Aerobrake Assessment, Comparison of Rigid and Flexible/Deployable Concepts," Program Development, July 1990.

15. Mease, K.D., and Vinh, N.X.: "Minimum-Fuel Aeroassisted Coplanar Orbit Transfer Using Lift Modulation," AIAA Paper 83-2094, August 1983.

16. Shinn, J.L., and Jones, J.J.: "Chemical Nonequilibrium Effects on Flow Fields for Aeroassisted Orbital Transfer Vehicles," Journal of Spacecraft and Rockets, vol. 22, January–February 1985, pp. 54–59.

17. Hair, L.M., Engel, C.D., and Sulyma, P.R.: "Low L/D Aerobrake Test at Mach 10," AIAA Paper 83-1509, June 1983.

18. Garcia, F., and Fowler, W.T.: "Thermal Protection System Weight Minimization for the Space Shuttle Through Trajectory Optimization," Journal of Spacecraft and Rockets, vol. 11, No. 4, April 1974, pp. 241–245.

19. Dickerson. T.D.: "LTV Aerobrake Sizing Methods," NASA, Marshall Space Flight Center Memo, PD32(90-130), September 19, 1990.

20. Halfman, R.L.: "Systems, Variational Methods and Relativity," Dynamics, vol. 2, Addison-Wesley, Reading Mass., 1962, pp. 448–469.

21. Oberle, H.J.: "Numerical Treatment of Minimax Optimal Control Problems With Application to the Reentry Flight Path Problems," Journal of the Astronautical Sciences, vol. 36, No. 1/2, January–June 1988, pp. 159–179.

22. Vinh, N.X., and Lu, P.: "Chebyshev Minmax Problems for Skip Trajectories," Journal of the Astronautical Sciences, vol. 36, No. 1/2, January– June 1988, pp. 179–197.

23. Vinh, N.X.: "Optical Trajectories in Atmospheric Flight," Elsevier Scientific Publishing Co., Amsterdam, 1981, pp. 296–313.

24. Willcockson, W.H.: "OTV Aeroassist With Low L/D," Acta Astronautica, vol. 17, No. 3, 1988, pp. 277–301.

25. Andrews, D.G., and Bloetscher, F.: "Aerobraked Orbital Transfer Vehicle Definition," AIAA Paper 81-0279, January 1981.

26. Dauro, V.A.: "Integrated Mission Program Users Manual Volume 1," NASA, Marshall Space Flight Center, April 1990. (Unpublished).

27. Fehlberg, E.: "Classical Fifth-, Sixth-, Seventh-, and Eighth-Order Runge-Kutta Formulas With Step Size Control," NASA TR-R-287, October 1968.

28. Kaplan, D., ed.: "Environment of Mars," NASA Technical Memorandum 100470, October 1988.

29. United States Government Printing Office, "U.S. Standard Atmosphere, 1962," Washington, DC, December 1962.,

30. "Space and Planetary Environment Criteria Guidelines for Use in Space Vehicle Development, 1982 Revision (Volume 1)," NASA Technical Memorandum 82478, January 1983.

APPROVAL

APPLICATIONS OF LOW LIFT TO DRAG RATIO AEROBRAKES USING ANGLE OF ATTACK VARIATION FOR CONTROL

By J.A. Mulqueen

The information in this report has been reviewed for technical content. Review of any information concerning Department of Defense or nuclear energy activities or programs has been made by the MSFC Security Classification Officer. This report, in its entirety, has been determined to be unclassified.

Charles R. Darwin

C.R. DARWIN
Director, Program Development

U. S. GOVERNMENT PRINTING OFFICE 1991 – 531-081/40104